Summer 8-11-2016

RNAi Nanotechnology: A Platform for siRNA Screening and Cancer Gene Therapy

Mayurbhai Ravikant Patel
Seton Hall University, mayurbhai.patel@student.shu.edu

RNAi Nanotechnology: A Platform for siRNA Screening and Cancer Gene Therapy

A thesis submitted to the Department of Chemistry and Biochemistry at Seton Hall University in partial fulfillment of the requirements for the degree of Doctor of Philosophy

By

Mayurbhai R. Patel

August 2016

Department of Chemistry and Biochemistry
Seton Hall University
South Orange, New Jersey, USA

DISSERTATION COMMITTEE APPROVALS

We certify that we have read this thesis and that in our opinion it is sufficient in scientific scope and quality as a dissertation for the degree of Doctor in Philosophy

APPROVED BY:

David Sabatino, Ph.D.

Advisor, Seton Hall University

Cecilia Marzabadi, Ph.D.

Reader, Member of Dissertation Committee, Seton Hall University

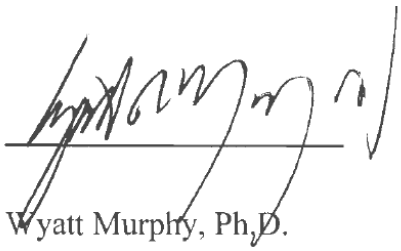

Wyatt Murphy, Ph.D.

Reader, Member of Dissertation Committee, Seton Hall University

Cecilia Marzabadi, Ph.D.

Chair, Department of Chemistry and Biochemistry, Seton Hall University

Dedicated to my father Ravikant, Vipinfua, my wife Mandakini, mother Dharmistaben and family. Thank you for your unconditional love and support. This thesis work wouldn’t have been possible without your sacrifices.

ABSTRACT

Over the past two decades, advances in RNA structural biology have improved our understanding of the structures and folding properties of naturally occurring RNAs. RNA sequences and structures participate in many specific biological functions, such as those performed by messenger RNA (mRNA), ribosomal RNA (rRNA), transfer RNA (tRNA), micro RNA (miRNA), short-interfering RNA (siRNA), small nuclear RNA (snRNA) and many others. The noncoding RNAs, such as siRNA, do not express proteins but have been utilized in a wide range of applications, including RNA interference (RNAi) and the regulation of mRNA expression. These important biological functions have been implemented in gene therapy and for screening malignant gene targets. In spite of their therapeutic potential, naturally occurring siRNAs are limited by poor pharmacological properties which has hindered their translation into the clinic. However, recent studies have highlighted the fruitful applications of modified siRNAs, including the use of siRNA nanostructures in cancer detection and treatment. In this thesis, the prerequisite conditions for forming stable RNA hybrid assemblies are described in Chapter 2. These conditions are critically important for the generation of stable higher-order RNA nanostructures. Inspired by the widespread biological function of self-assembled RNA hybrids, linear RNA templates and two complementary strands were self-assembled in order the determine the requirements for efficient RNA hybridization into stable three-component systems (3CS). In this study the RNA sequence composition and length were found to impact hybridization and self-assembly. Moreover, buffer conditions were also evaluated in order to explore the influence of ionic strength and metal cation composition on stable RNA hybridization. The complementary RNAs were annealed in buffer and analyzed by native PAGE, thermal denaturation and CD spectroscopy. The data supported the stable 3CS self-assembly on a thirty nucleotide (30nt) RNA template and with complementary 15nt and 23 nt RNA sequences in Tris buffer. These conditions were shown to favor the self-assembly of higher-order RNA structures, such as the siRNA nanostructures in Chapter 3.

The genetically encoded, self-assembled siRNA nanostructures targeting the Glucose Regulated Proteins (GRP) were developed for applications in siRNA screening of these important oncologic targets and for potentiating cancer gene therapy. In our RNAi nanotechnology approach, linear, V- and Y-shape RNA templates were synthesized by semi-automated solid phase RNA synthesis with the use of a ribouridine branchpoint synthon which was used generate the V- and

Y-shape RNA templates. The RNA templates were then hybridized in Tris buffer with their complementary strands, in stoichiometric ratios which favored hybridization and self-assembly into genetically encoded spheres, triangles, squares, pentagons and hexagons of discrete sizes and shapes. The siRNA self-assembly was confirmed by native PAGE while TEM imaging validated the sizes and shapes of the siRNA nanostructures. Moreover, thermal denaturation and CD spectroscopy were used to ascertain the prerequisite siRNA hybrids for their RNAi applications. In a 24 sample siRNA screen conducted within the AN3CA endometrial cancer cells known to overexpress tumorigenic GRP78 activity, the self-assembled siRNAs targeting multiple sites of GRP78 mRNA demonstrated more potent and long-lasting anticancer activity relative to their linear controls. Extending the scope of our RNAi screening approach, the self-assembled siRNA hybrids (5 nM) that targeted GRP-75, 78 and 95 were tested within endometrial (AN3CA), cervical (HeLa) and breast (MDA-MB-231) cancer cell lines with respect to the control non-cancerous lung (MRC5) cell line. The results indicated that the non-cancerous MRC5 lung cell line which displayed normal glucose regulated chaperone levels was found to tolerate siRNA treatment and demonstrated less toxicity relative to the cancer cells that were found to be addicted to glucose regulated chaperome. Therefore, the GRP targeting siRNAs were found to elicit more potent anti-cancer activity due to an overexpression and strong dependence of GRP activity in cancer. The serum stability of the self-assembled siRNAs was also investigated relative to the linear siRNA control. The data analyzed on a denaturing PAGE indicated a quick (< 4 h) degradation profile of the linear siRNA hybrid while the siRNA nanostructures were disassembled into their native RNA templates with no further degradation observed over the course of a 48 h fetal bovine serum (FBS) treatment. Thus, the RNA templates have been proposed to contribute to the prolonged (72 h) RNAi effect observed within the cancer cells. In sum, these remarkable self-assembled siRNA nanostructures may thus encompass a new class of potent siRNAs that may be useful in screening important oncogene targets while improving siRNA therapeutic efficacy and specificity in cancer.

KEYWORDS: siRNA nanostructures, RNAi nanotechnology, cancer gene therapy, Chaperones, Glucose Regulated Proteins (GRP), endometrial, cervical and breast cancer

ACKNOWLEDGEMENTS

They say that life's all about the journey, and at the beginning of this journey I started as a chemist. After deciding I didn't have enough experience in any one area I decided to go to graduate school. At the New Jersey Institute of Technology (NJIT) I completed my Master's degree in nucleic acid biochemistry. My interest and curiosity in this field propelled made me to pursue a Ph.D. degree in nucleic acid chemical biology at Seton Hall University. During my studies, I gained in depth knowledge of nucleic acid chemistry and biology. As the saying goes, "Success doesn't knock on your door easily", in reality, I learned that hard work and perseverance were the keys to success. This experience has definitely made me a better person. Not only because of the vast amount of knowledge I've gained, but also because of the people I've met along the way. Without the help and sacrifice of many great people, I would not have been able to accomplish my goals.

The first person I need to thank is my great advisor, Dr. David Sabatino. Thanks for providing all the lab resources necessary for my research project. You were a constant source of motivation and ideas for my projects. Dr. Sabatino always treats his students as a family instead of just a lab group and I am proud to be a part of the lab 419 family. He encouraged me to attend many regional and national conferences and made it possible to work with other research groups at Queens College and Memorial Sloan Kettering.

I would also like to thank my matriculation committee. Drs. Yufeng Wei (Chair Person), Cecilia Marzabadi, Sergiu Gorun, and Cosimo Antonacci, for putting time and effort to critically review, judge and provide feedback of my work. I'd like to especially thank Dr. Cecilia Marzabadi and Dr. Wyatt Murphy for reading and reviewing my dissertation. Thanks to Seton Hall University and the Department of Chemistry and Biochemistry faculty for teaching me great science in classes and providing additional feedback of my research, especially during our Petersheim Expositions. I would also like to thank Dr. Alan Blake, for his support of my studies and helpful discussions of my research work. Thanks to Dr. Nicholas Snow for always supporting my research and showing me how to become a leader. Thank you Ms. Maureen Grutt for making the impossible, possible, and helping me through difficult times.

During my Ph.D. I have experienced many challenges that have allowed me to mature as a scientist and human being. I'm especially grateful to our collaborators, for easing the scientific challenges while allowing me to expand my expertise. I gained additional knowledge of the material sciences in collaboration with Dr. Uri Samuni at Queens College, NY. I would like to thank Dr. Reeta Yadav and Ph.D. student Suiying Huang for helping me to obtain TEM and DLS data. Also, I am greatly indebted to Dr. Gabriela Chiosis at Memorial Sloan Kettering in NY, for offering all of the resources needed for the biological testing of my samples. My heartfelt thanks to Dr. John Koren for teaching me all molecular biology techniques.

I want to mention how lucky I was for being a part of Club 419. I thank, Mariana, Niki, Steve, Chris, Sunil, Gia, Erik for being part of my life, I consider you guys a family away from my home. I enjoyed each and every moment I spent in and outside of the lab with my group members that I also consider dear friends. I thank you all for the moral and emotional support. A special thanks is also extended to Anthony for introducing the RNA synthesis techniques, Steve for helping me synthesize RNA for my studies and Chris for assisting with the solution phase chemistry. I would also like to thank my morning coffee group; Pradeep, Emi, Lauren, Niki, andMariana for all the good times we shared together.

Thanks to my friends and family for all your support. I am very grateful to my uncle Vipin Patel whom I consider my god father for supporting me financially and emotionally. I appreciate my family for all their sacrifices so I can go abroad and pursue all my dreams. I don't have any words that can justly thank a great guy, my father Ravikant. I am what I am today because you believed in me, that I can conquer any obstacles in my path. Thanks to my mom Dharmistaben and my sisters Urja and Nehal for their love and support, you guys made me a better person. Thanks to my beautiful wife Mandakini for all sacrifices you made so I can focus on to my studies and all of your love and support.

I apologize to anyone I have unintentionally forgotten, or anything people have helped me with that I haven't properly acknowledged. To all of you, I sincerely thank you.

TABLE OF CONTENTS

CHAPTER 3: RNAi NANOTECHNOLOGY: APPLICATIONS OF siRNA NANOSTRUCTURES IN RNAi SCREENING AND CANCER GENE THERAPY

LIST OF FIGURES

CHAPTER 1

CHAPTER 2

CHAPTER 3

LIST of TABLES

CHAPTER 1

CHAPTER 2

CHAPTER 3

LIST OF SCHEMES

CHAPTER 2

ABBREVIATIONS AND SYMBOLS

%H	% hyperchromicity
®	registered
µmol/g	micro mole per gram
ºC	degree Celsius
©	copyright
Å	Angstrom
™	Trade Mark
ε	molar absorptivity
π	pi
A	Adenosine
A_{260} or Abs	UV absorbance measure at 260 nm
Ade	Adenine
AE	Anion Exchange
Ago2	Argonaute 2 complex
AKT	Protein kinase-B (PKB)
ATF6	Activating transcription factor 6
ATP	Adenosine triphosphate
BIK	BCL-2 interacting killer
BIM	Bcl-2-like protein 11
BuOH	butanol
C	cytosine
CD	circular dichroism

CEM	2’-cyanoethoxymethyl
CHOP	DNA-damage inducible transcript 3
CNET	cyanoethyl
CPG	controlled pore glass
Cyt	cytosine
DCA	dichloroacetic acid
DCM	dichloromethane
DLS	dynamic light scattering
DMEM	Dulbecco’s modified eagle’s medium
DMSO	dimethylsulfoxide
DMT	dimethyltrityl
DNA	deoxyribonucleic acid
e.g	for example
EDTA	ethylenediaminetetraacetic acid
EGFR	Epidermal growth factor receptor
eIF2α	Eukaryotic initiation factor 2 alpha
ER	endoplasmic reticulum
ESI-MS	electrospray ionization mass spectrometry
EtOH	ethanol
ETT	ethylthiotetrazole
FBS	fetal bovine serum
FDA	Food and Drug Administration
G	guanosine

GFP	Green fluorescent protein
GRP75	Glucose regulated protein 75 kDa
GRP78	Glucose regulated protein 78 kDa
GRP94	Glucose regulated protein 94 kDa
Gua	guanine
HCl	hydrochloric acid
HER-2	Human epidermal growth factor receptor-2
HSP	Heat shock protein
HSP70	Heat shock protein 70 kDa
INF	interferon
IP-RP-HPLC	ion-pairing reverse phase high resolution liquid chromatography
IRE1	Inositol requiring enzyme 1
LC/MS	liquid chromatography/ mass spectrometry
LCAA	long chain alkyl amine
Lv	levulinyl
m/z	mass per charge ratio
MALDI-TOF	matrix assisted laser desorption/ionization time of flight
Me	2’-methyl
MeCN	acetonitrile
$MgCl_2$	magnesium chloride
Min	minute
miRNA	microRNA
MOE	2’-methyloxyethyl

mRNA	messenger RNA
MS	mass spectrometry
Na_2HPO_4	sodium phosphate monobasic
N-Ac	N-Acetyl
NaCl	sodium chloride
NaOAc	sodium acetate
N-Bz	N-Benzoyl
NH_4OH	ammonium hydroxide
N-iBu	N-isobutyl
O.D.	optical density
O-Me	2'-O-methyl
P.G	protecting group
PAGE	polyacrylamide gel electrophoresis
PBS	phosphate buffered saline
PDT	photodynamic therapy
PERK	Protein kinase like ER kinase
PI3K	Phosphatidylinositide-3-kinase
PLGA	Poly(lactic-co-glycolic acid)
pmol	pico mole
PVDF	polyvinyldifluoride
RISC	Ribosomal initiation silencing complex
RNA	ribonucleic acid
RNase	Ribonucleases

rU	ribouridine and branchpoint unit V- and Y-shape RNA
shRNA	short hairpin RNA
siRNA	short interfering RNA
TBDMS	2’-tert-butyldimethysilane
TBE	tris borate EDITA buffer
TEA	triethylamine
TEAA	triethylammonium acetate
TEM	transmission electron microscope
tRNA	transfer RNA
TLR	toll like receptor
Tm	thermal melts
TNF	Tumor necrosis factor
TEA·3HF	trimethylamine trihydrofluoride
TRIS	tris(hydroxymethyl)aminomethane
U	uridine
UPR	unfolded protein response
Ura	uracil
UV	ultra-violet
VEGF	Vascular endothelial growth factor
Vis	visible
Vs.	Versus

CHAPTER 1: INTRODUCTION OF RNA SELF-ASSEMBLY AND ITS APPLICATIONS IN CANCER RESEARCH

1.1 Discovery of RNA Self-assembly

One of the biggest questions in science is based on the evolution of life on earth, dating back to the pre-biotic world that existed on early Earth. Many speculations and conspiracy theories that were later proved and disproved by ground breaking research provided an answer to the question of whether life originated from RNA or its close relative DNA? Studies on the origin of the world have shown that DNA and RNA might have evolved from nucleic acid building blocks which may have self-assembled into structures that represents the starting point of the 'RNA World' hypothesis. In this model, RNA was found to be the original scaffold for storing and expressing genetic information into the evolution of life on earth.[1] Through evolutionary changes, DNA synthesized by polymerases adopted the function as the carrier of genetic information in cells due to its more stable structure relative to RNA. The transcription of mRNA described a new role for RNA, as an intermediary molecule in between DNA and protein expression. Moreover, the creation of polypeptides or proteins by the translational machinery produced new RNAs with novel self-assembled architectures and functions inside the cell. These actions have been engineered in the laboratory in an effort to mimic the multiple structures and functions of RNA inside cells. For example, *in vitro* engineering of RNAs has led to the development of diverse RNAs with varied functions such as transcription, translation, degradation, maturation, and the catalytic activity related to the regulation of cellular bio-systems.[2] Thus technological advancements in RNA synthesis and engineering has led to the development of a wide range of synthetic RNAs for their growing applications in biology, biotechnology and medicine.[3]

Furthermore, RNAs are formulated with a wide range of carriers that contributes towards their fruitful applications.[4]

The varied sequences and self-assembled structures are key to the versatile functions RNA can adopt in cells and *in vivo*. Generally, RNA can be divided into three functional motifs, RNA can function as its primary sequence, as well as within its secondary and tertiary structures (**Figure 1.1**). The primary sequence of RNA is formed by covalent phosphodiester bonding while the secondary and tertiary structures are due to non-covalent Watson-Crick base pairing or hydrogen-bonding (H-bonding) and pi-stacking interactions (**Figure 1.1(A, B, C)**).[7,8] These RNA sequences and structures participate in many specific biological functions, such as those performed by messenger RNA (mRNA), ribosomal RNA (rRNA), transfer RNA (tRNA), micro RNA (miRNA), short-interfering RNA (siRNA), small nuclear RNA (snRNA) and many others.[5,9,10] The linear single stranded mRNA sequence functions as a carrier of genetic information, and serves as a template for protein synthesis with the use of additional RNAs that form part of the protein translational machinery. These include the secondary RNA self-assembled structures, tRNA, which adopts a series of stems and loops in a structure formulation that facilitates amino acid loading and transfer to the growing polypeptide. The tRNA forms part of the functional tertiary RNA structures, strongly associated with the ribosome and forming part of the catalytic RNA-protein complex for polypeptide synthesis (**Figure 1.1E**).[11] In a different application, the self-assembled miRNA and siRNA function to regulate gene expression for important applications in biotechnology and in medicine.[6] This new RNA application is supported by the fact that while less than 2% of the information stored in the entire human genome is designated for protein coding, more than 80% is transcribed into RNAs with still unspecified functions.[12] RNA structural motifs are routinely used as modules in a variety of combinations to code for distinctive and specialized

architectures that enable specific operations such as intermolecular recognition, catalytic, or mechanical functions. RNA thus provides functional self-assemblies for applications in nanotechnology. [7,13-17]

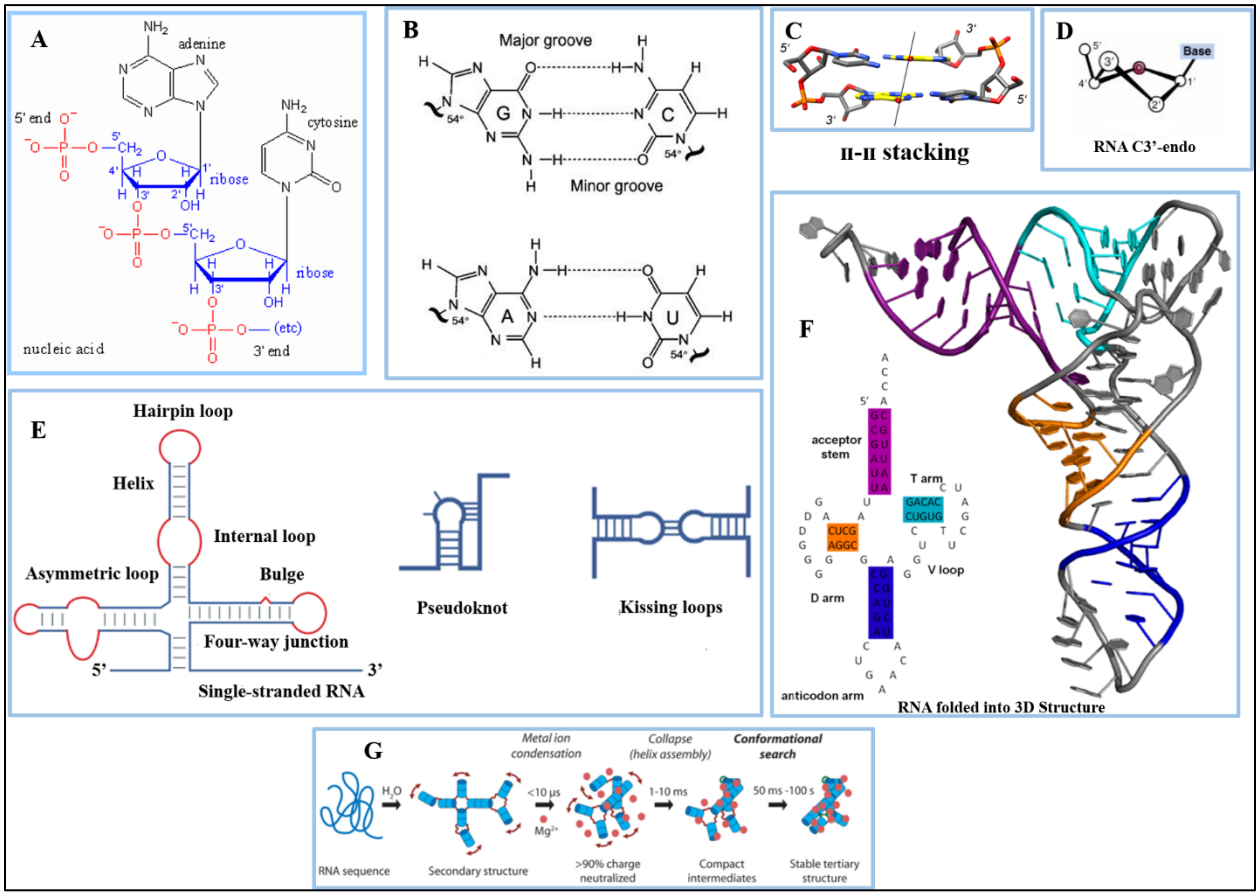

Figure 1.1 RNA primary, secondary and tertiary bonding interactions. (**A**) The primary bond formed by covalent phosphodiester linkage between two RNA nucleotides. (**B**) Watson-Crick hydrogen bonding interaction between RNA nucleosides to form RNA secondary and tertiary structures. (**C**) The π- π base stacking interaction for RNA stable A-type helix formation. (**D**) RNA pucker confirmation. (**E**) Various secondary RNA motifs. (**F**) Secondary and tertiary helical structure of tRNA demonstrating coaxial stacking and bonding interaction. (**G**) Effect of salt on stable RNA tertiary structure formation.

1.2 Methods of RNA Self-assembly

Over the past two decades, advances in RNA structural biology have improved our understanding of the structures and folding properties of naturally occurring self-folding RNAs. RNA self-assembly has led to functional RNAs, including RNA catalysts (ribozymes and ribosomes)[1,2], RNA receptors (riboswitches), and RNA adaptors (tRNA)[2,3]. The accumulation of knowledge regarding the modularity of RNA architectures also facilitates the number of small RNA modules (RNA motifs) that were used for the bottom-up design of artificial RNA structures (**Figure 1.2**). The architectural potential of RNA relies on the ability of a single RNA strand to fold into a stable 3D self-assembled structure. Incorporating functional and structural elements that could potentially allow the construction of complicated RNA nanomachines is a critical requirement for their technological and medical applications. From a structural point of view, the 2'-OH group in RNA locks the ribose sugar into a C3'-endo chair conformation (**Figure 1.1D**) facilitating the formation of the A-form RNA double helix, which is about 20% shorter and wider than B-form DNA.[4] Moreover, the presence of special structural motifs such as bends, stacks, junctions, loops and chelates with the presence of metal ions, such as Mg^{2+}, further improves the stability and functional utilities of the 3D RNA structures (**Figure 1.1G**).[18-24] Such inspirational functional architectures of RNA have ushered in a new era of artificial RNA nanotechnology for its applications in the medical as well as the material sciences.

Within the realm of RNA self-assembly methods there are two main strategies, template and non-template self-assembly. Templated assembly involves the interaction of RNA molecules under the influence of specific external sequences, forces, or spatial constraints. In contrast, non-templated assembly involves the formation of larger structures by individual components without the influence of external forces. Examples of non-template assembly are related to the ligation,

chemical conjugation, covalent linkage, and loop/loop interactions of RNA, especially in the formation of RNA multimeric complexes.[26-30] Within the context of this thesis, a templated self-assembly strategy will be discussed. In this application, a single stranded RNA functions as a template for the self-assembly of RNA hybrids that may lead to the generation of synthetic artificial nanoarchitectures.[22,24,30,31,40,42,56,65,70] There are four distinct methods for the templated assembly of RNAs, these include: (1) RNA architectonics, (2) single-strand RNA assembly, (3) RNA/DNA hybrid self-assembly, and (4) co-transcriptional assembly (**Figure 1.2**).

The concept of RNA tectonics was initially defined as RNA structures that can be decomposed and reassembled into new modular RNAs, called RNA tectonics (tectoRNAs).[25] This strategy recognizes the essential structural components of each RNA strand associated within its 3D shape. Furthermore, computer assisted 3D design provides a limitless number of self-assembling RNA units forming synthetic RNA nanostructures that can be generated through a tetraloop-receptor interactions and stable hairpin loop-loop dimerization.[16,26,31-34] The predefined/preorganized artificial RNA nanostructures can be self-assembled by taking advantage of thermodynamically stable motifs participating in the canonical Watson-Crick and non-canonical base pairing interactions. The shape and makeup of the RNA tectonics have resulted in 120° kissing loop motifs found in hexagonal nanorings and HIV kissing loops that resulted in the assembly of RNA tectosquares.[31,32,35] This strategy has also been applied in the library assembly of fibers,[36-38] triangles,[39-41] squares,[31,32,42] hexagons,[38,43] polyhedrons,[32,35,71] closed-ring structures[66] and 2D array[31,32,40] nanostructures. Thus, RNA tectonics offers the possibility of designing structurally complex architectures mimicking large naturally occurring RNA nanomachines.

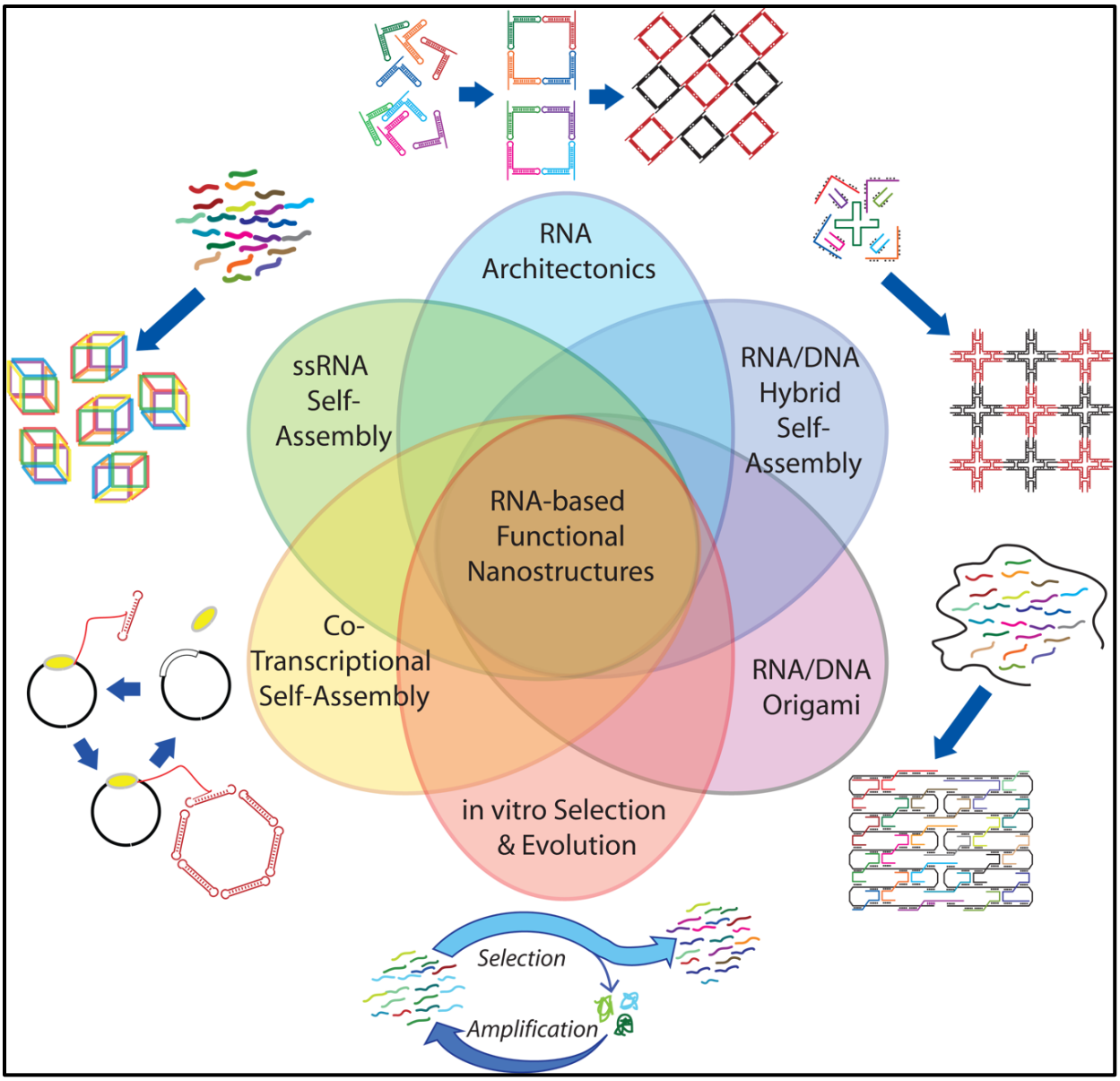

Figure 1.2. Self-assembly strategies and other principles governing the design of RNA-based functional nanostructures. Grabow, W.W.; Jaeger, L. *Acc. Chem. Res.* **2014**, *47*, 1871-1880.

Single strand RNA (ssRNA) assembly in contrast to RNA architectonics relies on complementary RNA strands that are unstructured by themselves but when mixed together are able to assemble through Watson Crick base pairs. Using base-pairing hybridization properties, RNA can also form nanostructures with elementary secondary structure motifs including crossover Holiday junctions.[39,44-48] Single stranded RNA can be used in conjunction with other strategies to promote programmed assembly of RNA units through complementary tail-tail interactions.[31,32,35,39,47,49] Although, this strategy is limited by mismatches in between bases, which can be addressed by computation-based complementary sequence optimization studies.[44,46] Moreover, self-complementarity or systematic repeats can be introduced to form naturally occurring nanostructures such as the DsrA and GcvB type arrays in cells.[50-53] In a more recent study, structurally well-defined RNA tiles by integrating a 90° bend of RNA and artificially designed T-junctions have been formed. Sufficient rigidity of the RNA tiles favored homo-oligomerization into a large and uniform RNA architecture, an octameric cube.[65] Another approach can be amenable to single stranded self-assembly with the use of hundreds of short (32-nucleotide) modular "bricks" (**Figure 1.3**).[53]

The unique properties of RNA and DNA can be integrated for the self-assembly of RNA-DNA hybrid nanostructures. Conventional Watson Crick base-pairing between RNA and DNA readily form helices resulting in a structural bias for the A-type helix. For example, RNA-DNA hybrids equipped with a toehold for selective strand displacement allowed the formation of functional RNA moieties.[54,55] Other examples include the formation of nucleic acid nanoparticles as a result of double stranded RNAs (pre-siRNAs) functionalized using DNA self-assembly with complementary sticky tails.[46,56] Crossover techniques have been developed for the self-assembly of large nucleic acid architectures using hundreds of DNA staples to fold long RNA templates into

simple shapes, such as ribbons, rectangles, triangles, and RNA templated square tiles. In this manner, a self-assembled RNA-DNA hybrid can be used to create well-programmed, stable RNA nanostructures having multi-functional utility in the materials and medical sciences.[57-60,67]

The ability of RNA to produce kinetically controlled self-assemblies using the endogenous transcription machinery has gained widespread attraction in the formation of bio-synthetic RNA nanostructures by coupling RNA synthesis with RNA self-assembly *in-vitro* or *in-vivo*.[61,46,52,62] For example, the RNA nanorings employed RNA tectonics and co-transcriptional self-assembly,[61,62] while the RNA nanocubes,[46,64] and organelle-like RNA[52] scaffolds were generated from the co-transcriptional assembly of single-stranded RNA. In addition, rolling circle transcription is a distinctive co-transcriptional strategy to form long RNAs (RNA microsponges) with periodic repeats resulting in lamellar-like structures.[63] On the other hand, RNA polymerization enables the construction of complex structures at relatively low cost. For example, a transcriptional method has been used to synthesize a long RNA strand which folded into RNA nanostructures.[68,69] Moreover, RNA polymerases have also been implicated in the self-assembly of RNA particles for efficient cellular uptake and biological activity.[70]

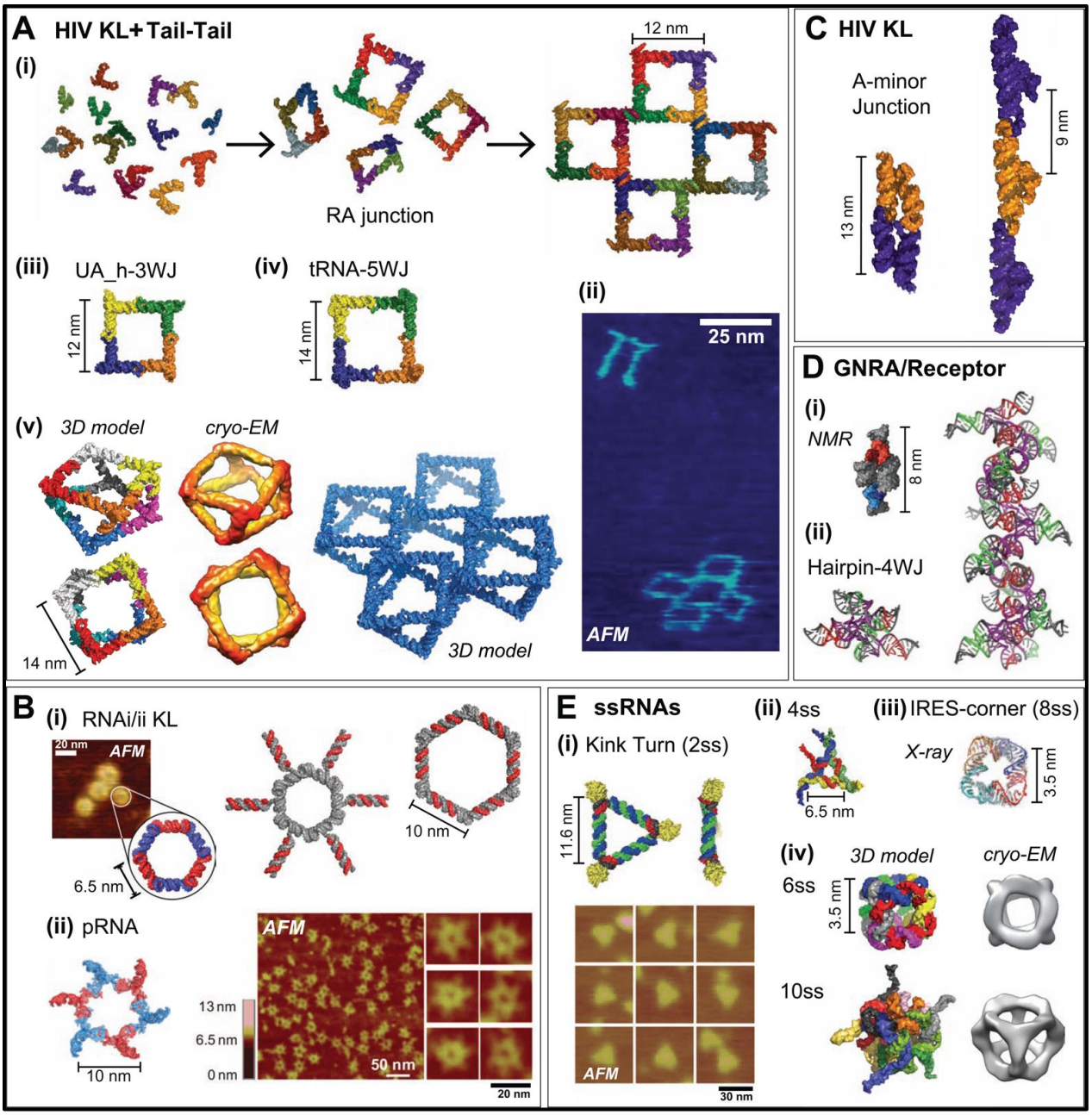

Figure 1.3. RNA nanostructures constructed using various RNA self-assembly strategies. (A) Several tertiary interactions directing a 90° bend between adjoining helices have been used to generate (i–iv) tectosquares[31, 32] and (v) antiprism shaped polyhedrons[35] including (i, ii) the right angle (RA), (iii) UA_h3WJ,[31] and (iv, v) tRNA-5WJ[31,35] motifs [parts i, ii reproduced from: Chworos, A.; Severcan, I.; Koyfman, A.Y.; Weinkam, P.; Oroudjey, E.; Hansma, H.G.; Jaeger, L. *Science* **2004**, *306*, 2068-2072.; parts iii, iv reproduced from: Severcan, L.; Geary, C.; Verzemnieks, E.; Chworos. A.; Jaeger, L. *Nano Lett.* **2009**, *9*, 1270-1277.; part v reproduced from: Severcan, I.; Geary, C.; Chworos, A.; Voss, N.; Jacoverry, E.; Jaeger, L. *Nat. Chem.* **2010**, *2*, 772-779. (B) Hexagonal nanoparticles[38,43] built from the (i) RNAI/IIi kissing loop[38] and (ii) the pRNA[43]

[part i reproduced from: Grabow, W. W.; Zakrevsky, P.; Afonin, K.A.; Chworos, A.; Shapiro, B.A.; Jaeger, L. *Nano Lett.* **2011**, *11*, 878-887.; part ii reproduced from: Zhang, H.; Endrizzi, J.A.; Shu, Y.; Haque, F.; Sauter, C.; Shlyakhtenki, L.S.; Lyubchenko, Y.; Guo, P.; Chi, Y.I. *RNA* **2013**, *19*, 1226-1237.] (C) RNA particles and fibers incorporating the HIV KL and A-minor Junction [reproduced from: Geary, C.; Chworos, A.; Jaeger, L. *Nucleic Acids Res*. **2011**, *39*, 1066-1080.] (D) Particles (i) and fibers (ii) using GNRA loop-receptor tectoRNAs [reproduced from: Nasalean, L.; Baudrey, S.; Leontis, N.B.; Jaeger, L. *Nucleic Acids Res*. **2006**, *34*, 1381-1392.] (E) RNA nanoparticles built using the ssRNA strategy: (i) Kink Turn triangle based on two single strands (ss) assembling with a protein [reproduced from: Ohno, H.; Kobayashi, T.; Kabata, R.; Endo, K.; Iwasa, T.; Yoshimura, S.H.; Takeyasu, K.; Inoue, T.; Saito, H. *Nat. Nanotechnol*. **2011**, *6*, 116-120.]; (ii) 4ss triangle [reproduced from: Bindewald, E.; Afonin, K.; Jaeger, L.; Shapiro, B.A. *ACS Nano* **2011**, *5*, 9542-9551.]; (iii) IRES nanosquare based on 8ss [reproduced from: Dibrov, S.M.; McLean, J.; Parsons, J.; Hermann, T. *Proc. Natl. Acad. Sci. USA* **2011**, *108*, 6405-6408.]; (iv) RNA nanocubes based on 6ss and 10ss [reproduced from: Afonin, K.A.; Bindewald, E.; Yaghoubian, A.J.; Voss, N.; Jacovetty, E.; Shapiro, B.A.; Jaeger, L. *Nat. Nanotechnol*. **2010**, *5*, 676-682.]. Nanostructures have been characterized by atomic force microscopy (AFM), cryo-electron microscopy (cryo-EM), NMR, or crystallography (X-ray) as indicated.[26,31,36]

1.3 Application of RNA Self-assemblies in Cancer Gene Therapy

Decoding the human genome has revealed that a substantial part (~98.5%) of our genetic make-up, the so called "junk" DNA, transcribes noncoding RNAs.[72] The noncoding RNAs do not express proteins but have been utilized for nanotechnology-based RNA gene therapy. These important bio-medical applications includes the use of small interfering RNA (siRNA), micro RNA (miRNA) and antisense RNA for the RNAi based mechanism of gene regulation.[153] Moreover, the catalytic RNAs ribozymes, have also been implemented for catalytic gene regulation.[1,2] The selective ligand binding RNAs, the RNA aptamers have been evolved for the detection of cancers. RNA nanotechnology has revolutionized the use of these therapeutic RNAs for the detection and therapy (theranostic) applications of cancer.[73]

Cancer gene therapy represents one of the most rapidly developing areas in preclinical and clinical cancer research. Viral vectors have been used as primary means to deliver genes to target cancer cells, although risks associated with toxicity, target specificity, immune and inflammatory responses have limited their clinical utility.[74] To address the limitations of viral gene transduction methods, liposome,[75] dendrimers,[76,99,100] carbon nanotubes,[77] synthetic polymers,[78] and gold nanoparticles[79] have been successfully implemented in gene delivery applications. Current advances in cancer gene therapy using multivalent RNA nanoparticles have shown promises to combat cancer using siRNA, miRNA, aptamer and with drugs by various methods such as conjugation and encapsulation.[15,82-85] Hence, RNA nanotechnology allows the self-assembly of multifunctional RNA motifs that may be administered into specific cells or tissues for targeted cancer therapy. Since the discovery of RNA interference (RNAi)[86] based therapy, siRNA, miRNA and shRNA have gained attention in the down-regulation of oncogenic protein expression which leads to cancer cell death.[87]

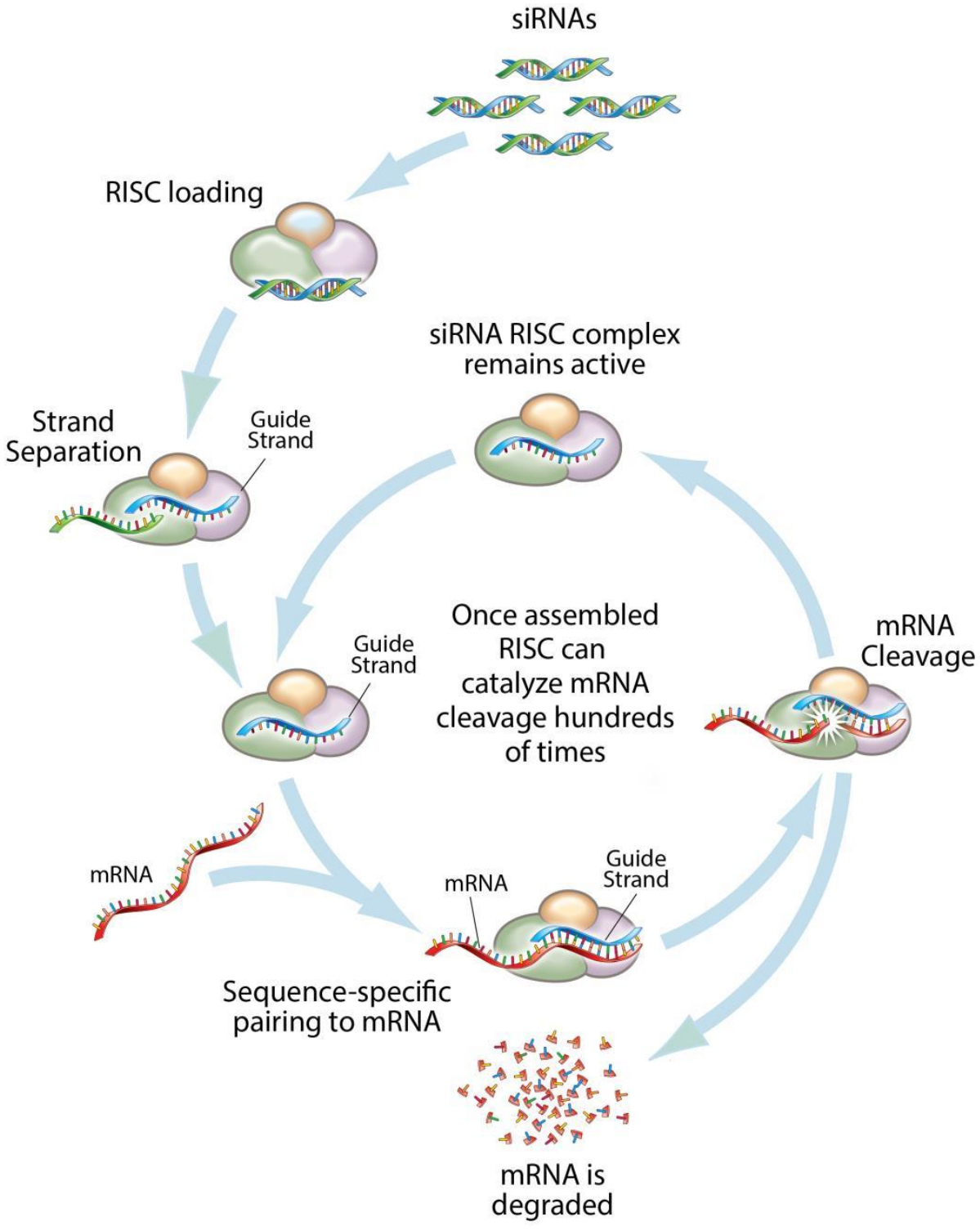

Figure 1.4 Schematic representation of siRNA mediated gene silencing via RNAi mechanism. Figure adapted from arrowheadpharma.com/science.

The RNAi mechanism applied to cancer gene therapy invokes the use of short, non-coding RNA hybrids (siRNA/miRNA/shRNA) that have the ability to act as substrates for the RNA Induced Silencing Complex (RISC). When bound to RISC, the RNAs are processed into the linear antisense RNA sequences by the nuclease activity of the Argonaute enzyme. This linear RNA functions as a template for the hybridization of the targeted oncogenic mRNA that is subsequently hydrolyzed leading to the inhibition of cancer cell proteins that ultimately lead to cancer cell death (**Figure 1.4**).[85-87] This mechanism has led to the development of a wide range of RNA-drug candidates for cancer gene therapy applications. The majority of RNAi based drugs are composed of multiple siRNA sequences or self-assemblies that can target a single or multiple oncogenic mRNAs for potent cancer gene therapy effects. (**Table 1.1**) Thus, siRNA have been formulated into potential cancer drug candidates due to their ability to specifically target oncogenic mRNA sequences and silence their protein expression which compromises cancer cell viability.[88-92]

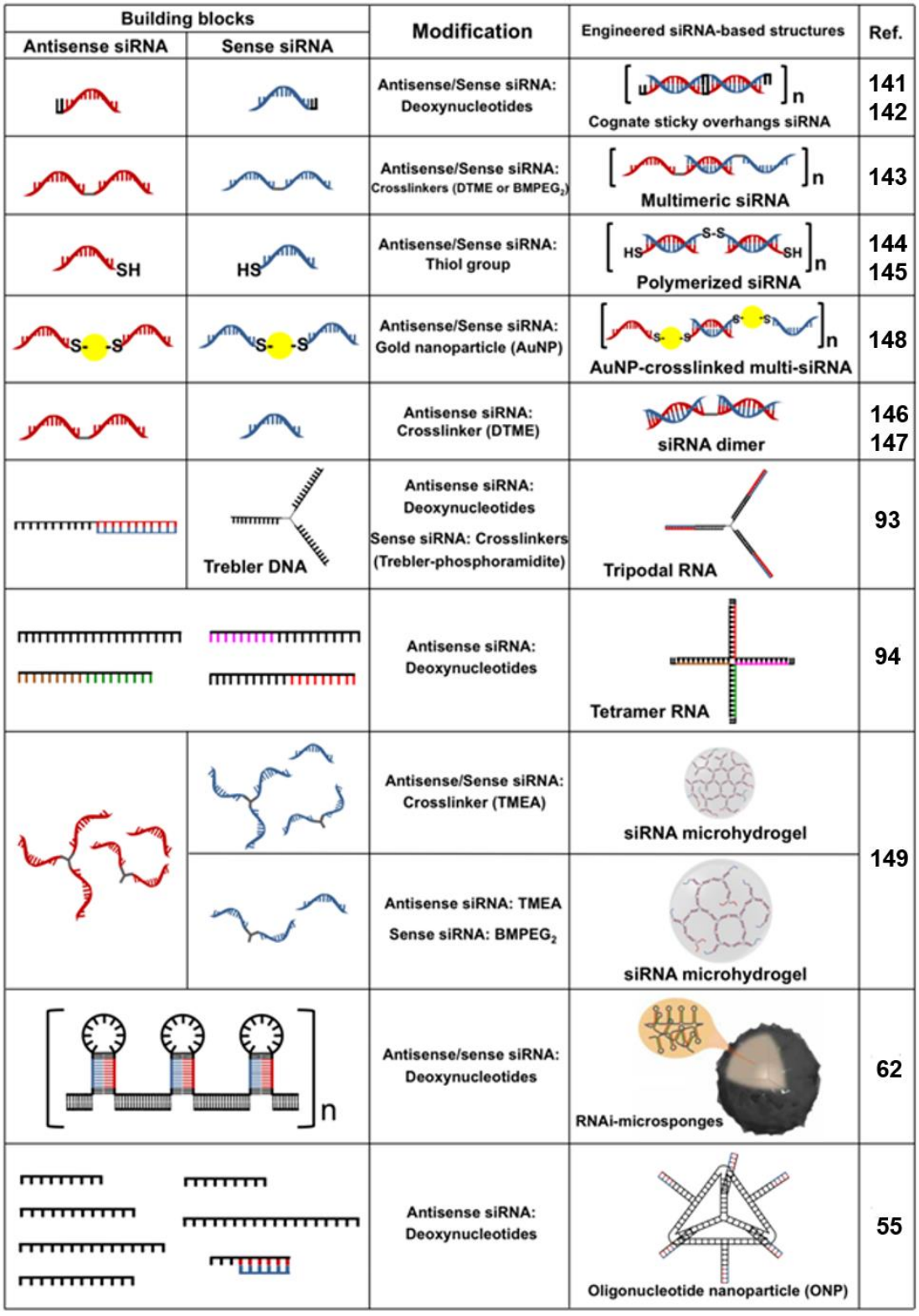

Figure 1.5 siRNA hybrid structures for RNAi activity. Figure has been adapted from: Hong, C.A.; Nam, Y.S. *Theranostics*, **2014**, *4*, 1211-1232.

To date, many RNA nanostructures have been designed to include: 1) identical siRNAs targeting the same gene locus; 2) different siRNAs targeting different loci on a single gene; 3) different siRNAs targeting different genes, thereby modulating multiple cell signaling pathways that generate synergistic or additive responses.[93,94] The design and delivery of multiple siRNA units for cancer gene therapy has been extensively studied by combining two,[95,96] three,[97] four,[97,98] and six[94,56] siRNAs by template-assisted hybridization into siRNA nanostructures. The design of siRNA nano-assemblies requires: 1) optimal siRNA sequence length (19-25 nucleotides with 2-nucleotide 3'-end overhangs); and 2) siRNA sequence prediction by computer generated softwares to prevent off-target mRNA silencing effects. After carefully designing the siRNA antisense and sense sequences, the functionalization of RNA into nanoparticle/nanostructure formulations requires minimal design steps to prevent any mis-folding of RNA scaffold strands. Additional examples of self-assembled RNA nanostructures applied to gene silencing include, the dumbbell-shaped nanocircular RNAs that have been designed to induce the RNAi. This effect was triggered by the Dicer enzyme cleaving activity of long non-coding RNA into active siRNAs for potent and long lasting RNAi activity.[100-102] Recently, branched RNA, called trimer or tetramer RNA, was also adopted to trigger the RNAi response and prolong the gene silencing activity by sterically shielding the siRNA from nucleases .[96,97] Chimeric DNA/RNA and RNA/pRNA oligomers were made and assembled into genetically encoded siRNA dendrimers.[76,98,99]

The nanoring shaped tectoRNAs have also been self-assembled for the efficient delivery of siRNAs that have shown resistance to exonucleases.[38,100] Furthermore, by exploiting the physical properties of siRNA structure formation, a sponge-like spherical structure referred to as an siRNA nano-sheet was synthesized by rolling circle transcription (RCT) and effectively processed by Dicer producing multiple siRNA precursors for gene silencing activity.[103] Another

example involves chimeric DNA/RNA self-assemblies, which employed a tetrahedral DNA template carrying six siRNAs. Imaging of the nanoparticles illustrated a DNA tetrahedral scaffold that positioned six siRNAs as 3' overhangs.[94]

1.4 Challenges, Solutions and Applications of siRNA Nanoparticles in Cancer Gene Therapy

A number of promising results suggests a great potential of siRNA nanostructures and assemblies in cancer treatment. However, a series of challenges remain and limit the full potential of translating the siRNA application into the clinic, and most siRNA drug delivery systems are still in preclinical studies. The existing barriers for the successful application of siRNAs in clinical cancer therapy includes; nuclease instability which results in short half-lives, limited cell uptake that restricts intracellular resident time for potent knockdown effects, off-target gene knockdown which leads to toxicity, early/late endosomal escape which restricts therapeutic efficacy, in addition to rapid, renal clearance and activation of innate immune responses which limits the pharmacological potential of the therapeutic siRNAs. Therefore, siRNA-based cancer gene therapy requires the careful design of therapeutics that may overcome these extra- and intra-cellular barriers and lead to their safe and effective administration for potent therapeutic activity (**Figure 1.6**).

As mentioned above, the design and chemical modification of siRNAs is an essential requirement for improving cancer gene therapy applications. Chemical modifications allows siRNAs to acquire serum stability and prolong their biological activity, while limiting the immune response which typically hinders siRNA access to the RNAi machinery.[154] Chemical modifications can be introduced at the 5' or 3' termini of the RNA oligonucleotides, but they may also effect the phosphodiester backbone, the ribo-sugar or nucleobase. The most common and essential siRNA

modifications alter the 2'-OH of the ribose sugar in order to prevent its involvement in RNA strand isomerization and degradation during acid, base or enzyme catalyzed hydrolysis.[155] The 2'-*O*-methyl (2'-OMe) and 2'-deoxy-2'-fluoro (2'-F) are the most acceptable and well tolerated modifications that have enhanced siRNA serum stability and increased their *in vivo* activity.[132] Other modifications include, backbone changes from the phosphodiester to phosphothioester or phosphothioate with and without 2' modifications.[132] Additionally, RNA cyclization has led to the generation of the locked nucleic acids (LNAs) that have shown enhanced nuclease stability and RNAi activity.[132] While other modifications such as boranophosphonate backbone modifications have improved nuclease stability but compromised RNAi activity. In order to enhance the RNAi activity, the siRNAs have been extended with 3'-overhang sequences by incorporating additional –AA or –UU nucleotides at the 3'-terminus. Currently the efficacy of siRNA is limited by its delivery methods, hence improvements in the specificity and efficacy of current delivery system is a necessary requirement for their clinical applications in cancer gene therapy. Advanced RNA nanotechnology can address this limitation by nanoparticle formulations that may potentiate the silencing of oncogenic mRNA.

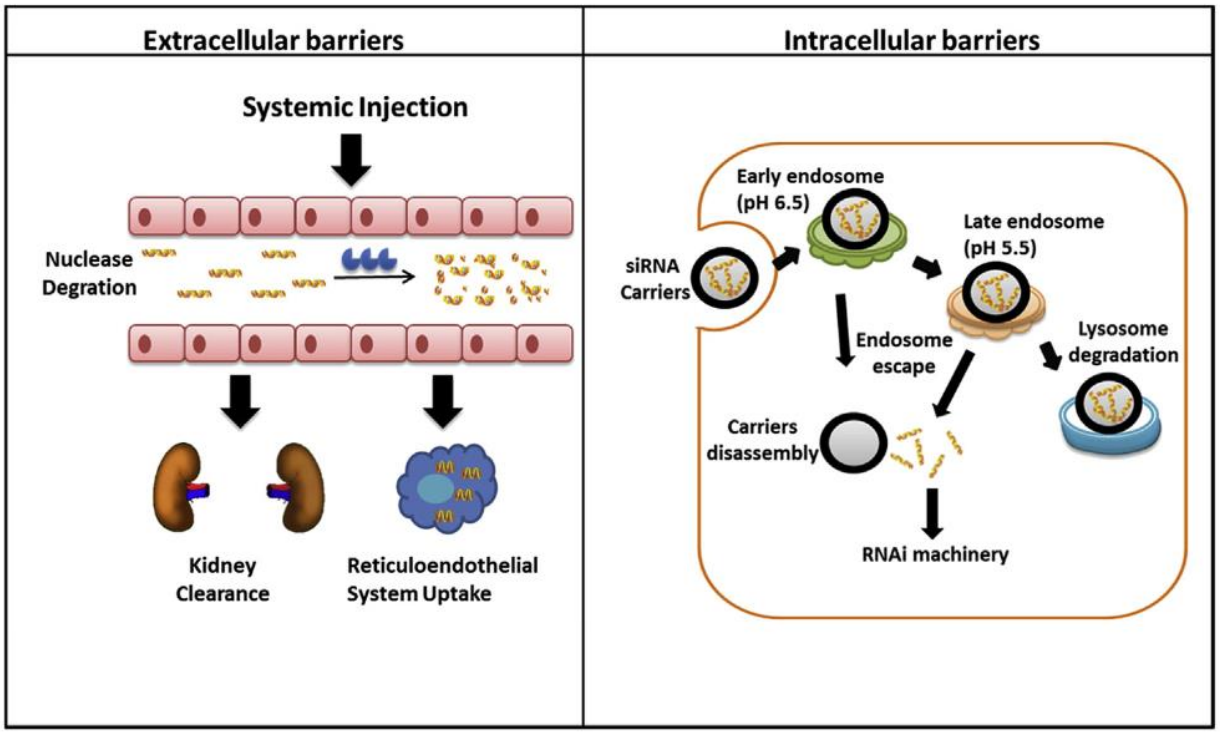

Figure 1.6 Barriers encountered by siRNA following their systemic administration. siRNA may be degraded in the blood or removed by renal excretion or macrophages. siRNAs may not reach their target cells because of electrostatic repulsions with the lipid bilayer. Once internalized, siRNAs may be prevented from reaching their intracellular targeted mRNA due to limited escape from the endosome-lysosome pathway. Figure has been adopted from: Liu, X.; Liu, C.; Laurini, E.; Posocco, P.; Pricl, S.; Qu, F. *Mol. Pharm*. **2012**, *9*, 470-481.

The encapsulation of siRNA within nanoparticles have shown improvements in shielding the siRNA from nucleases and immune responses while assisting in siRNA delivery. Furthermore ligand bound nanoparticles have been shown to increase the selectivity of siRNA delivery to tumor cells leading to the enhanced permeability and retention (EPR) effect.[105,106] For example, siRNA conjugation with drugs, cationic polymers and targeting ligands have demonstrated improved therapeutic utility by enhancing cell permeability and intracellular resident time which potentiates the RNAi response. Often, conjugated polymers are hydrophobic in nature which minimizes the water solubility of siRNAs thereby limiting their therapeutic potential.[156] Conjugation or

complexing of hydrophilic polymers with siRNA have been shown to significantly increase nanoparticle solubility, stability in biological media and increased oral absorption.[107-109] siRNA nanoparticles can be formed using biological additives, such as phospholipids[110] in addition to soft/organic and hard/inorganic materials (**Figure 1.7**).[118,119] Often cyclodextrins[114] and other synthetic polymers such as poly(lactic-co-glycolic acid) (PLGA)[113,115] (either degradable or non-degradable) with multiple copies of siRNA are formulated covalently or non-covalently into nanocarriers such as liposomes, nanoemulsions, and dendrimers that enhance siRNA compatibility and reduce cytotoxicity.[86,111,112] Several reviews have been published on the delivery of siRNA with a wide range of nano-carriers.[94,112,115-118] Thus, RNA nanotechnology has been widely applied for the therapeutic and diagnostic (theranostic) treatments of cancer.

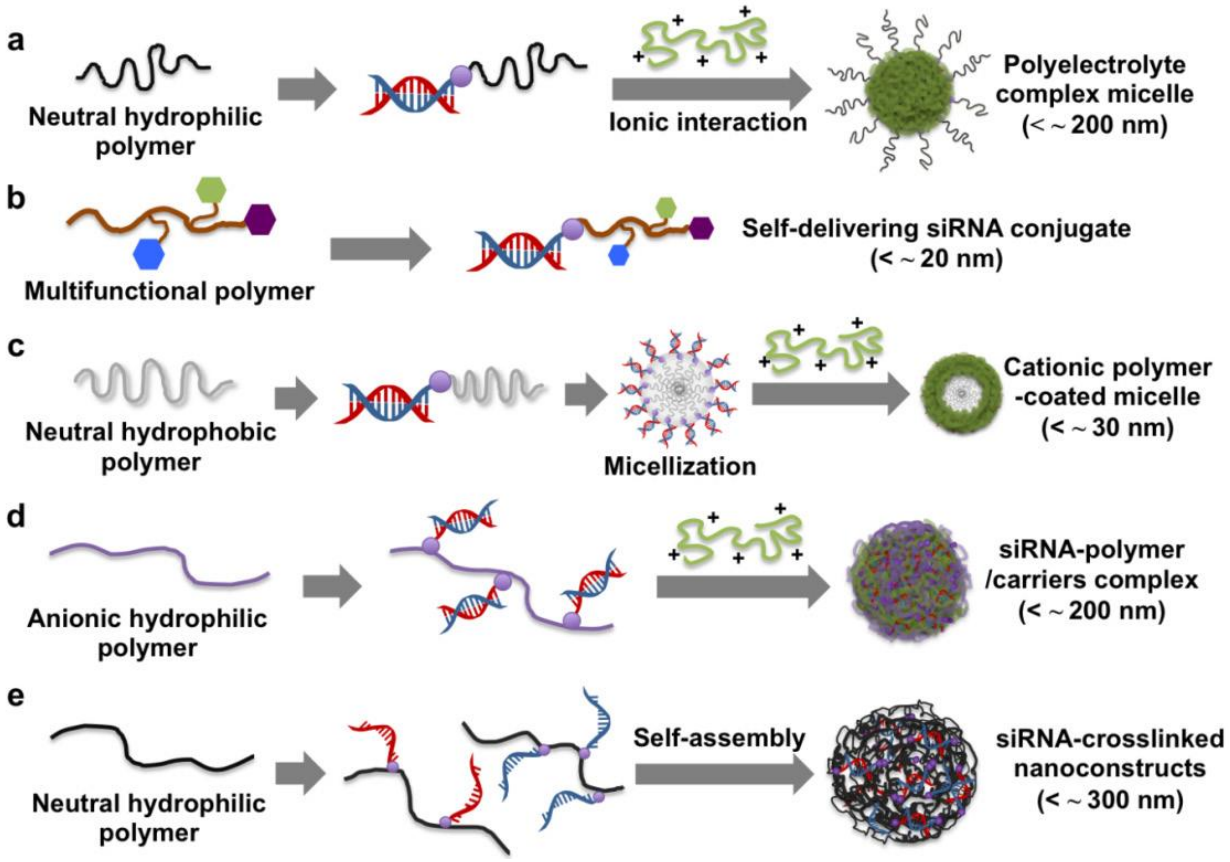

Figure 1.7. The various methods of siRNA formulation within a variety of nanoparticle formulations. Figure has been adapted from: Hong, C.A.; Nam, Y.S. *Theranostics*, **2014**, *4*, 1211-1232.

The shapes and sizes of RNA nanoparticles or nanostructures have also been shown to effect its activity *in vitro* and *in vivo*. For example, nanoparticle formulations of different sizes and shapes have led to different uptake capacities and half-lives within cells.[120-124] Particle sizes ranging from 20-120 nm are optimal because they limit elimination or destruction mechanisms and immunostimulatory reponses.[91,124,154]

Often endocytic pathways are dependent on the sizes of the endocytic vesicles. Gene transfection and tissue uptake can be well tolerated if the nanoparticle formulation is uniform and

less than 100 nm in size.[122,125,126] Surface characteristics of nanoparticles can also impact the internalization process via endocytosis or phagocytosis. More often, positive surface charged nanoparticles bind strongly to the anionic cell membrane facilitating a higher cellular uptake.[122,126] Considering the extracellular pH of tumors is slightly acidic (pH 6-7) while that of normal cells is about pH 7.6 the structural stability of the nanoparticle can be altered based on pH changes, allowing for the controlled disassembly of the nanoparticle and release of the siRNA within cancer cells.[127,128]

The tumor target specificity is another very crucial requirement to avoid off-target toxicity. Many studies have been accomplished by covalently and non-covalently conjugating siRNAs with targeting ligands such as folate,[56,30] proteins[113], antibody,[139] aptamers,[138] peptides[135-137] or with other polymer attached ligands[117,130,131,134,140,141]. Currently, many siRNA-based nanoassemblies targeting a variety of oncogenes against different cancer types are being evaluated in early-stage preclinical and clinical trials. The following table shows some of the ongoing clinical studies for siRNA based cancer gene therapy (**Table 1.1**). Thus, RNA nanoparticle formulations have gained widespread utility in pre-clinical and clinical cancer gene therapy.

Table 1.1. siRNA based drugs in the clinical trials.[a]

Table 1 RNAi based drugs in clinical trials.

Drug	Target	Delivery system	Administration route	Disease	Phase	Company	ClinicalTrials.gov identifier
TD101	K6a(N171K mutation)	Naked siRNA	Foot-pat injection	Pachyonychia Congenita	I	Pachyonychia Congenita Project	NCT00716014
AGN211745	VEGFR1	Naked siRNA	Single intravitreal injection	Age-Related Macular Degeneration, Choroidal Neovascularization	II	Allergan	NCT00363714
QPI-1007	CASP2	Naked siRNA	Single intravitreal injection	Optic Atrophy Non-arteritic Anterior Ischemic Optic Neuropathy	I	Quark Pharmaceuticals	NCT01064505
Bevasiranib	VEGF	Naked siRNA	Single intravitreal injection	Diabetic Macular Edema	II	Opko Health, Inc.	NCT00306904
SYL1001	TRPV1	Naked siRNA	Ocular topical administration	Ocular Pain, Dry Eye Syndrome	I, II	Sylentis, S.A.	NCT01776658
I5NP	p53	Naked siRNA	Intravenous injection	Injury of Kidney, Acute Renal Failure	I	Quark Pharmaceuticals	NCT00554359
SYL040012	ADRB2	Naked siRNA	Ophthalmic-drop administration	Glaucoma, Ocular Hypertension	I, II	Sylentis, S.A.	NCT01227291
ALN-RSV01	RSV nucleocapsid	Naked siRNA	Nebulization administration	Respiratory syncytial virus infections	II	Alnylam Pharmaceuticals	NCT00658086
PF-655	RTP801	Naked siRNA	Single intravitreal injection	Choroidal neovascularization, diabetic retinopathy, diabetic macular edema	II	Quark Pharmaceuticals	NCT01445899
siRNA-EphA2-DOPC	EphA2	LNP	Intravenous injection	Advanced Cancers	I	M.D. Anderson Cancer Center	NCT01591356
Atu027	PKN3	LNP	Intravenous injection	Advanced Solid Tumors	I	Silence Therapeutics GmbH	NCT00938574
PRO-040201	ApoB	LNP	Intravenous injection	Hypercholesterolemia	I	Tekmira Pharmaceuticals Corporation	NCT00927459
TKM-080301	PLK1	LNP	Hepatic intra-arterial administration	Multiple Cancers	I	National Cancer Institute (NCI)	NCT01437007
ALN-VSP02	KSP and VEGF	LNP	Intravenous injection	Solid tumors	I	Alnylam Pharmaceuticals	NCT01158079
TKM-100201	VP24, VP35, Zaire Ebola L-polymerase	LNP	Intravenous injection	Ebola-virus infection	I	Tekmira Pharmaceuticals	NCT01518881
ALN-PCS02	PCSK9	LNP	Intravenous injection	Hypercholesterolemia	I	Alnylam Pharmaceuticals	NCT01437059
ALN-TTR02	TTR	LNP	Intravenous injection	Transthyretin-mediated amyloidosis	II	Alnylam Pharmaceuticals	NCT01617967
CALAA-01	RRM2	Cyclodextrin NP	Intravenous injection	Cancer Solid Tumor	I	Calando Pharmaceuticals	NCT00689065
siG12D LODER	KRAS	LODER polymer	Intratumoral administration	Pancreatic Ductal Adenocarcinoma Pancreatic Cance	I	Silenseed Ltd	NCT01188785
RXi-109	CTGF	Self-delivering RNAi compound	Multiple intradermal administrations	Cicatrix scar prevention	I	RXi Pharmaceuticals	NCT01780077
ALN TTRsc	TTR	siRNA GalNAc conjugate	Subcutaneous injection	Transthyretin-mediated amyloidosis	I	Alnylam Pharmaceuticals	NCT01814839
ARC-520	Conserved regions of HBV	DPC	Intravenous injection	HBV	I	Arrowhead Research	NCT01872065

LNP, lipid nanoparticle; NP, nanoparticle; DPC, dynamic polyconjugate; VEGFR1, vascular endothelial growth factor receptor 1; CASP2, Caspase 2; TRPV1, transient receptor potential cation channel, subfamily V, member 1; PKN3, protein kinase N3; ApoB, apolipoprotein B; PLK1, polo-like kinase 1; PCSK9, Proprotein convertase subtilisin/kexin type 9; TTR, transthyretin; RRM2, ribonucleotide reductase M2; CTGF, connective tissue growth factor; HBV, hepatitis B virus.

[a]Data table adapted from ref 142. Xu, C.; Wang, J. *Asian J. Pharma. Sci.* **2015**, *1*, 1-12.

1.5 REFERENCES.

1) Joyce, G.F. *Annu. Rev. Biochem*. **2004**, *73*, 791-836.
2) Davidson, E.A; Ellington, A.D. *Trends Biotechnol*. **2005**, *23*, 109-112.
3) Famulok, M; Harting, J.S; Mayer, G. *Chem Rev.* **2007**, *107*, 3715-3743.
4) Keller, M. *J. Controlled Release* **2005**, *103*, 537-540.
5) a) Grabow, W.W.; Jaeger, L. *Acc. Chem. Res.* **2014**, *47*, 1872-1880.
   b) Wu, Q.; Huang, L.; Zhang, Y.; *Sci. China C. Life Sci*. **2009**, *52*, 232-244.
   c) Moore, P. B.; Steitz, T.A. *Cold Spring Harb. Perspect Biol*. **2011**, *3*, a003780.
   d) Cochrane, J.C.; Strobel, S.A. *Acc. Chem. Res.* **2008**, *41*, 1027- 1035.
   e) Baird, N.J.; Fang, X.W.; Srividya, N.; Pan, T.; Sosnick, T.R. *Q. Rev. Biophys.* **2007**, *40*, 113-161.
   f) Doherty, E.A.; Doudna, J.A. *Annu. Rev. Biophys. Biomol. Struct*. **2001**, *30*, 457-475.
6) a) Jaeger, L.; Chworos, A. *Curr. Opin. Struct. Biol.* **2006**, *16*, 531-543.
   b) Krishnan, Y.; Bathe, M. *Trends Cell Biol.* **2012**, *22*, 624-633.
7) Schroeder, R.; Barta, A.; Semrad, K. *Nat. Rev. Mol. Cell Biol*. **2004**, *5*, 908-919.
8) Lescoute, A.; Westhof, E. *Nucleic Acids Res.* **2006**, *34*, 6587-6604.
9) Collins, L.J.; Penny, D. *Trends Genet.* **2009**, *25*, 120-128.
10) St Laurent, G.; Savva, Y.A. *Front. Genet*. **2012**, *3*, 57-64.
11) Batey, T.R.; Rambo, P.R.; Doudna, A.J. *Angew. Chem. Int. Ed.* **1999**, *38*, 2326-2343.
12) Qu, H.; Fang, X. *Genomics, Proteomics Bioinf.* **2013**, *11*, 135-141.
13) Afonin, K.A.; Lindsay, B.; Shapiro, B.A. *RNA Nanotechnol.* **2013**, *1*, 1-15.
14) Grabow, W.; Jaeger, L. *F1000Prime Rep.* **2013**, *5*, 46.
15) Guo, P. *Nat. Nanotechnol*. **2010**, *5*, 833-842.
16) Ishikawa, J.; Furuta, H.; Ikawa, Y. *Wiley Interdiscip. Rev. RNA* **2013**, *4*, 651-664.
17) Chakraborty, S.; Mehtab, S.; Krishnan, Y. *Acc. Chem. Res.* **2014**, *47*, 1710-1719.
18) Draper, D.E. *Biophys. J.* **2008**, *95*, 5489-5495.
19) Woodson, S.A. *Annu. Rev. Biophys*. **2010**, *39*, 61-77.
20) Leipply, D.; Draper, D.E. *Biochemistry* **2011**, *50*, 2790-2799.
21) Abels, J.A.; Moreno-Herrero, F.; Van der Haijden, T.; Dekker, C.; Dekker, N.H. *Biophys. J.* **2005**, *88*, 2737-2744.
22) Barbeyron, R.; Vasseur, J.J.; Smietana, M. *Chem. Sci.* **2015**, *6*, 542-548.
23) Freier, S.M.; Kierzek, R.; Jaeger, J.A.; Sugimoto, N.; Caruthers, M.H.; Neilson, T.; Turner, D.H. *Proc. Natl. Acad. Sci. USA* **1986**, *83*, 9373-9377.
24) Kumar, V.; Kumar, A. *Methods Mol. Biol.* **2015**, *1316*, 195-210
25) Westhof, E.; Masguida, B.; Jaeger, L. *Fold Des*. **1996**, *1*, 78-88.
26) a) Jaeger, L.; Leontis, N.B. *Angew. Chem. Int. Ed. Engl.* **2000**, *39*, 2521-2524.
   b) Kireeva, L.M.; Komissarova, N.; Kashlev, M. *J. Mol. Biol.* **2000**, *299*, 325-335.
27) Shu, D.; Moll, W.D.; Deng, Z.; Mao, C.; Guo, P. *Nano Lett.* **2004**, *4*, 1717-1723.
28) Guo, S.; Tschammer, N.; Mohammed, S.; Guo, P. *Hum Gene Ther.* **2005**, *16*, 1097-1109.
29) Shu, D.; Huang, L.; Hoeprich, S.; Guo, P. *J. Nanotechnol*. **2003**, *3*, 295-302.

30) Khaled, A.; Guo, S.; Li, F.; Guo, P. *Nano Lett.* **2005**, *5*, 1797-1808.
31) Chworos, A.; Severcan, I.; Koyfman, A.Y.; Weinkam, P.; Oroudjey, E.; Hansma, H.G.; Jaeger, L. *Science* **2004**, *306*, 2068-2072.
32) Severcan, L.; Geary, C.; Verzemnieks, E.; Chworos. A.; Jaeger, L. *Nano Lett.* **2009**, *9*, 1270-1277.
33) Jaeger, L.; Chworos, A. *Curr. Opin. Struct. Biol*. **2006**, *16*, 531-543.
34) Bindewald, E.; Hayes, R.; Yingling, Y.G.; Kasprzak, W.; Shapiro, B.A. *Nucleic Acids Res.* **2008**, *36*, 392-397.
35) Severcan, I.; Geary, C.; Chworos, A.; Voss, N.; Jacoverry, E.; Jaeger, L. *Nat. Chem*. **2010**, *2*, 772-779.
36) Nasalean, L.; Baudrey, S.; Leontis, N.B.; Jaeger, L. *Nucleic Acids Res*. **2006**, *34*, 1381-1392.
37) Geary, C.; Chworos, A.; Jaeger, L. *Nucleic Acids Res*. **2011**, *39*, 1066-1080.
38) Grabow, W.W.; Zakrevsky, P.; Afonin, K.A.; Chworos, A.; Shapiro, B.A.; Jaeger, L. *Nano Lett.* **2011**, *11*, 878-887.
39) Ohno, H.; Kobayashi, T.; Kabata, R.; Endo, K.; Iwasa, T.; Yoshimura, S.H.; Takeyasu, K.; Inoue, T.; Saito, H. *Nat. Nanotechnol*. **2011**, *6*, 116-120.
40) Shu, D.; Moll, W.D.; Deng, Z.; Mao, C.; Guo, P. *Nano Lett.* **2004**, *4*, 17171-1723.
41) Khaled, A.; Guo, S.; Li, F.; Guo, P. *Nano Lett.* **2005**, *5*, 1797-1808.
42) Grabow, W.W.; Zhuang, Z.; Swank, Z.N.; Shea, J.E.; Jaeger, L. *J. Mol. Biol.* **2012**, *424*, 54-67.
43) Zhang, H.; Endrizzi, J.A.; Shu, Y.; Haque, F.; Sauter, C.; Shlyakhtenki, L.S.; Lyubchenko, Y.; Guo, P.; Chi, Y.I. *RNA* **2013**, *19*, 1226-1237.
44) Bindewald, E.; Afonin, K.; Jaeger, L.; Shapiro, B.A. *ACS Nano* **2011**, *5*, 9542-9551.
45) Afonin, K.A.; Ceiply, D.J.; Leontis, N.B. *J. Am. Chem. Soc.* **2008**, *130*, 93-102.
46) Afonin, K.A.; Bindewald, E.; Yaghoubian, A.J.; Voss, N.; Jacovetty, E.; Shapiro, B.A.; Jaeger, L. *Nat. Nanotechnol.* **2010**, *5*, 676-682.
47) Dibrov, S.M.; McLean, J.; Parsons, J.; Hermann, T. *Proc. Natl. Acad. Sci. USA* **2011**, *108*, 6405-6408.
48) Khisamutdinoy, E.F.; Jasinski, D.L.; Guo, P. *ACS Nano* **2014**, *8*, 4771-4781.
49) Koyfman, A.Y.; Braun, G.; Magonov, S.; Chworos, A.; Reich, N.O.; Jaeger, L. *J. Am. Chem. Soc.* **2005**, *127*, 11886-11897.
50) Busi, F.; Cayrol, B.; Lavelle, C.; LeDerout, J.; Pietrement, O.; Le Cam, E.; Geinguenaud, F.; Lacoste, J.; Regnier, P.; Arluison, V. *Cell Cycle* **2009**, *8*, 952-954.
51) Cayrol, B.; Nogues, C.; Dawid, A.; Sagi, I.; Siberzan, P.; Isambert, H. *J. Am. Chem. Soc.* **2009**, *131*, 17270-17276.
52) Delebecque, C.J.; Lindner, A.B.; Silver, P.A.; Aldaye, F.A. *Science* **2011**, *333*, 470-474.
53) Ke. Y.; Ong, L.L.; Shih, W.M.; Yin, P. *Science* **2012**, *338*, 1177-1183.
54) Afonin, K.A.; Desai, R.; Viard, M.; Kireeva, M.L.; Bindewald, E.; Case, C.L.; Maciag, A.E.; Kasprzak, W.K.; Kim, T.; Sappe, A.; Stepler, M.; Kewalramani, V.N.; Kashlev, M.; Blumenthal, R.; Shapiro, B.A. *Nucleic Acids Res.* **2014**, *42*, 2085-2097.

55) Afonin, K.A.; Viard, M.; Martins, A.N.; Lockett, S.J.; Maciag, A.E.; Freed, E.O.; Heldman, E.; Jaeger, L.; Blumenthal, R.; Shapiro, B.A. *Nat. Nanotechnol.* **2013**, *8*, 296-304.
56) Afonin, A.K.; Grabow, W.W.; Walker, M.F.; Bindewald, E.; Dobrovolskaia, A.M.; Shapiro, A.B.; Jaeger, L. *Nat. Protoc.* **2011**, *6*, 2022-2034.
57) Ko, S.H.; Su, M.; Zhang, C.; Ribbe, A.E.; Jiang, W.; Mao, C. *Nat. Chem*. **2010**, *2*, 1050-1055.
58) Endo, M.; Yamamoto, S.; Tatsumi, K.; Emura, T.; Hidaka, K.; Sugiyama, H. *Chem. Commun.* **2013**, *49*, 2897-2881.
59) Wang, P.; Ko, S.H.; Tian, C.; Hao, C.; Mao, C. *Chem. Commun*. **2013**, *49*, 5462-5464.
60) Zheng, H.N.; Ma, Y.Z.; Xiao, S.J. *Chem. Commun*. **2014**, *50*, 2100-2103.
61) Afonin, K.A.; Kasprzak, W.K.; Bindewald, E.; Kireeya, M.; Viard, M.; Kashlev, M.: Shapiro, B.A. *Acc. Chem. Res*. **2014**, *47*, 1731-1741.
62) Afonin, K.A.; Kireeva, M.; Grabow, W.W.; Kashlev, M.; Jaeger, L.; Shapiro, B.A. *Nano Lett.* **2012**, *12*, 5192-5195.
63) Lee, J.B.; Hong, J.; Bonner, D.K.; Poon, Z.; Hammond, P.T. *Nat. Mater.* **2012**, *11*, 316-322.
64) Afonin, K.A.; Viard, M.; Kagiampakis, I.; Case, C.L.; Dobrovolskaia, M.A.; Hofmann, J.; Vrzak, A.; Kireeva, M.; Kasprzak, W.K.; KewalRamani, V.N.; Shapiro, B.A. *ACS Nano* **2015**, *9*, 251-259.
65) Yu, J.; Liu, Z.; Jiang, W.; Wang, G.; Mao, C. *Nat. Commun*. **2015**, *6*, 5724-5729.
66) Novikova, I.V.; Hassan, B.H.; Mirzoyan, M.G.; Leontis, N.B. *Nucleic Acids Res.* **2011**, *39*, 2903-2917.
67) Horton, N.C.; Finzel, B.C. *J. Mol. Biol.* **1996**, *264*, 521-533.
68) Geary, C.; Rothemund, P.W.; Andersen, E.S. *Science* **2014**, *345*, 799-804.
69) Seyhan, A.A.; Vlassov, A.V.; Johnston, B.H. *Oligonucleotides* **2006**, *16*, 353-363.
70) Han, D.; Park, Y.; Nam, H.; Lee, J.B. *Chem. Commun*. **2014**, *50*, 11665-11667.
71) Dabkowska, A.P.; Michanek, A.; Jaeger, L.; Rabe, M.; Chworos, A.; Hook, F.; Nylander, T.; Sparr, E. *Nanoscale* **2015**, *7*, 583-596.
72) Lander, E.S.; Linton, L.M.; Birren, B.; Nusbau, C.; Zody, M.C.; Baldwin, J.; Davon, K.; Dewar, K. et al. *Nature* **2001**, *409*, 860-921.
73) Sailor, M.J.; Park, J.H. *Adv. Mater*. **2012**, *24*, 3779-3802.
74) Gao, Y.; Liu, X.L.; Li, X.R. *J. Nanomedicine* **2011**, *6*, 1017-1025.
75) Gao, J.; Yu, Y.; Zhang, Y.; Song, J.; Chen, H.; Li, W.; Qian, W.; Deng, L.; Kou, G.; Chen, J.; Guo, Y. *Biomaterials* **2012**, *33*, 270-282.
76) Zeng, X.; Pan, S.; Li, J.; Wang, C.; Wen, Y,; Wu, H.; Wang, C.; Wu, C.; Feng, M. *Nanotechnology* **2011**, *33*, 375102.
77) Kam, N.W.; Liu, Z.; Dai, H. *J. Am. Chem. Soc.* **2005**, *127*, 12492-12493.
78) Bonner, D.K.; Leung, C.; Chen-Liang, J.; Chingozha, L.; Langer, R.; Hammond, P.T. *Bioconjug. Chem.* **2011**, *22*, 1519-1525.
79) Lytton-Jean, A.K.; Langer, R.; Anderson, D.G. *Small* **2011**, *7*, 1932-1937.
80) Grabow, W.W,; Jaeger, L. *Acc. Chem. Res*. **2014**, *47*, 1871-1880.
81) Guo, P.; Haque, F.; Hallahan, B.; Reif, R.; Li, H. *Nucleic Acid Ther.* **2012**, *22*, 226-245.

82) Shu, D.; Shu, Y.; Haque, F.; Abdelmawla, S.; Guo, P. *Nat. Nanotechnol.* **2011**, *6*, 658-667.
83) Abdelmawla, S.; Guo, S.; Zhang, L.; Pulukuri, S.; Patankar, P.; Conley, P.; Trebley, J.; Guo, P.; Li, Q.X. *Mol. Ther.* **2011**, *19*, 1312-1322.
84) Shu, Y.; Haque, F.; Shu, D.; Li, W.; Zhu, Z.; Kotb, M.; Lyubchenko, Y.; Guo, P. *RNA* **2013**, *19*, 766-777.
85) Fire, A.; Xu, S.Q.; Montgomery, M.K.; Kostas, S.A.; Driver, S.E.; Mello, C.C. *Nature* **1998**, *391*, 806-811.
86) Davis, M.E.; Zuckerman, J.E.; Choi, C.H.; Seligson, D.; Tolcher, A.; Alabi, C.A.; Yen, Y.; Heidel, J.D.; Ribas, A. *Nature* **2010**, *464*, 1067-1070.
87) Sen, GL.; Blau, H. M. *FASEB J.* **2006**, *20*, 1293-1299.
88) Dogini, D.B.; Pascoal, V.D.; Avansini, S.H.; Vieira, A.S.; Pereira, T.C.; Lopes-Cendes, I. *Genet. Mol. Biol.* **2014**, *37*, 285-293.
89) Castonotto, D.; Rossi, J.J. *Nature* **2009**, *457*, 426-433.
90) Patil, V.S. Zhou, R., Rana, T.M. *Biochem. Mol. Biol*. **2014**, *49*, 16-32.
91) Resnier, P.; Montier, T.; Mathieu, V.; Benoit, J.P.; Passirani, C. *Biomaterials* **2013**, *34*, 6429-6443.
92) Shu, D.; Shu, Y.; Haque, F.; Abdelmawla, S.; Guo, P. *Nat. Nanotechnol*. **2011**, *6*, 658-667.
93) Haque, F.; Shu, D.; Shu, Y.; Shlyakhtenko, L.; Rychahou, P.; Evers, M.; Guo, P. *Nano Today* **2012**, *7*, 245-257.
94) Lee, H.; Lytton-Jean, A.K.; Chen, Y.; Love, K.T.; Park, A.I.; Karagiannis, E.D.; Sehgal, A.; Querbes, W.; Zurenko, C.S.; Jayaraman, M.; Peng, C.G.; Charisse, K.; Borodonysky, A.; Manoharan, M.; Donahoe, J.S.; Truelove, J.; Nahrendorf, M.; Langer, R.; Anderson, D. G. *Nat. Nanotechnol* **2012**, *7*, 389-393.
95) Maina, A.; Blackman, B.A.; Parronchi, C.J.; Morozko, E.; Bender, M.E.; Blake, A.D.; Sabatino, D. *Bioorg. Med. Chem. Lett.* **2013**, *23*, 5270-5274.
96) Chang, C.I.; Lee, T.Y.; Kim, S.; Sun, X.; Hong, S.W.; Yoo, J.W.; Dua, P.; Kang, H.S.; Kim, S.; Li, C.J.; Lee, D.K. *J. Gene Med*. **2012**, *14*, 138-146.
97) Nakashima, Y.; Abe, H.; Abe, N.; Aikawa, K.; Ito, Y. *Chem. Commun*. **2011**, *47*, 8367-8369.
98) Hong, C.A.; Eltoukhy, A.A.; Lee, H.; Langer, R.; Anderson, D.G.; Nam, Y.S. *Angew. Chem. Int. Ed. Engl.* **2015**, *54*, 6740-6744.
99) Li, Y.; Tseng, Y.D.; Kwon, S.Y.; D'Espaux, L.; Bunch, J.S.; McEuen, P.L.; Luo, D. *Nat. Mater.* **2004**, *3*, 38-42.
100) Abe, N.; Abe, H.; Ito, Y. *J. Am. Chem. Soc.* **2007**, *129*, 15108-15109.
101) Abe, N.; Abe, H.; Ohshiro, T.; Nakashima, Y.; Maeda, M.; Ito, Y. *Chem. Commun. (Camb).* **2011**, *47*, 2125-2127.
102) Abe, N.; Abe, H.; Nagai, C.; Harada, M.; Hatakeyama, H.; Harashima, H.; Ohshiro, T.; Nishihama, M.; Furukawa, K.; Maeda, M.; Tsuneda, S.; Ito, Y. *Bioconjug. Chem.* **2011**, *22*, 2082-2090.
103) Kim, H.; Park, Y.; Lee, J. *Sci. Rep*. **2015**, *5*, 12737.
104) Kim, H.; Lee, J.S.; Lee, J.B. *Sci. Rep.* **2016**, *6*, 25146.
105) Resnier, P.; Montier, T.; Mathieu, V.; Benoit, J.P.; Passirani, C. *Biomaterials* **2013**, *34*, 6429-6443.

106) Uchino, K.; Ochiya, T.; Takeshita, F. *Jpn. J. Clin. Oncol*. **2013**, *43*, 596-607.
107) Iyer, A.K.; Khaled, G.; Fang, J.; Maeda, H. *Drug Discov. Today* **2006**, *11*, 812-818.
108) Greish, K.J. *Drug Target* **2007,** *15*, 457-564.
109) Wu, J.; Huang, W.; He, Z. *ScientificWorldJournal* **2013**, 2013, 630-654.
110) Lee, S.E.; Sasaki, D.Y.; Perroud, T.D.; Yoo, D.; Patel, K.D.; Lee, L.P. *J. Am. Chem. Soc.* **2009**, *131*, 14066-14074.
111) Landen, C.N. Jr.; Chavez-Reyes, A.; Bucana, C.; Schmandt, R.; Deavers, M.T.; Lopez-Berestein, G.; Sood, A.K. *Cancer Res.* **2005**, *65*, 6910-6918.
112) Lee, J.M.; Yoo, T.J. Cho, Y.S. *Biomed. Res. Int.* **2013**, 782041.
113) Hong, C.A.; Nam, Y.S. *Theranostics*, **2014**, *4*, 1211-1232.
114) Hsiang, T.; Zhao, C.; Krug, M.R. *J. Virol*. **2009**, *83*, 5971-5977.
115) Singha, K.; Namgung, R.; Kim, W.J. *Nucleic Ther*. **2011**, *21*, 133-147.
116) Yin, H.; Kanasty, R.L.; Eltoukhy, A.A.; Vegas, A.J.; Dorkin, J.R.; Anderson, D.G. *Nat. Rev. Genet*. **2014**, *15*, 541-555.
117) Adjei, I.; Sharma, B.; Labhasetwar, V. *Adv. Exp. Med. Biol*. **2014**, *81*1, 73-91.
118) Ardana, A.J. *Chem. Technol. Biotechnol.* **2015**, *90*, 1196-1208.
119) Kim, T.; Hyeon, T. *Nanotechnology* **2014**, *25*, 012001.
120) Huang, C.; Zhang, Y.; Yuan, H.; Gao, H.; Zhang, S. *Nano Lett.* **2013**, *13*, 4546-4550.
121) Li, X. *J. Appl. Phys*. **2012**, *111*, 024702.
122) Murugan, K.; Choonara, Y.E.; Kumar, P.; Bijukumar, D.; du Toil, L.C.; Pillay, V. *Int. J. Nanomedicine* **2015**, *10*, 2191-2206.
123) Chithrani, B.D.; Ghazani, A.A.; Chan, W.C. *Nano Lett.* **2006**, *6*, 662-668.
124) Toy, R.; Peiris, P.M.; Ghaghada, K.B.; Karathanasis, E. *Nanomedicine (Lond)* **2014**, *9*, 121-134.
125) Prabha, S.; Zhou, W.Z.; Panyam, J.; Labhaswtwar, V. *Int. J. Pharm.* **2002**, *5*, 105-115.
126) Nam, H.Y.; Kwon, S.M.; Chung, H.; Lee, S.Y.; Jeon, H.; Kim, Y.; Park, J.H.; Kim, J.; Her, S.; Oh, Y.K.; Kwon, I.C.; Kim, K.; Jeong, S.Y. *J. Control. Release* **2009**, *135*, 259-267.
127) Danhier, F.; Feron, O.; Preat, V. *J. Control. Release* **2010**, *148*, 135-146.
128) Beddoes, C.M.; Case, C.P.; Briscoe, W.H. *Adv. Colloid. Interface Sci.* **2015**, *218*, 48-68.
129) Ho, C.C.; Ding, S.J. *J. Mater. Sci. Mater. Med.* **2013**, *24*, 2381-2390.
130) Whitehead, K.A.; Langer, R.; Anderson, D.G. *Nat. Rev. Drug Discov*. **2009**, *8*, 129-138.
131) Katas, H.; Alpar, H.O. *J. Control Release* **2006**, *115*, 216-225.
132) Deleavery, G.F.; Damha, M. *J. Chem. Biol.* **2012**, *19*, 937-954.
133) Wang, A.Z.; Langer, R.; Farokhzad, O.C. *Annu. Rev. Med.* **2012**, *63*, 185-198.
134) Jeong, J.H.; Mok, H.; Oh, Y.K. *Bioconjug. Chem.* **2008**, *20*, 5-14.
135) Chiu, Y.L.; Ali, A.; Chu, C.Y.; Cao, H.; Rana, T.M. *Chem. Biol*. **2004**, *11*, 1165-1175.
136) Moschos, S.A.; Jones, S.W.; Perry, M.M.; Williams, A.E.; Erjefalt, J.S.; Turner, J.J.; Barnes, P.J.; Sproat, B.S.; Gait, M.J.; Lindsay, M.A. *Bioconjug. Chem.* **2007**, *18*, 1450-1459.
137) Cesarone, G.; Edupuganti, O.P.; Wickstrom, E. *Bioconjug. Chem.* **2007**, *18*, 1831-1840.
138) Xu, W.; Pan, R.; Zhao, D.; Chu, D.; Wu, Y.; Wang, R.; Chen, B.; Ding, Y.; Sadatmousavi, P.; Yuan, Y.; Chen, P. *Mol. Pharm.* **2015**, *12*, 56-65.
139) Chu, T.C.; Twu, K.Y.; Ellington, A.D.; Levy, M. *Nucleic Acids Res.* **2006**, *34*, 73.

140) Toloue, M.M.; Ford, L.P. *Methods Mol. Biol*. **2011**, *764*, 123-39.
141) Lee, K.; Oh, M.H.; Lee, M.S.; Nam, Y.S.; Park, T.G.; Jeong, J.H. *Int. J. Pharm*. **2013**, *445*, 196-202.
142) Li, S.D.; Huang, L. *Curr. Opin. Investig. Drugs* **2008**, *9*, 1317-1323.
143) Bolcato-Bellemin, A.L.; Bonnet, M.E.; Creusat, G.; Erbacher, P.; Behr, J.P. *Proc. Natl. Acad. Sci*. *USA* **2007**, *104*, 16050-16055.
144) Liu, X.; Liu, C.; Laurini, E.; Posocco, P.; Pricl, S.; Qu, F. *Mol. Pharm*. **2012**, *9*, 470-481.
145) Mok, H.; Lee, S.H.; Park, J.W.; Park, T.G. *Nat. Mater.* **2010**, *9*, 272-278.
146) Lee, S.Y.; Huh, M.S.; Lee, S.; Lee, S.J.; Chang, H.; Park, J.H. *J. Control Release* **2010**, *141*, 339-346.
147) Lee, S.Y.; Mok, H.; Jo, S.; Hong, C.A.; Park, T.G. *Biomaterials* **2011**, *32*, 2359-2368.
148) Chung, H.J.; Hong, C.A.; Lee, S.H.; Jo, S.D.; Park, T.G. *Bioconjug. Chem*. **2011**, *22*, 299-306.
149) Jo, S.D.; Kim, J.S.; Joie, C.O.; Mok, H.; Nam, Y.S. *Macromol. Biosci.* **2014**, *14*, 195-201.
150) Kong, W.H.; Bae, K.H.; Hong, C.A.; Lee, Y.; Hahn, S.K.; Park, T.G. *Bioconjug. Chem*. **2011**, *22*, 1962-1969.
151) Hong, C.A. Lee, S.H.; Kim, J.S.; Park, J.W.; Bae, K.H.; Mok, H. *J. Am. Chem. Soc.* **2011**, *133*, 13914-13917.
152) Young, S.W.; Stenzel, M.; Yang, J.L. *Crit. Rev. Oncol. Hematol*. **2016**, *98*, 159-169.
153) Mansoori, B.; Shotorbani, S.S.; Baradaran, B. *Adv. Pharm. Bull*. **2014**, *4*, 313-321.
154) Forsbach, A.; Muller, C.; Montino, C.; Kritzler, A.; Curdt, R.; Benahmed, A.; Jurk, M.; Vollmer, J. *Immunol. Lett.* **2012**, *141*, 169-180.
155) Mikkola, S.; Kosonen, I.; Lonnberg, H. *Curr. Org. Chem.* **2002**, *6*, 523-538.
156) Lundy, B.B.; Convertine, A.; Miteva, M.; Stayton, S.P. *Bioconjug. Chem*. **2013**, *24*, 398-407.

CHAPTER 2: HYBRIDIZATION AND SELF-ASSEMBLY OF RNA INTO STABLE THREE COMPONENT SYSTEMS (3CS)

2.1 Abstract

In this chapter, the prerequisite conditions for forming stable hybrid RNA assemblies are described. The study involved the design of linear RNA template sequences and two complementary strands with base-pairing fidelity that facilitated higher-order self-assembly into stable three-component RNA systems. Solid phase RNA synthesis was performed in order to obtain the crude RNA sequences. All synthesized RNA sequences were then purified by RP-IP-HPLC and characterized by mass spectrometry. In order to optimize the conditions for self-assembly of the stable RNA hybrid three component system (3CS), parameters such as RNA sequence length, buffer conditions and salt concentration were screened for hybridization. The influence of the hybridization conditions on RNA self-assembly of the 3CS were analyzed by native polyacrylamide gel electrophoresis (PAGE), which distinguished hybrid *vs* non-hybrid RNA based on their differences in electrophoretic mobilities on the gel. Furthermore, the thermal stabilities (T_m) of the RNA hybrid 3CSs were evaluated by thermal denaturation which indicated the most stable hybrid conditions with the highest T_m values. The RNA hybrids were also found to form the canonical A-type helical hybrid structure in various buffer conditions as examined by circular dichroism (CD) spectroscopy. These characterization studies revealed that the 30 nucleotide (nt) long RNA template strand, **RNA_{T30}**, was required to self-assemble the two complementary RNA strands of 15 nt, **RNA_{C15}** and 23 nt, **RNA_{C23}** to form the stable RNA 3CS. Moreover, the self-assembled RNA 3CS was stably formed using Tris buffer, which supported the stabilizing effects of the salts present in the buffer.

2.2 INTRODUCTION

2.2.1 Solid Phase RNA Synthesis

Many synthetic strategies have been developed to generate biologically active RNAs for applications in biology, chemical biology, and medicine in addition to the advancement of bio-technologies. The synthesis of RNA has always been a challenge due to its many reactive functional groups and higher-order structures. Since the 1950s two widely developed strategies have been implemented: 1) Enzymatic synthesis and 2) Chemical synthesis, each method has gained in popularity with the rise of technological innovations in the field.[1,2,3] In this thesis, I will discuss the automated solid phase synthesis of RNA and underscore its benefits for producing a wide range of RNAs for the many applications that have evolved from chemical synthesis procedures. Solid phase RNA synthesis enables the incorporation of native or modified RNA monomers for making RNA oligonucleotides in sufficient quantities for biological and therapeutic applications.[4,5] The automated synthesis of RNA begins with the selection of the solid support. The solid support is preferably insoluble in organic or aqueous solvents and chemically inert throughout of the entire RNA synthesis cycle.[6,7] A variety of compatible polymeric materials have been designed and developed for RNA synthesis. These include: Divinylbenzene cross-linked Polystyrene[6] (DVB-PS), Macroporous[8] Polystyrene (MPPS) or Controlled Pore Glass[7] (CPG). Among the different types of solid supports that have been produced, CPG has been widely accepted for both small to commercial production levels of RNA. The CPG is commercially available with different pore sizes ranging from 500-3000 Å, with the larger pore sizes respectively facilitating the growth of lengthy and larger RNA sequences and structures.[7] Linkers have been functionalized onto the CPG for the efficient growth and isolation of RNA from the solid support. For example, the long chain alkyl amine linker such as the succinyl linker[9a], hydroquinone-*O*-*O'*-

diacetic acid derived Q- or HDQA-linker,[11] the photo- labile linker such as the *ortho*-nitrobenzyl linker[12] and the universal linkers [9,10] that allow the rapid and efficient synthesis of a wide range of RNA sequences. The first RNA monomers attached to the succinyl linkers on CPG are the most routinely used for RNA synthesis. The succinyl-linked CPG support contains the 3'-RNA monomer composed with the 5'-dimethoxytrityl (5'-ODMT) 2'-*tert*-butyldimethylsilyl (2'-OTBDMS) protecting groups (**Figure 2.1**). The 5'-ODMT group is acid labile with 3% trichloroacetic acid (TCA) or dicholoroacetic acid (DCA) in dichloromethane (DCM) and can be monitored during deprotection by trityl cation color analyses using UV-Vis spectroscopy. The loading capacity (μmol of RNA/ g of solid support) determines the stoichiometric quantity of RNA monomers attached to the solid support. It is used for calculating synthesis yields and efficiencies. The higher loading supports (i.e. 80-100 μmol/g) enable the production of greater RNA amounts and is especially useful in bulk RNA synthesis at lower costs.[13] Each chemical step is optimized to completion by introducing an excess of reagents to the column containing CPG, while facilitating RNA synthesis on solid support. Moreover, the solid phase synthesis procedure alleviates the need for step-wise work-up and purification steps. Following each reaction step, excess reagents are filtered through the column and into the waste container. Following RNA synthesis, a final post-synthesis cleavage and deprotection procedure is used to isolate the crude RNA from the solid support. The crude RNA is quantitated by UV-Vis spectroscopy, analyzed and purified by HPLC and finally characterized by MS which validates sequence identity based on molecular weight.

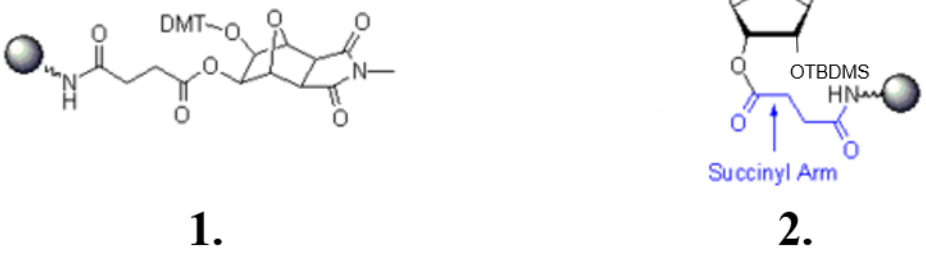

1. **2.**

Figure 2.1 Control pore glass (CPG) attached with (1) amino succinyl universal linker and (2) the first 5-ODMT 2'-OTBDMS RNA nucleotide (Base: $A^{N\text{-Bz}}$,$G^{N\text{-Ac}}$,$C^{N\text{-Ac}}$,U) attached to the succinyl linker CPG support.

2.2.2 RNA PHOSPHORAMIDITES FOR SOLID PHASE RNA SYNTHESIS

The conventional RNA building blocks for automated RNA solid phase synthesis contain three types of protecting groups: 1) 5'-OH acid labile protecting groups (DMT or MMT), 2) 2'-OH fluoride labile protecting groups (-OTBDMS), 3) exocyclic $-NH_2$ base labile protecting groups on bases (*N*-Bz, *N*-Ac, *N*-iBu) and a 3'-phosphoramidite facilitating coupling to the nascent support-bound RNA (**Figure 2.2**). Even though these RNA building blocks are commonly used in RNA synthesis, their application in lengthy RNA syntheses (> 50 nt) is limited due to the steric influence imparted by the bulky 2'-OTBDMS protecting groups. For the efficient synthesis of lengthy RNA sequences, a number of new 2'-protecting groups have been developed.[14] For example, the chemical synthesis of the 43 nt long RNA corresponding to the 3'-terminus of a formylmethionine tRNA of *Escherichia coli* on CPG solid support using 2'-OTBDMS protecting group has been carried out.[17] Another 110 nt long precursor-microRNA was synthesized using 2-cyanoethoxymethyl (CEM) as a 2'-*O*-protecting group by solid phase RNA synthesis.[15]

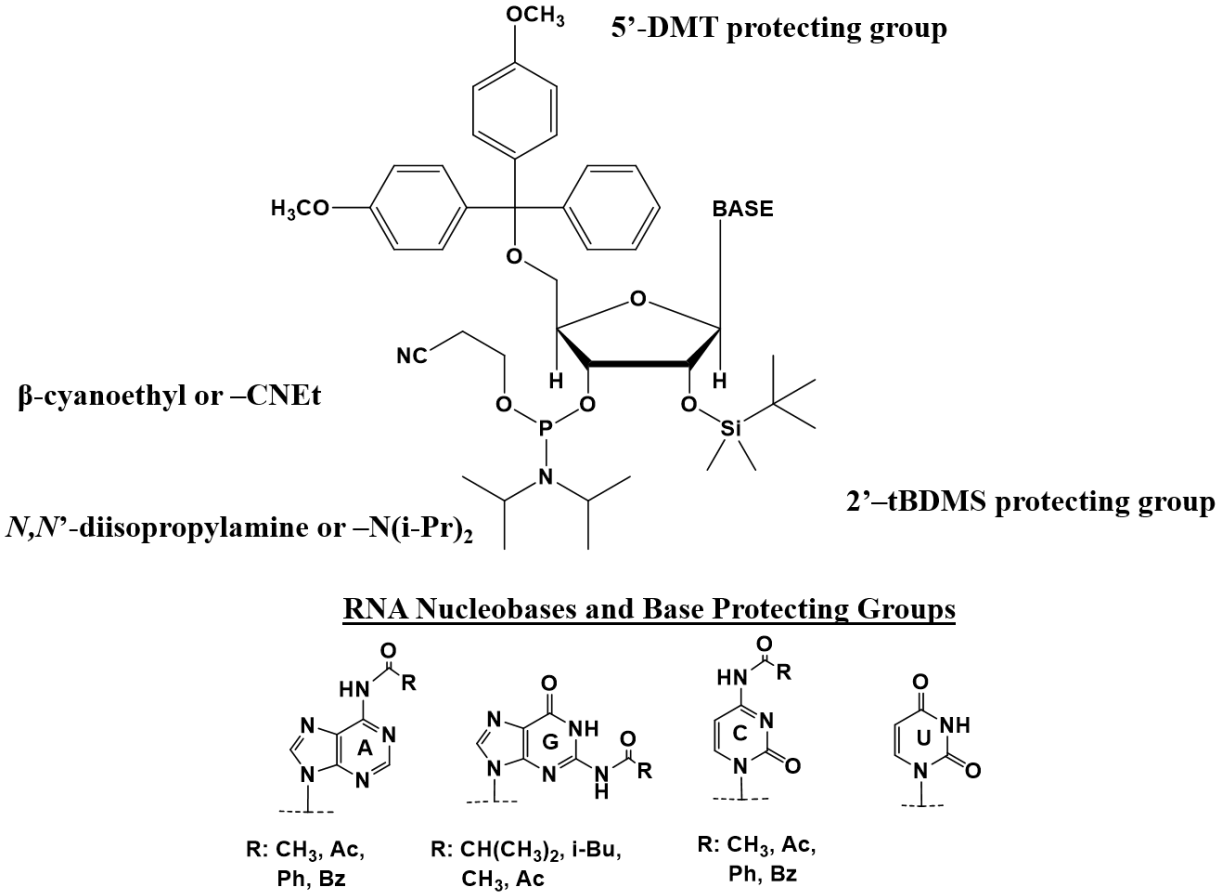

Figure 2.2 Commercially available RNA phosphoramidites with their protecting groups for solid phase RNA synthesis (RNA phosphoramidites commercially available at Chemgenes Inc. Wilmington, MA).

2.2.3 Automated Solid Phase RNA Synthesis, Cleavage and Deprotection from the Solid Support

The discovery of the automated RNA solid phase synthesis cycle has facilitated the small (microgram to milligram), and bulk (gram to kilogram) scale production of native and modified synthetic RNAs using various phosphoramidite RNA building blocks.[17]

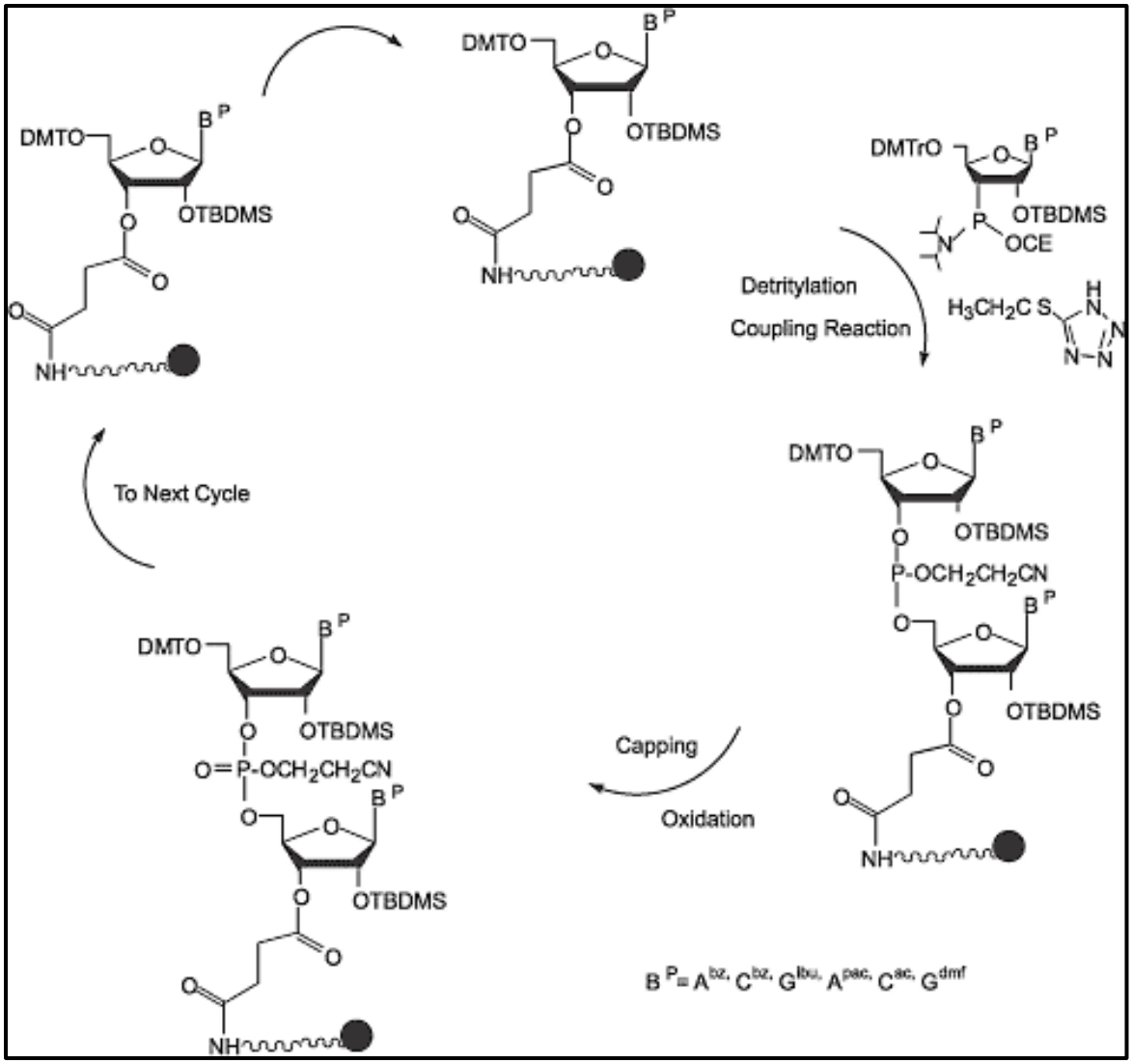

Scheme 2.1 Automated solid phase RNA synthesis cycle. Figure has been adapted from ref 16: Iyer, R.P.; Kuchimanchi, S.N.; Panday, R.K. *Drugs Fut.* **2003**, *28*, 51.

The automated solid phase RNA synthesis cycle (**Scheme 2.1**) allows the rapid growth of RNA on solid support from the 3'- to 5'-end of the target sequence. During the synthesis cycle, the very first detritylation step of the 5'-DMT group is conducted by delivering into the synthesizer column containing the CPG a solution of 3% DCA:DCM for 90 seconds to ensure complete detritylation. In the subsequent step, the CPG is washed with DCM to remove any residual DMT^+. In the following coupling step, the pre-dissolved RNA phosphoramidites (0.15 M) in anhydrous acetonitrile (MeCN), are mixed with the coupling reagent, 0.25 M 5-ethylthiotetrazole (ETT), in MeCN for activation and coupling to the RNA bound CPG solid support. Typically, the coupling reaction takes places in 6-10 minutes but coupling times can be varied based on the composition of the RNA phosphoramidites (e.g. riboguanosine requires 15 minute couplings due to the bulky *N*-iBu and 2'-TBDMS protecting groups) or to enhance coupling efficiencies of modified phorphoramidites (e.g. branchpoint ribouridine phosphoramidite).[18] After the coupling step, the RNA bound CPG is washed with MeCN and any uncoupled RNA is capped. The capping step is of prime importance to prevent the elongation of uncoupled RNA failure sequences (i.e. n-1, n-2, n-3……. etc.). In this step any uncoupled RNA is capped with the capping reagents (Cap A: 1:1:8 v/v/v acetic anhydride:pyridine:tetrahydrofuran, Cap B: 16% *N*-methyl imidazole in tetrahydrofuran) for 12-15 seconds. If incomplete capping is anticipated in difficult to couple sequences, two capping cycles may be applied to ensure 100% capping efficiency (e.g V-shape and Y-shape siRNA synthesis).[18] In this study, the RNA coupling steps were optimized to 96-98% coupling efficiency thereby minimizing the accumulation of failure sequences. Following capping, oxidation of the RNA backbone from the more reactive phosphite to the more stable phosphate triester[19] is accomplished using 0.02 M oxidant (I_2 in 75/20/5 v/v/v tetrahydrofuran/pyridine/water) for 14 seconds. This step is also essential because the trivalent

phosphite triester group is reactive and can lead to 3'- to 2'- isomerization and cleavage of the RNA strand under neutral, acidic and basic conditions.[20] The RNA bound support is then washed with MeCN and dried with argon prior to 5'-detritylation of the last attached RNA monomer. The synthesis cycle continues until the desired sequence has been completed.

Once the desired RNA sequence is synthesized, the RNA linked CPG is subjected to cleavage (removal of the RNA from the solid support) and deprotection (removal of the exocyclic nucleobase protecting groups and the cyanoethyl groups from the phosphate triester backbone) using alkaline conditions. Typically, a 1:1 v/v ammonium hydroxide: methylamine (1:1 AMA) solution is applied for 10 min at 65 ºC for the cleavage and deprotection step of RNA containing labile nucleobase protecting groups (e.g. *N*-Bz, *N*-Ac). However, harsher conditions are applied when the RNA base protecting groups (e.g. Guanine base, *N*-iBu) are more resilient to the AMA conditions. These conditions use a 3:1 v/v ammonium hydroxide in ethanol (3:1 v/v NH_4OH:EtOH) solution for 14 -18 hours at 55 ºC. The alkaline solution is volatile and can be then evaporated on a Speedvac® concentrator. The dried, crude RNA is then recovered from the CPG by extraction with sterile, autoclaved distilled water and evaporated to obtain the dried crude RNA pellet. The crude RNA is then treated with a 1:1 v/v dimethylsufoxide:trimethylamine trihydrofluoride (1:1 DMSO:TEA·3HF, 125 µL each) solution at 65 ºC for 2 hours to remove the 2'-OTBDMS protecting group. In the very last step, the crude RNA is precipitated with 3 M NaOAc (30 µL) in n-BuOH (1 mL), isolated by centrifugation and redissolved in autocleaved distilled water for further quantitative analysis by UV-Vis Spectroscopy. Crude RNA analysis and purification is next accomplished by IP-RP-HPLC[27] and/or polyacrylamide gel electrophoresis.[21]

2.2.4 Qualitative Analysis and Purification of RNA by IP-RP-HPLC

Many techniques are currently available for the isolation, purification and quantification of RNA. The crude qualitative analysis of RNA is commonly accomplished by ion-pair reverse-phase high performance liquid chromatography (IP-RP-HPLC).[25] This method is especially useful for the analyses of double-stranded RNA under non-denaturing conditions, and single-stranded RNA using partially and completely denaturing conditions by varying salt concentrations and buffer pH. The denaturing HPLC conditions have gained widespread acceptance for RNA analysis and purification.[22-25]

In IP-RP-HPLC, the RP column contains a non-polar stationary phase, typically C-18 (although C-8 columns have been used) derivitized silica with different particle sizes.[26-29] The particle sizes of 8-30 μm have been most commonly used for the separation of lengthier, more hydrophobic RNA sequences that have greater retention and separation on the RP column.[30] The buffer conditions also play a critical role in IP-RP-HPLC. A commonly used ion pairing buffer for RNA analysis is composed of the alkyl ammonium salts (eg. TEAA) formed from the acid/base reaction in between acetic acid (AA) and triethylamine (TEA). The buffer is maintained near neutral pH and serves a very important function in stabilizing the hydrophobic interactions in between the eluting RNA in the mobile phase and the stationary phase. Also, the use of organic solvents such as acetonitrile (MeCN) is combined with the TEAA buffer in the mobile phase to facilitate RNA elution and the washing of non-polar synthetic RNA impurities, such as those accumulated from incomplete deprotection of the bulky, hydrophobic protecting groups. **Figure 2.3** shows a typical IP-RP-HPLC chromatogram with increased resolution in between the desired RNA target sequence and the n-1 failure sequences which are typically shorter, more hydrophilic and faster eluting with shorter retention times. The lengthier (n+1) RNA sequences as a result of

the incorporation of additional RNA monomer units or due to incomplete deprotection will lead to more hydrophobic RNA sequences that elute slower with longer retention times. The n-1 and n+1 sequences are typically difficult to separate from the target RNA sequence, therefore, careful optimization of the gradient elution system is necessary in order to obtain pure RNA product.[28] Moreover, the crude RNA may also be susceptible to self-folding into higher-order secondary structures which makes the analysis and purification more difficult to accomplish. In these instances, denaturing conditions may be applied by increasing the column temperatures to 50-70 ºC which causes the denaturation of any high-order structures and clean analyses of the native RNA primary sequence. The RNA analysis on HPLC is monitored by the UV absorbance at 260 nm.[28,29] Following analysis and purification of the crude RNA, the volatile eluent components can be evaporated on a Speed Vac concentrator, leaving behind the pure RNA pellet that can be further characterized by a combination of gel electrophoresis, mass spectrometry and UV-Vis, CD spectroscopy.

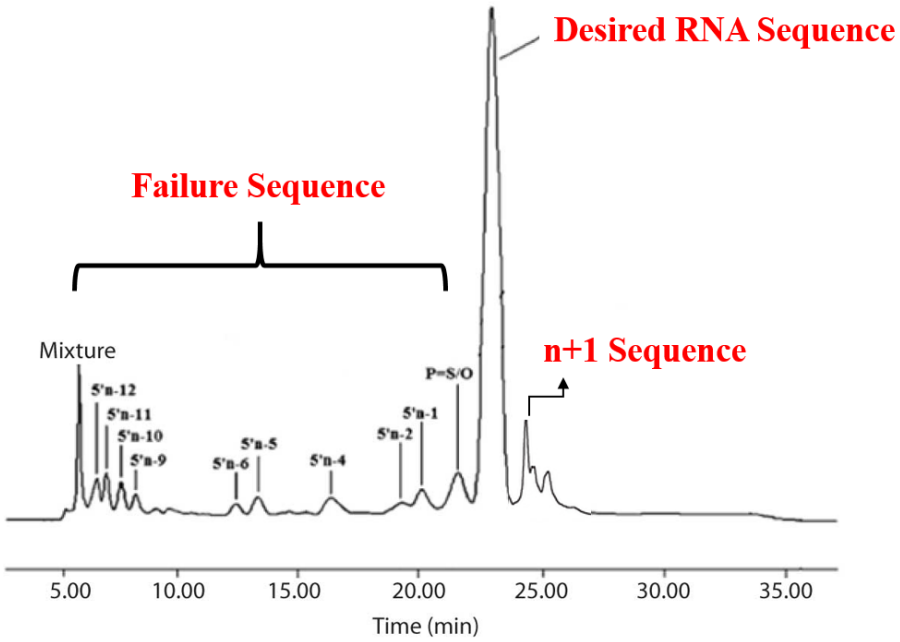

Figure 2.3 A typical IP-RP-HPLC chromatogram of a crude RNA sequence.

2.2.5 Qualitative Analysis of RNA by Polyacrylamide Gel Electrophoresis (PAGE)

The polyacrylamide gel electrophoresis (PAGE) technique is a useful analytical technique to assess RNA purity (under denaturing conditions) and for the characterization of self-assembled hybrid structures (under native conditions).[32-35] The separation of crude RNA under denaturing PAGE conditions requires the preparation of the RNA sample in 0.1% formamide in TBE buffer and with a PAGE gel containing urea. These conditions separate crude RNA samples based on RNA sequence composition, size, shape and charge differences. The RNA migrates through pores of the gel with an applied electric current, with the smaller sequences (<18 nucleotides) migrating faster while the lengthier sequences (>30 nucleotides) migrate slower and with shorter electrophoretic mobilities on the gel, **Figure 2.4**.[31] Native PAGE analysis can be useful in characterizing hybrid RNA structures in a non-denaturing sucrose-TBE buffer and with a PAGE gel prepared without urea. Moreover, the amount of polyacrylamide varies from preparation to preparation and typically accounts for 18-25 nt long RNA, as a 20-24% PAGE and for RNA >45 nt, as a 10-18% PAGE solution. Under these conditions, native PAGE analyses has been used to track hybrid RNA,[36] ligand-RNA[37] and peptide/protein-RNA[38] complex formation. Following RNA PAGE analysis, the gel can be visualized under a UV light (260 nm absorbance) or with an intercalating dye solution (such as ethidium bromide) which displays the RNA as purple colored bands, **Figure 2.4**.

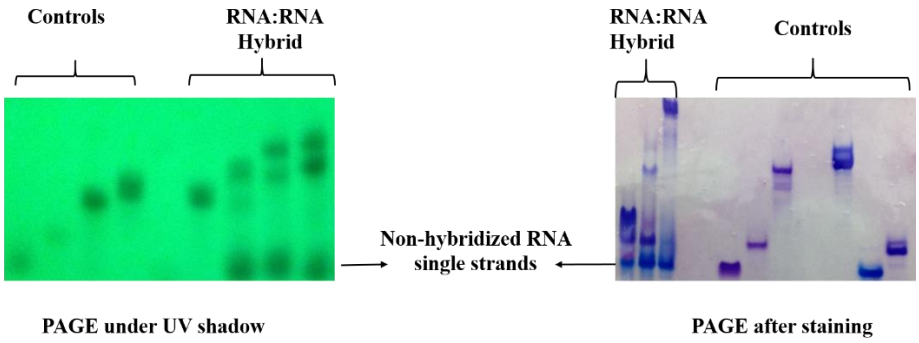

Figure 2.4 Polyacrylamide gel electrophoresis of RNA:RNA hybrids under UV shadow and after staining with ethidium bromide.

2.2.6 Mass Spectrometry Analysis of RNA

Mass spectrometry (MS) is a very sensitive RNA analysis technique due to its ability to provide molecular weight and sequence information of a limited amount of sample.[39,40] The analysis of RNA by mass spectrometry is based on sample ionization with an ion source under high pressure and temperature conditions, followed by mass ion separation and fragmentation within the mass analyzer leading to the detection of ions as mass to charge ratios. The computer aided software algorithms enable interpretation of RNA fragment ion data by providing mass to charge ratios (*m*/*z*). Sample ionization for RNA is typically accomplished by electron spray ionization (ESI).[41] This ESI ion source is coupled with a triple quadrupole or time of flight mass analyzer which facilitates high resolution mass spectra (HRMS) data collection. This provides exact molecular weight identification of RNA in addition to mass ion fragmentation patterns collected from MS/MS methods that are designed to provide information on the sequence composition. The latter has been applied to the sequencing of biological RNA and entire RNA genomes.[42] Matrix-assisted laser desorption/ionization of time flight mass spectroscopy (MALDI-TOF-MS) has also been used as an analytical approach for obtaining mass information of RNAs.[43] MALDI-TOF MS requires the RNA sample to be embedded within a suitable matrix, typically

composed of aza-thiothymine/spermine and L-fucose, which is then subjected to a UV laser beam causing sample absorption, followed by desorption from the matrix and ionization. The ions generated are then separated and detected by the TOF-MS producing a mass spectrum of the RNA sample in positive (protonated) or negative (deprotonated) mode.

In ESI mass spectrometry the parent ions are typically not observed. Rather, multiple negatively charged species are detected in the mass spectrum and deconvoluted to provide mass sequence identity. The ESI method provides better mass accuracy, resolution, and sensitivity for lengthy RNAs (from 20-120 base-pairs) while MALDI-TOF analysis has been used to characterize very large, genomic RNA sequences.[44] Moreover, RNA mass analysis may also be accomplished by coupling mass spectrometry with HPLC, for in-line chromatographic separation and mass characterization.[45] Thus, LC-MS provides a nice instrumental technique for rapidly separating RNA sequences and characterizing their composition.

2.2.7 UV-Vis Spectroscopy Analysis of RNA Thermal Denaturation

Thermal denaturation analysis is commonly used to assess RNA hybrid stability. The experiment uses a UV-VIS spectrophotometer to measure the changes in absorption of the RNA bases in the hybrid *vs.* non-hybrid form. In this assay, the RNA nucleobases will exhibit greater changes in UV absorption with increasing temperatures (% hyperchromicity) as the RNA hybrid denatures into separate, single-stranded sequences (**Figure 2.5**). The nucleobases within the RNA sequences have absorptivities in the far-UV (210-310 nm) region. Thus, any change in RNA secondary structure can be effectively quantitated at 260 nm (A_{260}). The typical UV absorption at 260 nm increases when the RNA hybrid duplex transitions to random, single-stranded RNA sequences. In the denatured single-stranded form, RNA owns the ability to absorb light more strongly relative to the hybrid duplex form. The stable WC hydrogen bonding interactions in

between the hybrid RNA strands can be disrupted by denaturing agents such as formamide, urea and heat. Therefore, thermal denaturation provides a measure of RNA thermal stability by monitoring the % changes in hyperchromicities at 260 nm with increasing temperatures. The experiment yields a phase transition (helix-coil transition) or denaturation curve signaling the transition of an RNA hybrid duplex to single stranded form. The midpoint of this curve provides the melting temperature (T_m ºC) at which 50% of the RNA duplex has denatured to single-stranded form. The higher the melting temperature the more stable the RNA hybrid structures (**Figure 2.5**).

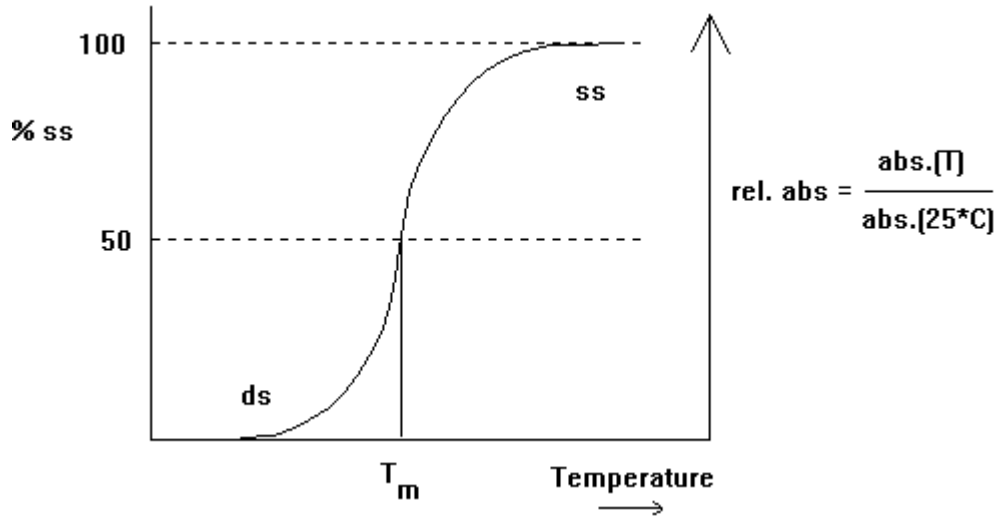

Figure 2.5 A typical melting curve of a hybrid RNA duplex.

Melting experiments have been used to determine the thermal stabilities of homopurine-homopyrimidine oligonucleotide duplexes. In these experiments, RNA hybrids were found to be more stable when compared to DNA or DNA:RNA hybrids[(rPu)(rPy) > (rPu)(dPy) > (dPu)(dPy) > (dPu)(rPy)].[46] The inherent stabilities of RNA hybrids has been related to their conformational properties, in which the more compact C3'-endo RNA conformation contributes to a tighter, more stable hybrid assembly.[47] Thus, RNA may function as a stable template for the self-assembly of higher-order RNA structures.

2.2.8 CD spectroscopy analysis of RNA

The chiral, optical activity of RNA is results from its ability to absorb and rotate circularly polarized light in the far-UV region (200-300 nm). The frequency dependent differences in the absorption of circularly polarized light provides a circular dichroism (CD) signal indicative of the RNA secondary structure in solution. The CD spectra of duplex RNA hybrids are indicative of an A-type RNA helical trajectory (**Figure 2.6**). A typical A-type RNA CD spectra features a positive maximum band near 260 nm and negative minima near 210 nm and also in between 235-250 nm.[48] The amplitude of the positive band is usually within 7-12 M^{-1} cm^{-1} depending on the base sequence. Another important characteristic of the CD spectra of the A-type RNA hybrids is the peak intensity in between 235-250 nm is present as a larger minimum when compared to the peak intensity at 210 nm; whereas the maximum positive band at 260 nm is typically broad and intense.

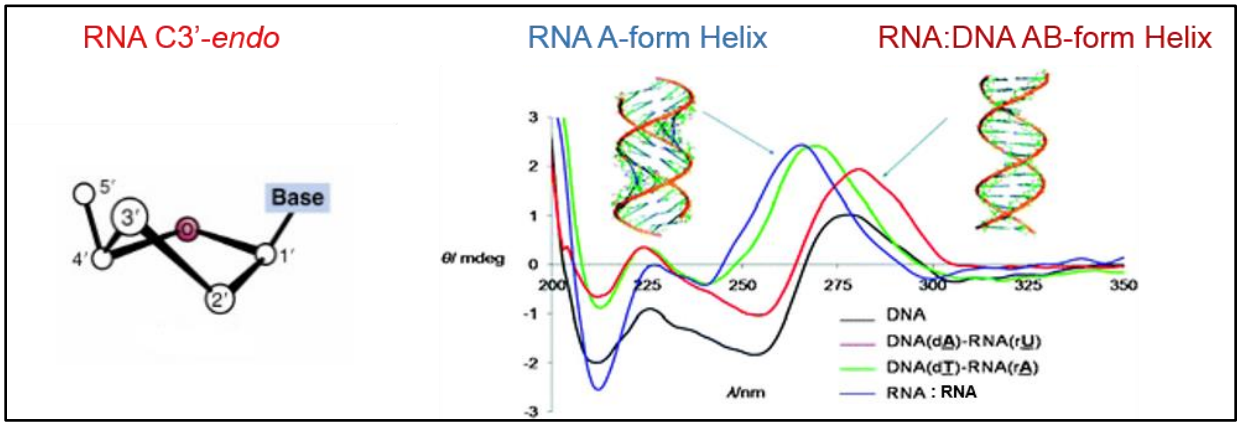

Figure 2.6. Structure of the A-type RNA hybrid duplex and the corresponding CD spectrum.

2.3 PROJECT OBJECTIVES

Inspired by the widespread biological function of self-assembled RNA hybrids, this chapter examines the requirements for efficient RNA hybridization and self-assembly. This study is important for the design and selection of complementary RNAs and the buffer conditions that can facilitate efficient hybridization and self-assembly into 3CS. The 3CS RNA structure is composed of a linear template strand with base-pairing fidelity which guides the self-assembly with two complementary RNA sequences (**Figure 2.7**). The 3CS is anticipated to be tightly held together in favorable buffer conditions. In order to evaluate this hypothesis, solid-phase RNA synthesis, purification, hybridization and stability studies of the RNA hybrids are reported in this chapter. The hybridization capabilities of the 3CS was evaluated in different buffering conditions in order to analyze the effect of the buffer on RNA hybrid stability. The RNA 3CS were characterized by PAGE analysis in order to determine the hybridization capabilities. UV-thermal denaturation analysis validated the hybrid stabilities in the various buffer systems. Meanwhile, CD spectroscopy provided insights on the influence of sequence composition and buffer on RNA secondary structure. At the end of this study, optimized conditions for stable RNA hybrid formation are described for the efficient self-assembly of RNA hybrids that may have useful applications as RNA nanomedicines (Chapter 3).

2.4 CRITERIA FOR STABLE RNA HYBRIDIZATION AND SELF-ASSEMBLY

A rising interest in the structure and stability of RNA hybrids is in part based on the development of regulatory, non-coding RNAs such as siRNA and miRNA that have been successfully applied in the gene therapy of infectious and metabolic disorders, including cancer.[49] RNA conformation, primary sequence composition, and secondary structure each contribute to the stability of RNA hybrids. Moreover, external factors such as choice of solvent, sample and salt concertation, buffer composition and pH changes each contribute to the self-assembly and hybridization potential of RNA. In our design for studying the influence of intrinsic and external factors on RNA self-assembly and hybridization, a template RNA was used to pre-organize the self-assembly of complementary RNA sequences that led to the formation of stable RNA 3CS (**Figure 2.7**). In order to gain a better understanding of the requirements for the efficient self-assembly of higher-order RNA 3CS factors such as, 1) sequence composition, 2) secondary structure, 3) buffer conditions were explored and optimized to provide the most efficient conditions for RNA hybridization and self-assembly.[50-54]

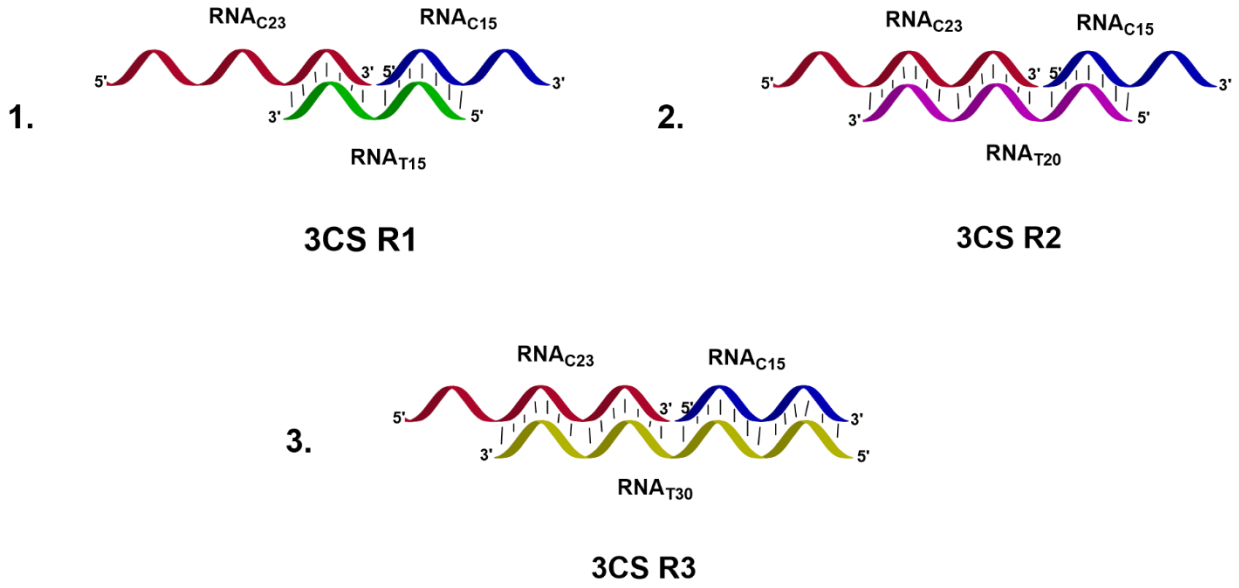

Figure 2.7 Schematic representation of RNA hybrid three component system (3CS). RNA complemtary strands **RNA$_{C15}$** (Blue) and **RNA$_{C23}$** (Red) shown to hybridize with RNA templates **RNA$_{T15}$** (Green), **RNA$_{T20}$** (Pink), **RNA$_{T30}$** (Yellow) to form the three component hybrids **1** (**3CS R1**), **2** (**3CS R2**) and **3** (**3CS R3**).

The sequence composition of RNA is of prime importance due to its implications in secondary and tertiary structure folding.[54] In terms of the individual purines and pyrimidine nucleobases found within RNA, the absence of the 5'-methyl group in uracil contributes to a small decrease in base-pairing free-energy when compared to the base-pairing capabilities of thymine. In addition, the greater number of G:C base pairs within the RNA primary sequences has also been shown to increase the hybridization stability. This is due to the increase in number of H-bonding interactions found within the G:C base pairs (3) when compared to the A:U base pairs (2).[55] Long RNA sequences are known to fold onto themselves (self-folding) into secondary and tertiary structures that are typically associated with proteins (e.g. rRNA, tRNA). RNA self-folding is based on Watson-Crick and Hoogsteen base pairing interactions and must be taken into account when selecting RNA templates and complementary strands that can participate in efficient cross-pairing interactions while minimizing self-folding effects.[54]

The RNA conformation of the phosphodiester backbone also plays an important role in the hybridization and self-assembly of complementary sequences.[55] The secondary structure of double stranded RNA typically forms A-type helical structures, due to the pre-organized ribose sugar pucker which adopts a *Northern* or C3'-*endo* geometry. In this conformation, the C3' and C5' carbons lie above the median plane defined by C1'-O4'-C4' such that the C5'-C3'-phosphate diester bond distance is reduced to 5.9 Å, resulting in a more compact and thermodynamically stable duplex formation, (**Figure 2.6**).[56]

Many comparative thermodynamic stability studies according to the nearest-neighboring effect (based on sequence composition) have been accomplished on RNA:RNA, DNA:DNA, and DNA:RNA hybrid systems.[51,53,57-59] However, these studies limit the contributing effects of external factors, such as salt composition and concentration, buffer pH changes on stable hybrid formation. RNAs are dependent on a variety of cations found in salt buffers, and their concentrations influence RNA hybridization and self-assembly. In the presence of high salt concentration (1 M NaCl), stable RNA hybrids persist although RNA hybridization and self-assembly has also been shown to efficiently occur at physiological salt concentrations (100 mM NaCl and $MgCl_2$). The monovalent (Na^+, K^+) and divalent (Mg^{2+}) cations have profound effects on RNA hybrid stability that cannot be ignored.[60] In general, the presence of monovalent cations enhances thermal stability (T_m) of the hybrid duplex but the divalent cations stabilizes the duplex more effectively. These cations are considered to have different binding sites on the ribonucleotides; with Na^+ coordinating preferentially with the phosphate group and Mg^{2+} with the N7 of purine bases, including those found in the major and minor groove of RNA hybrids.[61,62] Therefore, the base sequence composition and the ionic strength of monovalent and divalent cations play an important role in RNA hybrid duplex stability.[51]

2.5. EXPERIMENTAL SECTION

2.5.1 Solid Phase Synthesis of Linear RNA Sequences

The RNA sequences synthesized in this study (**Table 2.1**) were chosen for their assembly into the three component hybrid systems (3CS). The automated solid-phase synthesis cycle for RNA was accomplished on a nucleoside derivitized controlled pore glass (CPG) support using the ABI 3400 automated solid-phase DNA/RNA synthesizer. The first step involved removal of the 5′-dimethoxytrityl (DMT) group in acidic conditions (i.e. 3% trichloroacetic acid in dichloromethane) followed by coupling of the ribonucleoside phosphoramidites in the presence of an activating reagent (i.e. ethylthiotetrazole). Any unreacted starting material was capped by an acetylation reaction followed by oxidation of the phosphite to the phosphate triester backbone and continuation of the synthesis cycle to generate the full length oligonucleotide. Following cleavage of the oligonucleotide from the solid-support and deprotection of phosphate and nucleobase protecting groups using alkaline conditions (i.e. 3:1 v/v NH_4OH:EtOH), crude RNAs were subjected to 2′-desilylation reactions in a triethylamine trihydrofluoride/DMSO mixture. Deprotected crude RNAs were desalted by precipitation in cold *n*-butanol, centrifuged down and dried after decanting *n*-butanol. The dried RNA pellets were then dissolved in autoclaved water for further analysis.

Table 2.1 Characterization data for the RNA sequences synthesized in this study.

No.	Name	Sequence[a]	Size[b]	%Crude[c] Purity	%Yield[d]	%Purity[e]	MW (g/mol)[f] Observed	Calculated
4.	RNA_{I15}	5'-CAG UGG AAU CCA GGA-3'	15	97	90	99	4838.6	4838.5
5.	RNA_{I20}	5'-GCA GUG GAA UCC AGG ACG CA-3'	20	92	87	98	6453.8	6453.6
6.	RNA_{I30}	5'-AUA GCA GUG GAA UCC AGG ACG CAC CGA AGC-3'	30	91	86	98	9681.1	9681.0
7.	RNA_{38}	5'-ACG CGC UUC GGU GCG UCC UGG AUU CCA CUG CUA UGG AC-3'	38	88	84	99	12009	12009
8.	RNA_{C15}	5'-UCC ACU GCU AUC CAC-3'	15	93	89	99	4633	4632.8
9.	RNA_{C23}	5'-ACG CGC UUC GGU GCG UCC UGG AU-3'	23	90	87	98	7411	7411.8

Characterization data for sequences synthesized in this study. [a]Sequence composition, [b]size of the RNA sequence, [c]%crude yields were determined by UV-Vis Spectroscopy, [d]%yield of isolated RNA pure product obtained, [e]%purity determined by reverse-phase ion-pairing HPLC on a WATERS Symmetry C-18 reverse phase column (4.6 x 150 mm, 5 μm particle size) using gradient of 10-95% (20% MeCN in 0.1M TEAA) over 23 minutes. [f]Molar mass (g/mol) were calculated from the oligo-analyzer software provided by IDT (https://www.idtdna.com/calc/analyzer) and the experimental masses (g/mol) were obtain from ESI-MS analyses in negative mode (NOVATIA LLC, Newton PA)

2.5.2 Purification and Mass Analysis of RNA Sequences

The crude RNA sequences were analyzed by IP-RP-HPLC to determine crude purities. Briefly, HPLC analyses (0.1 OD) and purification (1 OD) were performed on a Waters® 2695 Alliance Separations Module. Crude RNA templates were dissolved in autoclaved water (1 mL) and injected into a Waters® Symmetry C-18 reverse phase column (4.6 x 150 mm, 5 µm particle size, 120 Å) heated at 60 ºC. HPLC analyses and purifications were conducted using a gradient of 5-95% eluent B (20% acetonitrile in 0.1 M triethylammnonium acetate) in eluent A (0.1 M triethylammonium acetate) with a HPLC flow rate of 1 mL/min, run times of 26 minutes and with absorbance detection at 260 nm using a Waters 2489 UV/Visible detector. Retention times (min.) and peak areas (% area) were integrated with Empower II (Waters®) and used to confirm RNA purities ≥96% following sample purifications. Following purification, RNA sequences (0.1-0.4 µM) were dissolved in Millipore water (1 mL) and analyzed by Dr. Mark Hail at Novatia LLC, Newtown, PA. Samples were analyzed on an Oligo HTCS equipped ESI/MS in negative mode. The data was obtained and deconvoluted using the ProMass software. Theoretical molecular weights were calculated by entering each sequence identity on IDT OligoAnalyzer. https://www.idtdna.com/calc/analyzer.

2.5.3 Hybridization of RNA Sequences

A 50 µM stock solution of each RNA sample was prepared in autoclaved Millipore H_2O. The templates (1 µL, 50 µM) were added to the each complementary RNA strand (1 µL, 50 µM) in 18 µL of the respective buffer conditions: A) Tris-HCl buffer : 10 mM Tris-HCl, 100 mM NaCl, 50 mM $MgCl_2$, 1 mM EDTA (pH 8.0) (B) Phosphate Buffer : 5 mM Na_2HPO_4, 140 mM KCl, 1 mM $MgCl_2$ (pH 7.2) (C) MES buffer : 250 mM MES, 20 mM $MgCl_2$ (pH 7.6) (D) 30% Sucrose Tris-Acetate buffer : 89 mM Tris Acetate, 2.5 mM EDTA (pH 5.0), to afford the hybrid mixtures

(20 μL, 1 μM). The resulting mixtures were heated to 95 ºC for 3-5 minute in a heating block to denature any high-order structures. The samples were slowly cooled to room temperature (22 ºC) over 2 h followed by overnight storage in the refrigerator at 4 ºC prior to analysis. The RNA hybrid 3CS prepared in this study are represented in **Figure 2.7**.

2.5.4 Native PAGE Analysis of the RNA Hybrids

With hybridized RNA sequences in hand, a native PAGE analysis was conducted in order to evaluate the possibility of RNA hybridization into the 3CS (**Figure 2.8**). The hybridized RNA samples (1 μM), in their respective annealing buffers, were suspended in non-denaturing 30% sucrose loading buffer (5 μL in 5X TBE). RNA hybrid samples were then loaded on an 18% native, non-denaturing PAGE and run at 300 V, 100 mA and 12 W for 2.5 h. Following electrophoresis, the RNA bands were visualized under UV shadowing (260 nm) and stained with a Stains-All (Sigma-Aldrich™) solution.

2.5.5 Thermal Stability of RNA Hybrids

All RNA hybrids were prepared as previously described in the RNA hybridization method. Thermal denaturation of the RNA hybrids was performed using a CARY 3E, UV-Vis spectrophotometer, with a temperature range of 5 – 95 ºC, at a temperature ramping rate of 0.5 ºC /min. The changes in absorption at 260 nm as a function of temperature were collected and the first derivative plot was used to determine the melting temperatures (T_m) of the RNA samples (**Figure 2.9**). The data was transferred and plotted in Microsoft Excel™ and reported as changes in the hyperchromicities (% H) observed at 260 nm as a function of temperature (5 – 95 ºC).

2.5.6 CD Spectroscopic Analysis of RNA Hybrids

RNA hybrid samples were prepared as previously described. RNA samples were then transferred to fused quartz cells (1 cm path length) incubated at 10 ºC under N_2 for 10 minutes prior to spectral acquisition. CD spectra were collected using an AVIV 62A DS CD spectrophotometer as an average of 3 scans with a 1.0 nm band width interval and a 0.5 nm step interval. CD spectra were analyzed in between 210 and 310 nm, blank corrected and smoothed prior to analyses (**Figure 2.10**). The raw data was exported into Microsoft Excel™ and plotted as changes in molar ellipticities (θ) with increasing wavelengths (210 – 310 nm).

2.6 RESULTS AND DISCUSSION

The template RNA strands were designed and synthesized as 15-30 nt long sequences that favor Watson-Crick (WC) base pairing with the 15 nt and 23 nt long RNA complementary strands without producing self-folded structures. More specifically, three RNA template strands were designed and synthesized: **RNA$_{T15}$**, **RNA$_{T20}$**, and **RNA$_{T30}$** (**4**-**6**) to hybridize with two complementary RNA sequences **RNA$_{C15}$** and **RNA$_{C23}$** (**8**, **9**). The hybridization of these RNA sequences into the putative 3CS was assessed by native PAGE in order to evaluate the influence of the length and base sequence composition of the guiding template strands and the complementary RNA sequences, in addition to the role of the buffer and its cation concentrations on hybrid RNA stability. The hybrid 3CS was found to be most favored in Tris buffer (**Figure 2.8A**), based on the larger proportion of self-assembled RNAs that were found to be more retained on the gel relative to the non-hybrid sequences, which migrated faster and were visualized towards the bottom of the gel. The Tris buffer conditions contained the highest concentration of monovalent (Na^+) and divalent (Mg^{2+}) cations which have been reported to provide greater stability in RNA secondary and tertiary structure folding.[63-66] Moreover, the combination of two complementary strands **RNA$_{C15}$** and **RNA$_{C23}$** (**8**, **9**) that have RNA sequence lengths of 15 and 23 nt respectively, were found to have little hybridization propensity with the template sequence **4**, **RNA$_{T15}$**, composed of 15 nt. In this case, the poor hybridization and self-assembly can be attributed to minimal WC base pairing interactions between the pairing RNA strands (**Figure 2.8, lanes 1**). When the template strands were increased to 20 nt or greater, **RNA$_{T20}$**, and **RNA$_{T30}$** (**5**-**6**) hybridization is observed with the complementary RNA sequences **RNA$_{C15}$** and **RNA$_{C23}$** (**8**, **9**). The multiple bands observed in lanes 2 of the gel suggests the formation of duplex RNA hybrids with the 20 nt RNA template, **RNA$_{T20}$**, (**5**) in place of the anticipated 3CS. The hybridization

propensity improves and favors the formation of the desired 3CS when the template strand is lengthened to a 30 nt RNA sequence **RNA_{T30}**, (**6**) **Figure 2.8, lanes 3**. The 30 nt long RNA complementary strand formed a completely stable 3CS by effectively increasing the WC base-pairing interactions. These lengthier sequences also contain a greater proportion of G:C base-pairs that contribute to more stable self-assembly. These trends were found to be consistent in phosphate, Tris and MES buffer conditions but with little hybridization detected in the sucrose buffer conditions (**Figure 2.8**). The self-assembled RNA hybrids were subsequently studied for their thermal stabilities (T_m) and structural (CD) properties.

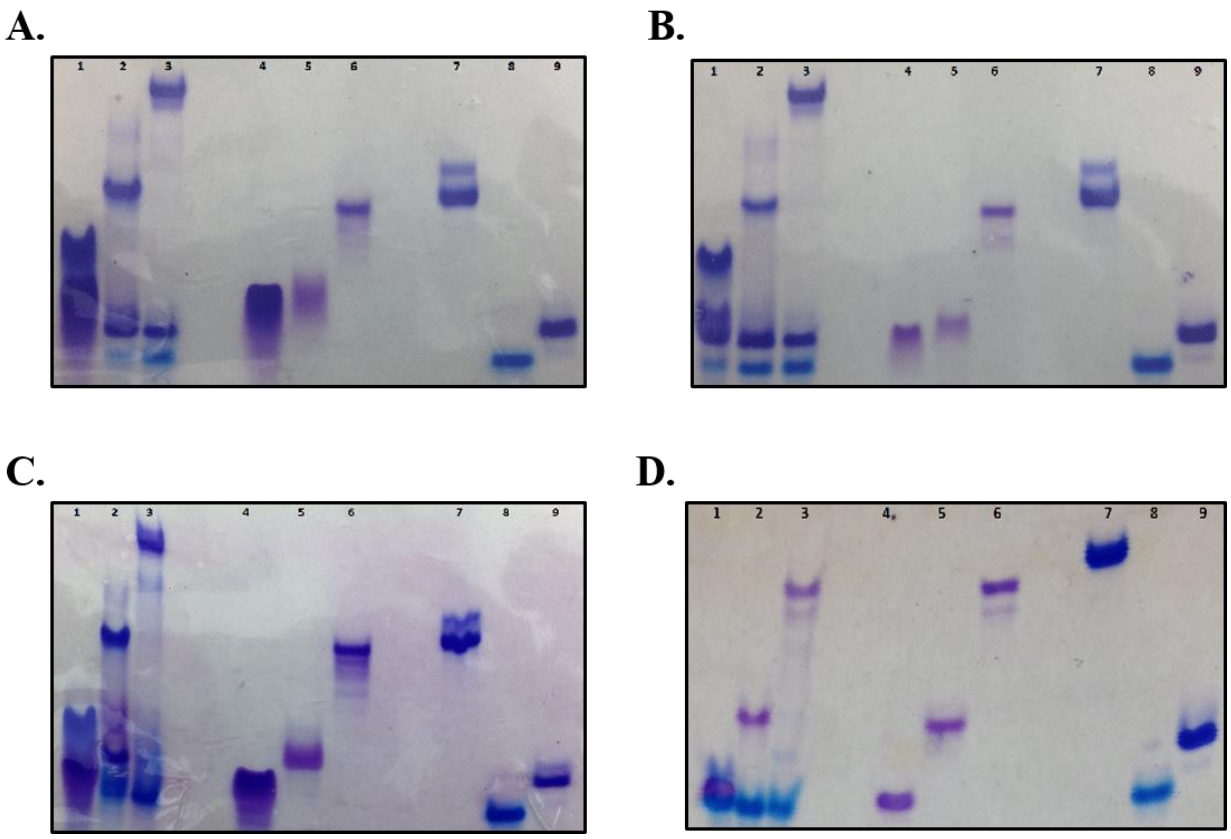

Figure 2.8 Native 18% PAGE analysis for RNA 3-component hybrid system. Analysis of RNA hybrid 3CS for the stability analysis. 3CS hybrid samples (0.75 μmol) were prepared by annealing equimolar quantities of complementary RNAs and template RNA sequences at 95 °C for 2-3 min in 20 μL of respective buffer followed by incubation (37 °C) for 14 h. (**A**) Tris-HCl buffer : 10 mM Tris-HCl, 100 mM NaCl, 50 mM $MgCl_2$, 1 mM EDTA (pH 8.0) (**B**) Phosphate Buffer : 5 mM Na_2HPO_4, 140 mM KCl, 1 mM $MgCl_2$ (pH 7.2) (**C**) MES buffer : 250 mM MES, 20 mM $MgCl_2$ (pH 7.6) (**D**) 30% Sucrose Tris-Acetate buffer : 89 mM Tris Acetate, 2.5 mM EDTA,(pH 5.0). Lanes 1-3: 3-component system using complementary RNA strands **RNA$_{C15}$** and **RNA$_{C23}$** (**8**, **9**) with RNA templates **RNA$_{T15}$**, **RNA$_{T20}$** and **RNA$_{T30}$** (**4-6**), Lanes 4-6: RNA **15**, **20**, **30nt** (**4-6**), Lanes 7: RNA **38nt** (**7**), Lanes 8, 9: RNA **15**, **23nt** (**8**, **9**) complementary sequences.

The thermal denaturation of the hybrid RNA 3CS was tested in Tris, Phosphate MES and sucrose buffer conditions using UV-Vis spectrophotometry (**Figure 2.9**). In Tris buffer, the thermal denaturation data indicated a single phase duplex to single strand transition for the R2 3CS, whereas little hybridization stability was observed for the R1 3CS and multiple transitions for the more stable R3 3CS. This data correlates nicely with the gel data observed in **Figure 2.8A**, which indicated little hybridization of the 3CS assembled with the shorter 15 nt RNA template and validated by the thermal denaturation curve of R1 3CS, duplex formation with the 3CS assembled with the 20 nt template and confirmed with the thermal denaturation curve of R2 3CS and a stable 3CS RNA hybrid structure with the 30 nt RNA template which displayed multiple phase transitions in the case of R3 3CS. These results underscore the importance of the lengthy, 30 nt RNA template for the stable self-assembly of the RNA 3CS in Tris buffer conditions. The phosphate and MES buffer conditions indicated similar trends, albeit with lower T_m values observed for the helix-to-coil transitions (Table 2.2). More specifically, a ΔT_m: +9 ºC was observed for the R3 3CS in Tris buffer when compared with the MES buffer conditions. In addition, the T_m values of the R3 3CS also increased with the addition of divalent Mg^{2+} cations in the Tris buffer conditions, underscoring the importance of divalent cations on the stability of the hybrid RNA 3CS. Comparatively, the sucrose buffer conditions failed to produce a thermally stable RNA hybrid. This result is unsurprising considering the lack of stabilizing counterions in the sucrose buffer. Taken altogether, the thermal denaturation experiments serves to support the hybridization trends delineated from the native PAGE assays. That is, the RNA 3CS effected by the hybridization of the template 30 nt RNA, **RNA$_{T30}$**, (**6**) with the complementary RNA strands, **RNA$_{C15}$** and **RNA$_{C23}$** (**8**, **9**) forms the most thermally stable RNA 3CS, R3 3CS, in Tris buffer (**Figures 2.8 and 2.9**).

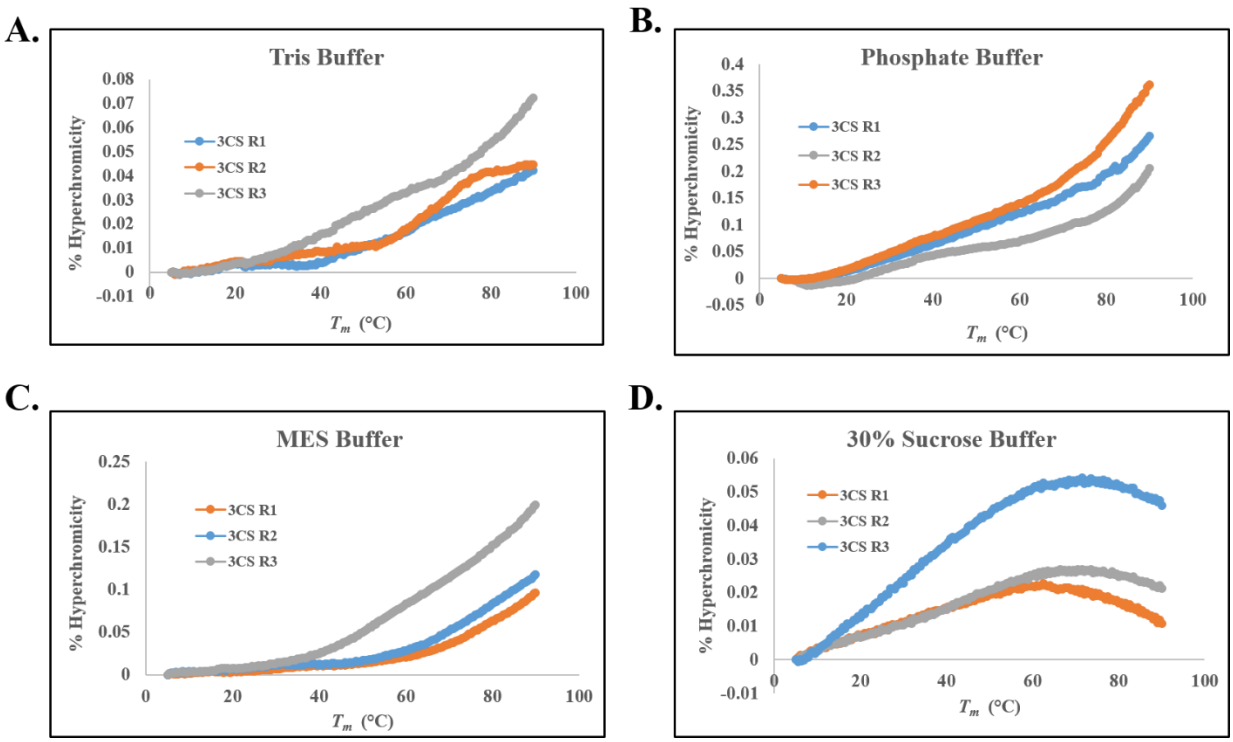

Figure 2.9 Thermal denaturation of the RNA 3-component hybrid system. The thermal stability of the RNA hybrid 3CSR1, R2 and R3 in (A) Tris-HCl buffer : 10 mM Tris-HCl, 100 mM NaCl, 50 mM MgCl2, 1 mM EDTA (pH 8.0) (B) Phosphate Buffer : 5 mM Na_2HPO_4, 140 mM KCl, 1 mM $MgCl_2$ (pH 7.2) (C) MES buffer : 250 mM MES, 20 mM $MgCl_2$ (pH 7.6) (D) 30% Sucrose Tris-acetate buffer : 89 mM Tris Acetate, 2.5 mM EDTA, (pH 5.0). Data was collected on a Cary 3E UV/Vis Spectrophotometer at 260 nm with temperature ranging from 5-90 ºC at a heating rate of 0.5 ºC/min. The data was transported to Excel and plotted as changes in hyperchromicity versus temperature. The T_m (ºC) of the curve was calculated from the first derivative plot which represents the value at which 50% of the hybrid dissociated to single strands.

Tris Buffer	T_m **(1)**	T_m **(2)**
3CS R1: RNA_{C15}+RNA_{C23}+RNA_{T15}	55 ºC	-
3CS R2: RNA_{C15}+RNA_{C23}+RNA_{T20}	34 ºC	67 ºC
3CS R3: RNA_{C15}+RNA_{C23}+RNA_{T30}	45 ºC	77 ºC
Phosphate Buffer		
3CS R1: RNA_{C15}+RNA_{C23}+RNA_{T15}	51 ºC	-
3CS R2: RNA_{C15}+RNA_{C23}+RNA_{T20}	31 ºC	64 ºC
3CS R3: RNA_{C15}+RNA_{C23}+RNA_{T30}	39 ºC	74 ºC
MES Buffer		
3CS R1: RNA_{C15}+RNA_{C23}+RNA_{T15}	58 ºC	-
3CS R2: RNA_{C15}+RNA_{C23}+RNA_{T20}	67 ºC	-
3CS R3: RNA_{C15}+RNA_{C23}+RNA_{T30}	42 ºC	68 ºC
30% Sucrose Buffer		
3CS R1: RNA_{C15}+RNA_{C23}+RNA_{T15}	47 ºC	-
3CS R2: RNA_{C15}+RNA_{C23}+RNA_{T20}	49 ºC	-
3CS R3: RNA_{C15}+RNA_{C23}+RNA_{T30}	44 ºC	-

Table 2.2 The thermal denaturation (T_m, ºC) data of the RNA hybrid 3CS in different buffer conditions.

The CD spectra, of the RNA hybrids in the tested buffer conditions generally maintained the canonical A-type RNA helical geometry (**Figure 2.10**). This conformation was characterized by the strong positive absorption bands at 260 nm and the negative absorption bands at 210 nm and in between 235-250 nm. The RNA hybrid R1 3CS formed with the 15 nt RNA template, **RNA_{T15}, 6**, and the complementary RNA strands, **RNA_{C15}** and **RNA_{C23}** (**8**, **9**) indicated a decrease in the molar ellipticities at these characteristic wavelengths. This result indicates a decrease in the stability of the A-type helical arrangement for the R1 3CS. When the template strand was lengthened to the 30 nt, **RNA_{T30}, 8**, much more intense molar ellipticities were observed at 260 nm and 235-250 nm correlating a stable A-type helix for the R3 3CS. The R3 3CS maintained a stable A-type helix in all buffer conditions indicating the importance of the lengthy RNA template strand in the preorganization of the RNA hybrid structure.

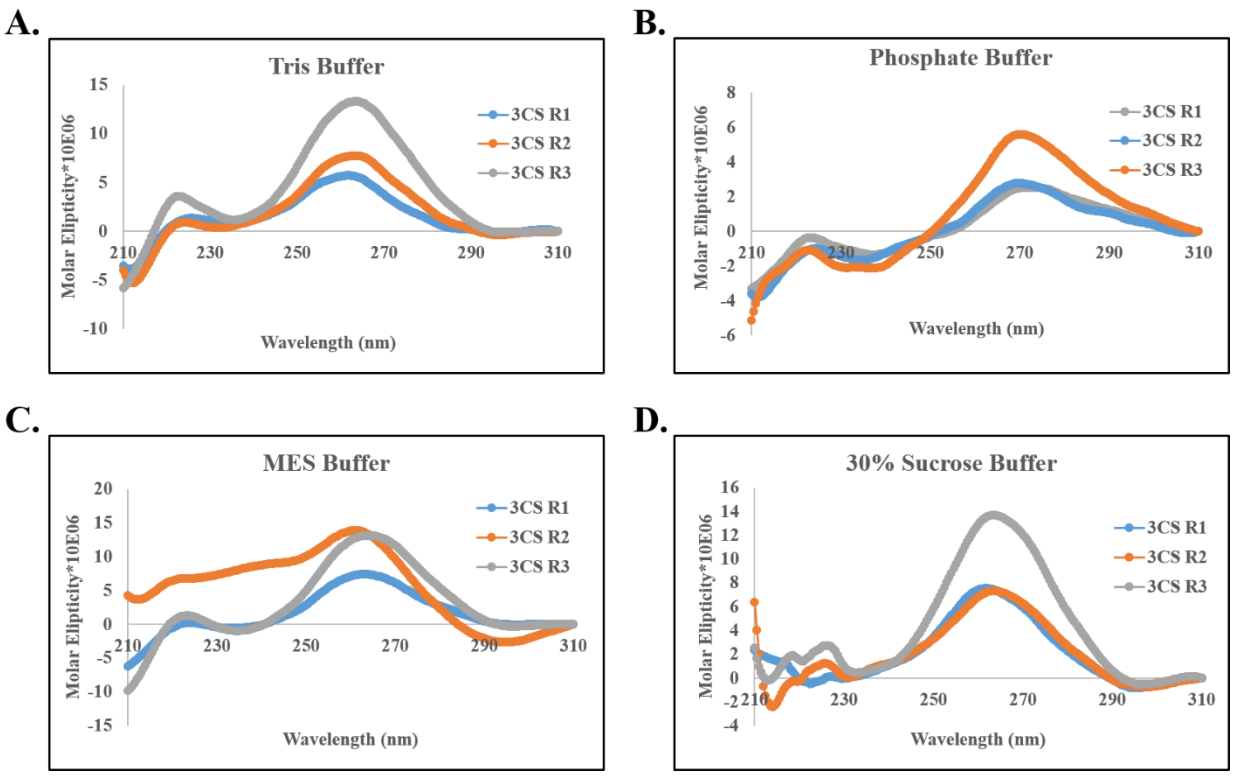

Figure 2.10 Circular dichroism spectra of the RNA 3CS R1, R2 and R3in (**A**) Tris-HCL buffer : 10 mM Tris-HCl, 100 mM NaCl, 50 mM $MgCl_2$, 1 mM EDTA (pH 8.0) (**B**) Phosphate Buffer : 5 mM Na_2HPO_4, 140 mM KCl, 1 mM $MgCl_2$ (pH 7.2) (**C**) MES buffer : 250 mM MES, 20 mM $MgCl_2$ (pH 7.6) (**D**) 30% Sucrose Tris-Acetate buffer : 89 mM Tris Acetate, 2.5 mM EDTA,(pH 5.0). Circular Dichorism (CD) Spectrophotometer (Model: Aviv 62A DS). CD spectra were collected on an average of three scans using 1 nm bandwidth and 0.5 min step size at 25 ºC from 310-210 nm. Samples were blank corrected, smoothed and the data converted to molar ellipticity values from the equation $[\theta] = \theta /cl$, where θ is the relative ellipticity (mdeg), c is the molar concentration of the 3CS (µM) and l is the path length of the cell (1 cm). The data was imported into Microsoft Excel and the CD spectra were plotted in terms of molar ellipticity vs wavelength.

2.7 CONCLUSIONS

In this chapter, the stable three component (3CS) RNA hybridization conditions have been evaluated. The solid-phase synthesis of RNA was used to synthesize RNA template strands (**RNA_{T15}**, **RNA_{T20}**, **RNA_{T30}**) and RNA complementary strands (**RNA_{C15}**, **RNA_{C23}**, **RNA_{C30}**). All RNA sequences were purified by IP RP HPLC and their mass identities were confirmed by ESI-MS. In order to promote a stable RNA three component hybrid system, the effect of the RNA template and complementary strands length and composition in varying buffer conditions were tested. The native PAGE analysis confirmed the hybridization capabilities of the RNA strands to generate the hybrid 3CS. Furthermore, the thermal denaturation experiments confirmed the thermal stability of the RNA hybrid 3CS containing the 30 nt template strand, **RNA_{T30}** hybridized with the complementary 15 and 23 nt RNA strands, **RNA_{C15}**, **RNA_{C23}** in Tris buffer. The RNA hybrid 3CS secondary structures were confirmed as A-type helical geometries by CD spectroscopy. This data also confirmed the most stable helical arrangement for the RNA 3CS composed of the template 30 nt RNA along with the complementary 15 nt and 23 nt RNA strands in Tris buffer conditions. This study revealed the importance of RNA hybridization conditions in the design of RNA self-assembled hybrids. These structures may have biological importance and therapeutic relevance for cancer gene therapy applications (Chapter 3).

2.8 REFERENCES

1) Caruthers, M.H. *J. Biol. Chem.* **2013**, *288*, 1420-1427.
2) Beckert, B.; Masquida, B. *Methods Mol. Biol.* **2011**, *703*, 29-41.
3) Sherlin, L.D.; Bullock, T.L.; Nissan, T.A.; Perona, J.J.; Lariviere, F.J.; Uhlenbeck, O.C.; Scaringe, S.A. *RNA* **2001**, *7*, 1671-1678.
4) Marshall, W.S.; Kaiser, R.J. *Curr. Opin. Chem. Biol.* **2004**, *8*, 222-229.
5) Verma, S.; Eckstein, F. *Annu. Rev. Biochem.* **1998**, *67*, 99-134.
6) Letsinger, R.L.; Mahadevan, V. *J. Am. Chem. Soc.* **1965**, *87*, 3526-3527.
7) Ellington, A.; Pollard, J.D. Jr. *Curr. Protoc. Mol. Biol.* **2001**, Chapter-2:Unit2, *11*.
8) Stetsenko, D.A.; Malakhov, A.D.; Gait, M.J. *Org. Lett.* **2002**, *4*, 3259-3262.
9) Zhang, X.; Gaffney, B.L.; Jones, R.A. *Nucleic Acids Res.* **1997**, *25*, 3980-3983.
10) Azhayev, A.V. *Tetrahedron*, **1999**, *55*, 787-800.
11) Pon, R.T.; Yu, S. *Nucleic Acids Res.* **1997**, *25*, 3629-3635.
12) Dell'Aquila, C.; Imbach, J.; Rayner, B. *Tetrahedron Lett.* **1997**, *38*, 5289-5292.
13) Patnaik, A.K.; Rao, N.S.; Kumar, P.; Sharma, A.K.; Garg, B.S.; Gupta, K.C. *Helv. Chim. Acta* **2000**, *83*, 322-327.
14) Somoza, A. *Chem. Soc. Rev.* **2008**, *37*, 2668-2675.
15) Shiba, Y.; Masuda, H.; Watanabe, N.; Ego, T.; Takagaki, K.; Ishiyama, K.; Ohgi, T.; Yano, J. *Nucleic Acids Res.* **2007**, *35*, 3287-3296.
16) Iyer, R.P.; Kuchimanchi, S.N.; Panday, R.K. *Drugs Fut.* **2003**, *28*, 51.
17) Usman, N.; Ogilvie, K. Jiang, M.Y.; Cedergren, R.J. *J. Am. Chem. Soc.* **1987**, *109*, 7845-7854.
18) Maina, A.; Blackman, B.A.; Parronchi, C.J.; Morozko, E.; Bender, M.E.; Blake, A.D.; Sabatino, D. *Bioorg. Med. Chem. Lett.* **2013**, *23*, 5270-5274.
19) Westheimer, F.H.; Huang, S.; Covitz, F. *J. Am. Chem. Soc.* **1988**, *110*, 181-185.
20) Sontakke, V.; Shinde, V.S.; Lonnberg, H.; Ora, M. Eur. *J. Org. Chem.* **2014**, *22*, 6806-6813.
21) Wyatt, J.R.; Chastain, M.; Puglisi, J.D. *Biotechniques* **1991**, *11*, 764-769.
22) Kelmers, A.D.; Noveli, G D.; Stulberg, M.P. *J. Biol. Chem.* **1965**, *240*, 3979-3983.
23) Wincott, F.; DiRenzo, A.; Shaffer, C.; Grimm, S.; Tracz, D.; Workman, C.; Sweedler, D.; Gonzalez, C.; Scaringe, S.; Usman, N. *Nucleic Acids Res.* **1995**, *23*, 2677-2684.
24) Fountain, K.J.; Gilar, M.; Gebler, J.C. *Rapid Commun. Mass Spectrom.* **2003**, *17*, 646-653.
25) Dickman, M.J.; Hornby, D.P. *RNA* **2006**, *12*, 691-696.
26) McCarthy, S.M.; Gilar, M.; Gebler, J. *Anal. Biochem.* **2009**, *390*, 181-188.
27) Gilar, M.; Fountain, K.J.; Budman, Y.; Neue, U.D.; Yardley, K.R.; Rainville, P.D.; Russell, R.J. 2nd.; Gebler, J.C. *J. Chromatogr. A* **2002**, *958*, 167-182.
28) Snyder, L.R.; Stadalius, M.R.; Quarry, M.A. *Anal. Chem.* **1983**, *55*, 1412-1430.
29) Azarani, A.; Hecker, K.H. *Nucleic Acids Res.* **2001**, *29*, e7.
30) Ketterer, T.; Von Der Mulbe, F.; Reidel, L.; Mutzke, T. *United States patent* US 8,383,340, **2013**.
31) Rio, D.C.; Ares, M.; Hannon, G J.; Nilsen, T.W. *Cold Spring Harb. Protoc.* **2010**, *469*, 189-208.
32) McMaster, G.K.; Carmichael, G.G. *Proc. Natl. Acad. Sci. USA* **1977**, *74*, 4835-4838.
33) Lehrach, H.; Diamond, D.; Wozney, J.H.; Boedtker, H. *Biochemistry* **1977**, *16*, 4743-4751.

34) Lima, W.F.; Monia, B.P.; Ecker, D.J.; Freier, S.M. *Biochemistry* **1992**, *31*, 12055-12061.
35) Woodson, S.A.; Koculi, E. *Methods Enzymol.* **2009**, *469*, 189-208.
36) Afonin, K.A.; Bindewald, E.; Yaghoubian, A.J.; Voss, N.; Jacovetty, E.; Shapiro, B.A.; Jaeger, L. *Nat. Nanotechnol.* **2010**, *5*, 676-682.
37) Lemay, J.; Lefontaine, D.A. *RNA* **2007**, *13*, 339-350.
38) Weeks, K.M.; Crothers, D.M. *Biochemistry* **1992**, *31*, 10281-10287.
39) Meng, Z.; Limbach, A.P. *Brief Funct. Genomic. Proteomic.* **2006**, *5*, 87-95.
40) Crain, P.F.; McCloskey, J.A. *Curr. Opion. Biotechnol.* **1998**, *9*, 25-34.
41) Lin, Z.J.; Li, W.; Dai, G.J. *Pharm. Biomed. Anal.* **2007**, *44*, 330-341.
42) Thomas, B.; Akoulitchev, A.V. *Trends Biochem. Sci.* **2006**, *31*, 173-181.
43) Pieles, U.; Zurcher, W.; Schar, M.; Moser, H.E. *Nucleic Acids Res.* **1993**, *21*, 3191-3196.
44) Stanssens, P.; Zabeau, M.; Meersseman, G.; Remes, G.; Gansemans, Y.; Storm, N.; Hartmer, R.; Honisch, C.; Rodi, C. P.; Bocker, S.; Van den Boom, D. *Genome Res.* **2004**, *14*, 126-133.
45) Thuring, K.; Schmid, K.; Keller, P.; Helm, M. *Methods* **2016**, doi: 10.1016/j.ymeth.2016.03.019. [Epub ahead of print].
46) Venkiteswaran, S.; Vijayanathan, V.; Shirahata, A.; Thomas, T.; Thomas, J.T. *Biochemistry* **2005**, *44*, 303-312.
47) Gyi, J.I.; Conn, G.L.; Lane, A.N.; Brown, T. *Biochemistry* **1996**, *35*, 12538-12548.
48) Romainczyk, O.; Endeward, B.; Prisner, T.F.; Engels, J.W. *Mol. Biosyst.* **2011**, *7*, 1050-1052.
49) Carthew, R.W.; Sontheimer, E.J. *Cell* **2009**, *136*, 642-655.
50) Guo, P. *J. Nanosci. Nanotechnol.* **2005**, *5*, 1964-1982.
51) Nakano, S.; Fujimoto, M.; Hara, H.; Sugimoto, N. *Nucleic Acids Res.* **1999**, *27*, 2957-2965.
52) Hopkins, F.J.; Panja, S.; McNeil, A.S.; Woodson, A.S. *Nucleic Acids Res.* **2009**, *37*, 6205-6213.
53) Lesnik, A.E.; Freier, M.S. *Biochemistry* **1995**, *34*, 10807-10815.
54) Draper, E.D. *Biophys. J.* **2008**, *95*, 5489-5495.
55) Roberts, R.W.; Crothers, D.M. *Science* **1992**, *258*, 1463-1466.
56) Egli, M.; Saenger, W. "Principle of Nucleic Acid Structure" *Springer-Verlag*, **1984**.
57) Venkiteswaran, S.; Vijayanathan, V.; Shirahata, A.; Thomas, T.; Thomas, J.T. *Biochemistry* **2005**, *44*, 303-312.
58) Xia, T.; SantaLucia, J.; Burkard, E.M.; Kierzek, R.; Schroeder, J.S.; Jiao, X.; Cox, C.; Turner, H.D. *Biochemistry* **1998**, *37*, 14719-14735.
59) Freier, S.M.; Kierzek, R.; Jaeger, J.A.; Sugimoto, N.; Caruthers, M.H.; Neilson, T.; Turner, D.H. *Proc. Natl. Acad. Sci. USA* **1986**, *83*, 9373-9377.
60) Draper, E.D. *RNA* **2004**, *10*, 335-343.
61) Bukhman, Y.; Draper, E.D. *J. Mol. Biol.* **1997**, *273*, 1020-1031.
62) Philips, A.; Milanowska, K.; Lach, G.; Boniecki, M.; Rother, K.; Bujnicki, J.M. *Bioinfomatics* **2012**, *28*, 198-205.
63) Soukup, A.G.; Breaker, R.R. *RNA*, **1999**, *5*, 1308-1325.
64) Lambert, D.; Leipply, D.; Draper, D.E. *J. Mol. Biol.* **2009,** *390*, 791-804.
65) Koculi, E.; Hyeon, C.; Thirumalai, D.; Woodson, S.A. *J. Am. Chem. Soc*. **2007**, *129*, 2676-2682.
66) Klein, D.J.; Moore, P.B.; Steitz, T.A. *RNA* **2004**, *10*, 1366-1379.

CHAPTER 3: RNAi NANOTECHNOLOGY: APPLICATIONS OF siRNA NANOSTRUCTURES IN RNAi SCREENING AND CANCER GENE THERAPY

3.1 ABSTRACT

The emerging field of RNA nanotechnology has been used to design well-programmed, self-assembled nanostructures for applications in chemistry, biology and medicine. At the forefront of its utility in cancer is the unrestricted ability to self-assemble multiple siRNAs within a single nanostructure formulation for the RNAi screening of a wide range of oncogene targets while potentiating cancer gene therapy effects. In our RNAi nanotechnology approach, V- and Y-shape RNA templates were designed and constructed for the self-assembly of discrete, higher-ordered siRNA nanostructures targeting the oncogenic glucose regulated chaperones. The GRP78-targeting siRNAs self-assembled into genetically encoded spheres, triangles, squares, pentagons and hexagons of discrete sizes and shapes according to TEM imaging. Furthermore, gel electrophoresis, thermal denaturation and CD spectroscopy validated the prerequisite siRNA hybrids for their RNAi application. In a 24 sample siRNA screen conducted within the AN3CA endometrial cancer cells known to overexpress tumorigenic GRP78, the self-assembled siRNAs targeting multiple sites of GRP78 mRNA demonstrated more potent and long-lasting anticancer activity relative to their linear controls. Extending the scope of our RNAi screening approach, the self-assembled siRNA hybrids (5 nM) targeting of GRP-75, 78 and 95 resulted in significant (50-95%) knockdown of the glucose regulated chaperones, which led to synergistic effects in tumor cell cycle arrest (50-80%) and death (50-60%) within endometrial (AN3CA), cervical (HeLa) and breast (MDA-MB-231) cancer cell lines. Interestingly, a non-cancerous lung (MRC5) cell line

displaying normal glucose regulated chaperone levels was found to tolerate siRNA treatment and demonstrated less toxicity (5-20%) relative to the cancer cells that were found to be addicted to the glucose regulated chaperome. These remarkable self-assembled siRNA nanostructures may thus encompass a new class of potent siRNAs that may be useful in screening important oncogene targets while improving siRNA therapeutic efficacy and specificity in cancer.

3.2 INTRODUCTION

3.2.1 Discovery and Functions of GRPs

The discovery of the Glucose Regulated Proteins (GRPs) in 1977 by Pastan and co-workers occurred thorough the keen observation that two proteins of 78 and 94 KDa were strongly induced in chicken embryo fibroblasts cultured in glucose-free medium.[1] These proteins were subsequently identified as GRP78 (also referred to as the immunoglobulin binding protein Bip and HSPA5) and GRP94 (also identified as gp96 and HSP90B1). GRP94 is the most abundant glycoprotein in the endoplasmic reticulum (ER). GRP78 is evolutionarily conserved from yeast to humans and abundantly located in the lumen of the ER. Although GRP78 and GRP94 are primarily located in the ER, they are also found in several other subcellular compartments such as the mitochondria, the plasma membrane and the cytosol where they display a myriad of functions. Another important GRP includes GRP75 (also known as mortalin/heat shock protein 70, HSP70/HSPA9) which was first identified and characterized by Welch and co-workers in 1989.[2] GRP75 is primarily localized in the mitochondria, and related forms may also be found in the cytosol or on the surface of the extracellular membrane. The glucose regulated proteins, GRP-75, 78 and 94 are stress-inducible molecular chaperones belonging to heat-shock protein (HSP) family.[3] The GRPs serve multiple functions related to chaperoning ER protein translocation, folding, quality control and export to a variety of organelles for function. The GRPs own subcellular localization is in the endoplasmic reticulum where it chaperones protein folding activity, in the mitochondria where it interacts with pro-apoptotic executors and at the cell surface where it directs cell signaling activity.[11] More specifically, GRPs guide misfolded proteins towards processing and degradation by the unfolded protein response (UPR) mechanism and can signal a variety of anti- and pro-apoptotic pathways (i.e. caspase activation) that regulate cell survival (**Figure 3.1**). In the UPR mechanism, ER stress

signaling stimulates the release of sequestered GRP78 from protein kinase like ER kinase (PERK), inositol requiring enzyme 1 (IRE1) and activating transcription factor 6 (ATF6).[11-14] This results in PERK-catalyzed phosphorylation of the eukaryotic initiation factor 2 alpha (eIF2α), preventing the translocation of additional proteins in the ER for protein translation.[13] Dimerization of IRE1 results in endoribonuclease activity which splices XPB1 mRNA for the expression of a basic leucine zipper family of transcription factors that assists in the production of chaperone proteins.[14] Similarly, ATF6 is cycled into the Golgi where it is cleaved and released into a functional transcription factor that promotes the expression of the GRPs that assists in protein folding as part of the UPR mechanism.[12] In this manner, the UPR elevates GRP expression levels and activity to release the ER biosynthetic burden in stressed cells.[11] Therefore, GRPs are known to maintain cellular integrity and homeostasis under physiological or pathological stress conditions. During physiological stress in the presence of misfolded proteins, hypoxia, embryonic development and aging, GRPs bind ATP to regulate Ca^{2+} flux and to facilitate protein folding events which inhibits the activation of pro-apoptotic executors and maintains normal cellular function under stressed conditions.[3-5] Therefore, the GRPs function as part of a cluster of proteins referred to as the chaperome which surveils cellular insults under stressed conditions and mitigates their impact on cellular malfunction. Therefore, GRP induction is an indicator of ER stress and many studies have revealed their activation mechanisms and intracellular signaling pathways.[4,5] Cellular stress due to protein misfolding occurs by intrinsic and extrinsic factors, including altered cell metabolism, hyperproliferation, hypoglycemia, hypoxia, acidosis, viral infection and genetic lesions that may also lead to cancer initiation.[3,9]

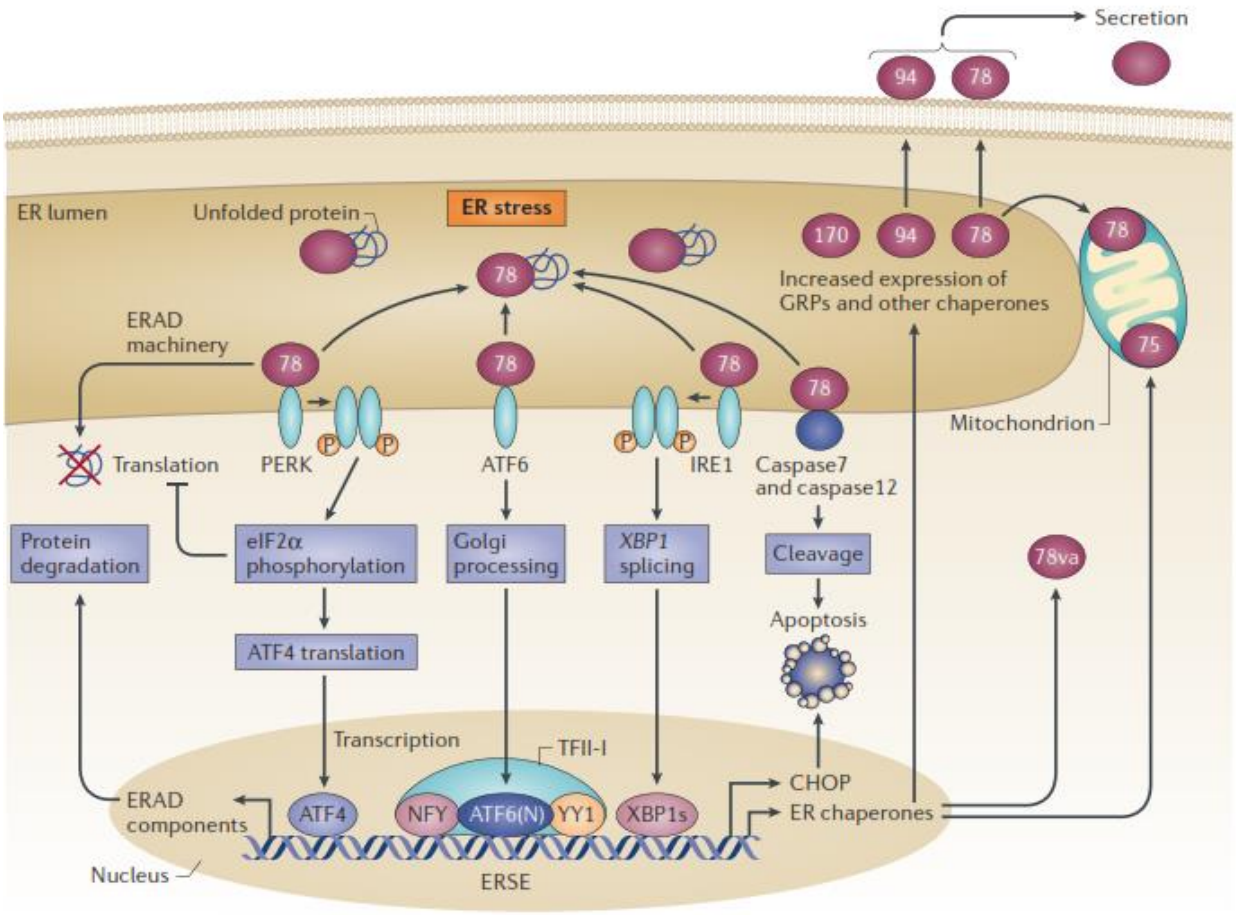

Figure 3.1 GRPs function in unfolded protein response and stress response. Figure has been adapted from ref 15: Lee, A.S. *Nat. Rev. Cancer* **2014**, *14*, 263-276.

3.2.3 Roles of GRPs in Cancer

Due to their induction during pathological stress conditions, GRPs have also been implicated in tumorigenic activity. Many studies have shown that the aggressive growth and invasive properties of many cancer types are due to the distinctive functions of GRP overexpression, especially related to GRP-75, 78 and 94 (**Table 3.1**).[15] For example, GRP78 regulates cancer cell viability and apoptosis by maintaining a balance in between ER protein folding events and the release of pro-apoptotic executors from their inactive state.[6] While GRP94 has been found to be essential in the processing of proteins that have been implicated in tumorigenesis, such as the insulin-like growth factor 1 (IGF-1), Toll-like receptors (TLRs) and integrins.[7] Also, GRP75 interacts with the tumor suppressor p53, inactivating the capacity of p53 to arrest cell growth and to trigger apoptosis at the onset of cancer.[8]

Type of Cancer	GRP78	GRP94	GRP75
Bladder	+		
Brain	+		+
Breast	+	+	+
Colorectal	+	+	+
Endometrial	+		
Esophageal	+	+	
Gastric	+	+	
Head and Neck	+	+	
Leukemia	+		+
Liver	+	+	+
Lung	+	+	+
Melanoma	+		
Multiple myeloma	+	+	
Nasopharyngeal		+	
Oral	+	+	
Osteosarcoma		+	
Ovarian	+		+
Pancreatic	+	+	+
Prostate	+		
Renal	+		
Thyroid			

Table 3.1 Overexpression of GRPs in different types of cancers. Table adapted from reference 15, Lee, A.S. *Nat. Rev. Cancer* **2014**, *14*, 263-276.

GRP78 has been found to play a pivotal role in promoting the inhibition of cell apoptosis under pathological stress conditions that have resulted in the progression, invasion and the rise of treatment resistance of cancer.[15] Contributing to the pathological role of GRP78 in cancer is an overexpression and cell surface localization which functions as a signaling receptor for oncogenic activity.[16] Interestingly, GRP-75, 78 and 94 have all been found on the surface of cancer cell types but not on normal tissues making them clinically relevant biological markers for the specific detection and treatment of cancer.[17] Moreover, GRP78 is associated with other stress-inducible members of the GRP family of chaperones, including GRP-75 and 94 which altogether form members of the cancer chaperome that contributes to the progression of some of the most aggressive and resilient forms of cancers.[15] Thus, GRPs play important roles in regulating a variety of essential functions in cancer through a UPR-dependent and independent manner. As an ER chaperone, GRP78 controls processing and maturation of a wide range of cell surface receptors and secretory proteins that are crucial for the ability of cancer cells to respond to extrinsic proliferative signals.[3] Furthermore, GRP78 has also been found to stabilize Wnt-β-catenin in the ER by regulating Wnt proliferative signaling.[18] Under hypoxic conditions GRP78 dissociates from Wnt inhibiting its function leading to proteasome degradation and reduced Wnt secretion. GRP78 has also been implicated in protein transport, such as the MTJ-1 (murine tumor cell DnaJ-like protein 1) in macrophages and PAR-4 (Prostate apoptosis response 4), which promotes cancer cell proliferation.[19,20] GRP78 also serves as a multifunctional receptor in prostate cancer cells in the activated form with the plasma proteinase inhibitor α2-macroglobulin (α2-M*), which triggers ERK (extracellular signal-regulated kinases) and AKT (also known as Protein kinase B, PKB) activation. This signaling pathway results in increased levels of DNA and protein synthesis that contribute to cancer cell proliferation and the inhibition of apoptosis.[21,22] In human leukemic cells,

the overexpression of GRP78 led to increased PI3K (Phosphoinositide 3-kinase) and PIP3 (Phosphatidylinositol (3,4,5)-trisphosphate) production.[23] Cell surface interactions in between GRP78 and Cripto-1 (also known as teratocarcinoma-derived growth factor 1) have also been implicated in the activation of the oncogenic MAPK and PI3K pathways and modulating activing-A, activing-B, nodal and transforming growth factor-β1 signaling activity.[24]

GRP94 controls the maturation and secretion of the important mitogenic insulin growth factors, IGFs which leads to the activation of the oncogenic PI3K-AKT cell growth signaling pathway.[25] Deletion of GRP94 in B-cells[26] and macrophages[27] have resulted in the attenuation of multiple myeloma and inflammatory colorectal cancer. Conversely, GRP94 overexpression was shown to enhance the growth of breast cancer cells under chronic exposure to reactive oxygen species (ROS).[28] This effect was counteracted by the production of antioxidants and the formation of disulfide bonds in proteins located in the ER.[28] The down-regulation of p53 target genes such as *Cdkn1a* and *Mdm2* have also been correlated with an overexpression of GRP75. In this case, GRP75 functions as a mitochondrial protein importer due to its ability to sequester p53 in the cytoplasm of neuroblastomas.[29] The mitogenic activities of fibroblast growth factor-1 (FGF-1) in association with GRP75 has also shown enhanced endothelial cell migration and proliferation.[30]

Recently, a close functional relationship between the GRP78, the pro-apoptotic protein BIK (BCL2 interacting killer) and anti-apoptotic protein BCL-2 (B-cell lymphoma 2) suggests that GRP78 and BCL-2 form separate complexes with the different domains of BIK.[31] The high levels of GRP78 resulted in BIK sequestration, which led to the inhibition of the BCL-2:BIK binding interaction, resulting in the relocation of the downstream pro-apoptotic protein BAX (Bcl-2-associated X protein) into the mitochondria. This led to the inhibition of cytochrome c release into the cytosol which prevented cellular apoptosis and triggered oncogenic activity in breast cancer.[31]

Moreover, cell surface GRP78 along with PAR4 (Protease-activated receptor 4) prevents TNF-related apoptosis-inducing ligand (TRAIL) apoptosis activation in HeLa[20] and MDA-MB-231[32] cells and therefore functions as a pro-survival factor. GRP78 and GRP94 overexpression is associated with lymph node metastasis and carcinoma recurrence, and silencing of GRP94 was found to inhibit migration and proliferation of MDA-MB-231 breast cancer cells *in vitro*.[28] More recently, the whole cell surface expression levels of GRP78 and GRP94 in HeLa cells were observed following treatment with BFA (brefeldin A) in the absence and presence of the ER stress stimuli Tg (thapsigargin) and Tu (tunicamycin). This treatment resulted in suppressed cell surface expression of GRP78 and GRP94.[33] The effect of chemotherapy drugs on MDA-MB-231 breast cancer cells was enhanced by siRNA mediated silencing of GRP78, which was implicated in drug resistance.[34] In comparison with normal healthy cells, GRP75/Mortalin was significantly up-regulated in the cytoplasm of breast cancer MDA-MB-231 cells according to an immunofluorescence (IF) assay.[35] Therefore, Mortalin/GRP75 has also been implicated as a biomarker for cancer therapy and for the prognostic evaluation of breast cancer progression.[35] The overexpression of Mortalin/GRP75 protein coincides with the acquisition of invasiveness, contribution to proliferation, anti-apoptosis, ATP production, chaperoning and inactivation of tumor suppressor p53 and PI3K/AKT activities.[36] Targeting of Mortalin by siRNA[37], ribozymes[38] and small molecules[39] resulted in growth arrest and led to apoptosis of cancer cells. Another interesting study showed the functional role and mechanism of cell surface GRP75 in HSPG (heparan sulfate proteoglycan core protein) mediated endocytosis of macromolecule magnetic nanoparticles in HeLa cells.[40] Interaction between caspase-7 and GRP78 at the ATP-binding site leads to inhibition of apoptotic event. (-)-Epigallocaterchin Gallate (EGCG) treatment of etoposide-treated MDA-MB-231 cells prevented the formation of the inhibitory complex

compromising endogenous GRP78 and caspase-7, which contributed to development of drug resistance.[41] The overexpression of wild-type tumor suppressor BRCA1 (breast cancer 1) was found to suppress the expression of GRP78 in cancer cells. siRNA mediated silencing of BRCA1 showed enhanced level of GRP78, GRP94 and CHOP indicating survival of cancer cell by GRP-78 and 94. The simultaneous knockdown of GRP78 and BRCA1 by siRNA showed increase sensitivity towards apoptosis in breast cancer cells (MDA-MB-231, MCF-7) and ovarian cancer cells (OVCAR-3).[42] Moreover, GRP78 overexpression also been linked with the progression of endometrial cancer (EC). GRP78 has been implicated in EC cell proliferation according to cell cytotoxicity and proliferation assays which underscored the role of GRP78 within the AN3CA EC cells. Reduction of GRP78 by siRNA knockdown was found to attenuate the invasion rate and led to the inhibition of cell growth resulting in apoptosis in EC cells.[43,44] Thus, GRP knockdown or inhibition has been shown to sensitize cancer cells to treatment, trigger tumor cell cycle arrest and apoptosis resulting in potent anticancer effects.[15,28,45-49] Thus, GRP78 and the related GRPs have been validated as clinically relevant molecular targets in cancer.[15]

3.2.4 siRNA Nanostructures for Cancer Gene Therapy

Gene therapy has re-emerged as a powerful modern day treatment modality in the search for a cure for cancer.[50] Several cancer gene therapy methods have already been realized *in vitro*, as well as *in vivo*, paving the way for their successful use in human clinical oncology.[51] Leading the way are the growing applications of siRNA in cancer therapy.[52] Technological advances in synthetic biology have ushered in a new wave of modified siRNAs that have improved the silencing of oncogenic mRNA expression ultimately resulting in tumor cell death.[53] This RNAi mechanism has shown exceptional catalytic efficacy and tolerance for a wide range of modified

siRNAs that can effectively screen a variety of oncogene targets while potentiating gene silencing effects.[54]

The rise of RNA nanotechnology has led to the evolution of functional RNA materials for a variety of applications, including the development of nanomedicines.[55,56] Recently, siRNA nanostructures have been formulated and applied for silencing single or multiple gene targets. For example, hybrid RNA nanocubes composed of six double-stranded dsRNA Dicer substrates have been formulated and shown to simultaneously release multiple siRNAs in breast cancer cells upon Lipofectamine-mediated transfection.[57] The intracellular release of the siRNAs was found to trigger the RNAi response and effectively down-regulated the reporter, enhanced green fluorescent protein, (eGFP) for up to twelve days. In a related case study, multifunctional RNA nanorings embedding six siRNAs within the nanoparticle formulation were shown to silence eGFP expression at concentrations as low as 1 nM.[58] Moreover, the siRNA nanoparticles were functionalized with RNA aptamers which were selected for binding to the epidermal growth factor receptor (EGFR) overexpressed on human breast cancer cells. These RNA nanoparticles demonstrated targeted tumor binding and cellular uptake, which led to persistent eGFP knockdown over a nine day period. This effect was found to be equivalent to the transfection of the linear eGFP-siRNAs at six-fold higher concentrations. In another proof-of-concept study, the branched siRNA nanostructures targeting multiple mRNA sites of the luciferase firefly reporter gene were shown to self-assemble into three- and four-way junctions.[59] These nanoparticle formulations released multiple siRNAs upon Dicer cleavage and effectively silenced luciferase activity for up to five days in HeLa cells. Taken altogether, these representative examples demonstrate the ability for higher-ordered siRNA nanostructures to behave as Dicer substrates, resulting in the release of multiple siRNAs that are processed by the RNAi mechanism, ultimately leading to synergistic

gene knockdown effects. These results underscores the potential utility of siRNA nanostructures in RNAi screening and cancer gene therapy applications.

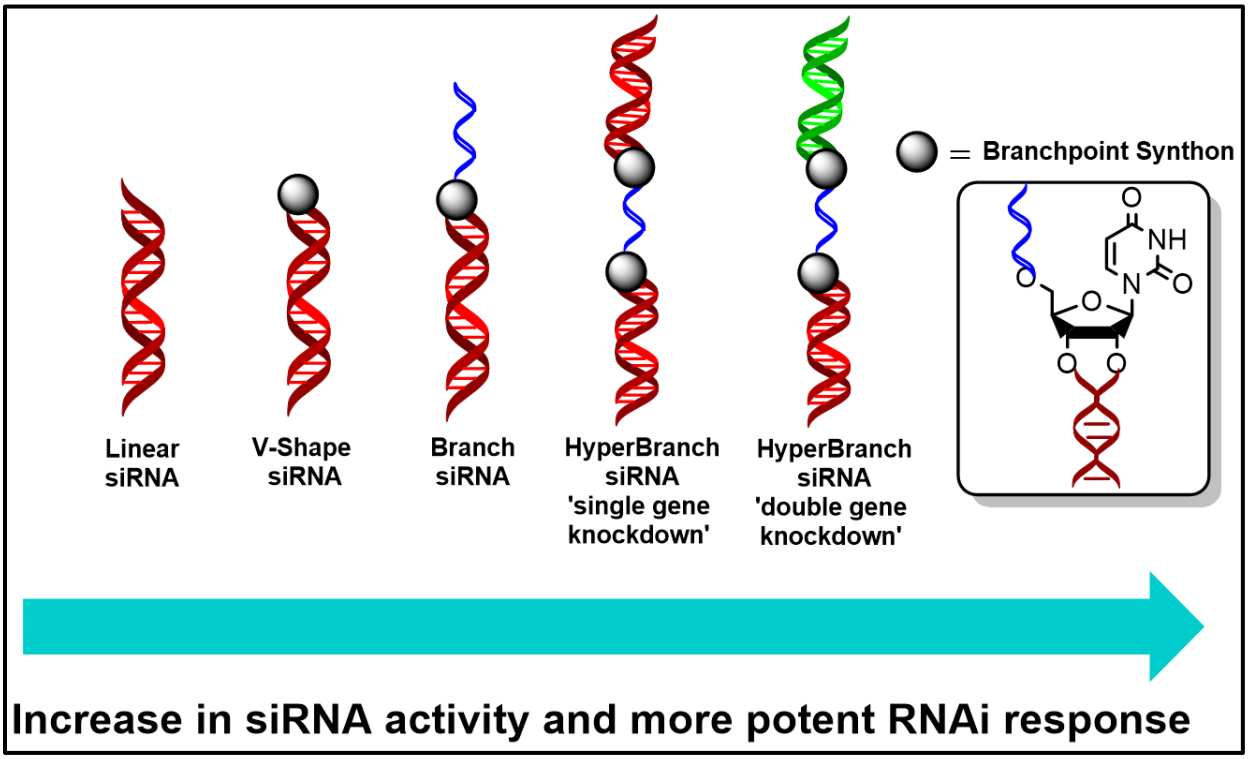

Figure 3.2 Assembly of GRP78 targeting V-shape, Y-branch and >-< hyperbranch siRNAs based on the ribouridine branchpoint phosphoramidite synthon.[60]

We previously reported the synthesis, characterization and RNAi evaluation of branch and hyperbranched siRNAs (**Figure 3.2**).[60] These novel molecular structures were built by semi-automated solid phase RNA synthesis and incorporated a branchpoint synthon which facilitated the extension of single or double siRNAs targeting the GRP78 oncogene. The branch and hyperbranch siRNAs led to 50-60% silencing of GRP78 expression which translated to approximately 20% cell death of the HepG2 liver cancer cells.[60] Therefore, the branch and hyperbranch siRNAs have effectively extended the repertoire of modified siRNA motifs that may be useful in the development of more potent RNAi oncogene therapeutics.

3.3 PROJECT OBJECTIVES

Inspired from previous studies in RNA nanotechnology, this chapter will discuss the synthesis, characterization and biological assessment of siRNA nanostructures in human cancer cell lines. The study begins with the design of linear, V-shape and Y-shape RNA templates which target one, two or three sites of oncogenic GRP78 mRNA and those related to the GRP-75 and 94 mRNA sequences.[49,61] The assembly of the complementary linear, V-shape and Y-shape RNA sequences is based on the canonical Watson-Crick Base-pairing interactions that results in the formation of hybrid structures. Moreover, the RNA templates function as guide strands, that pre-organize the self-assembly of hybrid siRNA into higher-order structures having distinct sizes and shapes (**Figure 3.3**). The solid-phase RNA synthesis strategy based on our previous study[60] was used to generate V-shape and Y-shape RNA templates using the ribouridine branch-point synthon (**Figure 3.2**). LCMS was used to characterize the purity and identity of the RNA templates for their self-assembly capabilities. The proposed hybrid siRNA nanostructures were characterized by Polyacrylamide Gel Electrophoresis (PAGE), Thermal Denaturation (T_m) and Circular Dichroism Spectroscopy (CD). The siRNA nanostructures were imaged by Transmission Electron Microscopy (TEM) to provide their distinct shapes and size distributions. Moreover, the application of siRNA nanostructures in cancer cell biology was screened within EC (AN3CA), cervical (HeLa), breast (MDA-MB-231) and within a non-tumorigenic, control lung cell line (MRC5). The study began with the optimization of siRNA transfections using RNAiMAX™, Lipofectamine 2000™ and SilenFect™ within AN3CA EC cells. Next, a 24-siRNA sample screen was conducted within the AN3CA cells to determine the structure-activity relationships (SARs) of the GRP78-targeting siRNAs. The most promising siRNA leads were then selected to further investigate the RNAi mediated GRP78 silencing efficiency. Finally, the most potent Y-shape

siRNA was synthesized for the synergistic knockdown of GRPs (GRP78, GRP94, GRP75), within the GRP overexpressing HeLa (cervical cancer cells), MDA-MB-231 (breast cancer cells), and AN3CA (endometrial) cancer cells and also within the non-cancerous MRC5 (epithelial normal lung) cells displaying normal GRP function. This study will describe a correlation of the GRP silencing effects of the siRNAs with their observed anti-cancer activities. Taken altogether, this combinatorial self-assembly approach has enabled the formulation of a library (30) of siRNA nanoparticles for exploring SARs within GRP overexpressing cancer cell lines.

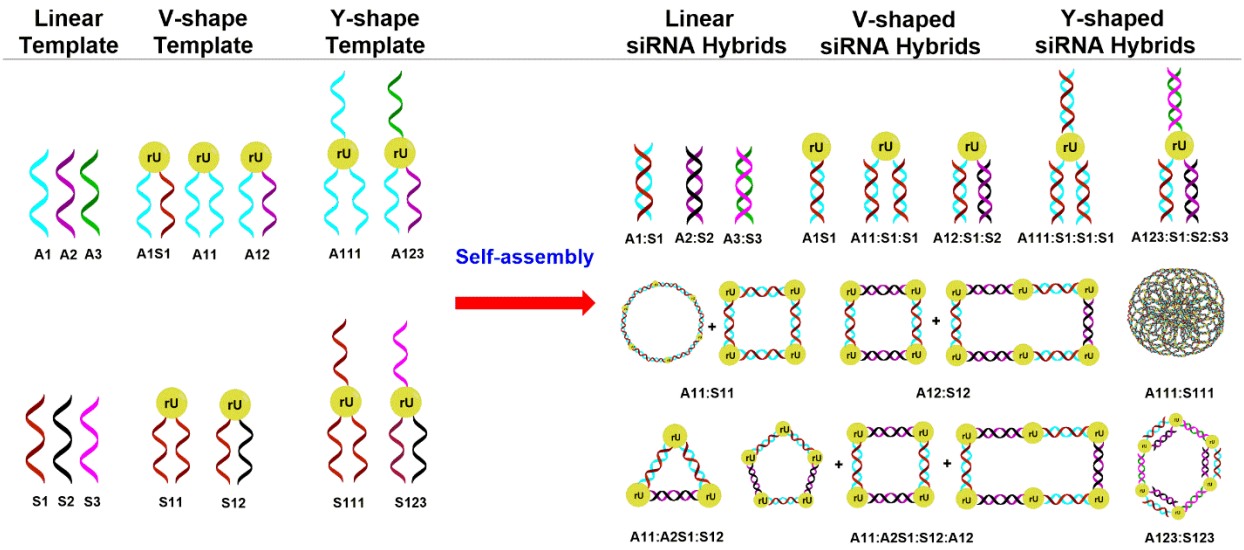

Figure 3.3 Design and self-assembly of siRNA nanostructures. The RNA templates, namely, linear, V- and Y-shaped RNA were designed and synthesized according to our previously described methodology.[56] The V- and Y-shaped templates incorporate a branchpoint ribouridine (rU) which facilitates the incorporation of sense (**S**) and antisense (**A**) RNA. These templates preorganize the self-assembly of siRNA hybrid nanostructures having discrete sizes and shapes, including those belonging to circles, triangles, squares, rectangles, pentagons, hexagons and porous-type structures. These siRNA nanostructures are genetically encoded to target a single (1), double (1, 2) and triple (1, 2, 3) sites of oncogenic GRP-75, 78 and 94 mRNA.

3.4 EXPERIMENTAL SECTION

3.4.1 Solid Phase Synthesis, Cleavage and Deprotection of Linear, V- and Y-shape siRNAs

Synthesis of linear siRNAs were accomplished on the ABI solid-phase RNA synthesizer as previously described in Chapter 2. The solution phase synthesis of orthogonally protected 5'-OLv 2'-OMMT ribouridine phosphoramidite and its incorporation into branch siRNA structures by solid phase RNA synthesis have also been reported in an earlier study.[60] Taking full advantage of this existing methodology, the synthesis of V-shape and Y-shape RNA templates and their complementary sequences **Table 3.2**, were completed on solid-phase. Briefly, the synthesis strategy involves RNA synthesis on the CPG up to the branchpoint ribouridine. The decyanoethylation step using 4:6 v/v Et_3N:MeCN for 90 min was used to remove the phosphate protecting groups in order to make the more stable phosphodiester bond. The next step involved the removal of 2'-MMT protecting group at the branchpoint position. The detritylation reaction was accomplished using 3% DCA:DCM for 3 min to ensure complete deprotection. Elongation of the second RNA sequence at the liberated 2'-OH of the branchpoint synthon afforded the V-shape RNA template. A capping step, resulting in acetylation of the terminal 5'-hydroxyl group was completed in order to prevent side-reactions. The 5'-Lv group at the branchpoint position was removed using 0.5M $NH_2NH_2{\cdot}H_2O$, buffered in 3:2 v/v pyridine:acetic acid for 20 min. Synthesis of the third RNA strand from the branchpoint 5'-position led to the generation of the Y-shape RNA template. Following synthesis, the RNAs were cleaved and deprectected from the CPG solid support. Deprotection of the exocyclic amino nucleobase and cyanoethyl phosphate protecting groups were accomplished using 7:3 v/v NH_4OH: EtOH at 60 ºC for 12-14 h. The 2'-TBDMS protecting groups was desilylated using 1:1.2 v/v trimethylamine-trihydrofluoride TEA-3HF:DMSO at 55 ºC for 2 h. Finally the crude RNA pellets were precipitated in 3M NaOAc (25

μL) and n-BuOH (1 mL). The crude RNA pellets were dissolved in autoclaved, Millipore H_2O for analysis and purification.

3.4.2 RP IP HPLC

The crude RNA templates were analyzed by Reverse Phase Ion Pairing High Performance Liquid Chromatography (RP IP HPLC) to determine crude purities. Briefly, HPLC analyses (0.1 OD) and purifications (1 OD) were performed on a Waters® 2695 Alliance Separations Module. Crude RNA templates were dissolved in autoclaved water (1 mL) and injected into a Waters® Symmetry C-18 reverse phase column (4.6 x 150 mm, 5 μm particle size, 120 Å) heated at 60 ºC. HPLC analyses and purifications were conducted using a gradient of 5-95% eluent B (20% acetonitrile in 0.1 M triethylammnonium acetate) in eluent A (0.1 M triethylammonium acetate). The HPLC flow rate was set at 1 mL/min, with run times of 26 min and with absorbance detection at 260 nm using a Waters® 2489 UV/Visible detector. Retention times (min.) and peak areas (% area) were integrated with Empower II software (Waters®) and used to confirm RNA purities≥96% following sample purifications.

3.4.3 Mass Spectrometry

RNA templates (0.1-0.4 μM) were dissolved in millipore water (1 mL) and analyzed by Dr. Mark Hail at Novatia LLC, Newtown, PA. Samples were analyzed on an Oligo HTCS equipped ESI/MS in negative mode. The data was obtained and deconvoluted using ProMass software. Theoretical molecular weights were calculated by entering each sequence identity on IDT OligoAnalyzer. https://www.idtdna.com/calc/analyzer

3.4.4 siRNA Hybridization

A 50 µM stock solution of each RNA sample was prepared in autoclaved Millipore H_2O. To the templates (20 µL, 50 µM) was added the complementary RNA strands (20 µL, 50 µM) and annealing buffer (60 µL, 50 mM Tris-HCl, pH 8.0, 100 mM NaCl, 5 mM EDTA) to afford the hybrid mixtures (100 µL, 10 µM). The resulting mixtures were heated to 95 ºC for 3-5 min on a heating block, slowly cooled to room temperature (22 ºC) over 2 h and stored in the fridge at 4 ºC overnight (12- 14 h) prior to analysis.

3.4.5 Non-denaturing, Native Polyacrylamide Gel Electrophoresis (PAGE)

The hybridized siRNA samples (20 µM) in annealing buffer (10 mM Tris, 50 mM NaCl, 1 mM EDTA, pH 7.5–8.0, 8 µL) were suspended in 30% sucrose loading buffer (15 µL in 5X TBE). Samples were then loaded on a 16% native, non-denaturing PAGE and run at 300 V, 100 mA and 12 W for 2.5 h. Following electrophoresis, the siRNA bands were visualized under UV shadowing (260 nm) and stained with a Stains-All (Sigma-Aldrich™) solution.

3.4.6 Thermal Denaturation (T_m)

All siRNA hybrids were prepared as previously described in annealing buffer (0.75 µM, 10 mM Tris, 50 mM NaCl, 1 mM EDTA, pH 7.5–8.0, 1 mL). Thermal denaturation of the siRNA hybrids was performed using a CARY 3E, UV-Vis spectrophotometer, from 5 – 95 ºC, with temperature ramping of 0.5 ºC /min. The changes in absorption at 260 nm as a function of temperature was collected and the first derivative plot was used to determine the melting temperatures (T_m) of the siRNA samples. The data was transferred and plotted in Microsoft Excel™ as changes in the hyperchromicities (% H) observed at 260 nm as a function of temperature (5 – 95 ºC).

3.4.7 CD Spectroscopy

siRNA samples were hybridized in annealing buffer (0.75 µM, 10 mM Tris, 50 mM NaCl, 1 mM EDTA, pH 7.5–8.0, 1 mL) as previously described. Samples were then transferred to fused quartz cells (1 cm path length) and incubated at 10 ºC under N_2 for 10 minutes prior to spectral acquisition. CD spectra were collected using an AVIV 62A DS CD spectrophotometer as an average of 3 scans with a 1.0 nm bandwidth interval and a 0.5 nm step interval. CD spectra were analyzed in between 210 and 310 nm, blank corrected and smoothed prior to analyses. The raw data was exported into Microsoft Excel™ and plotted as changes in molar ellipticities (θ) with increasing wavelengths (210 – 310 nm).

3.4.8 TEM Imaging

siRNA hybrid samples (50 µL, 50 µM) were suspended in sodium phosphate buffer (50 mM, pH 7, 1 mL) and sonicated for 15 minutes for complete dissolution. Samples were then mixed in 1:1 v/v ratio with 1% uranyl acetate and sonicated for an additional 10 minutes. An aliquot (5 µL) of siRNA sample was placed on a carbon film coated copper grid, 300 mesh (Electron Microscopy Sciences Inc., Hatfield, PA) dried overnight and viewed under the transmission electron microscope (JEOL, model JEM-1200 EX). Images were taken with a SIA–L3C CCD camera (Scientific Instruments and Applications, Inc.) using the software Maxim DL5 (Diffraction Limited, Ottawa, Canada). TEM images were collected by Dr. Reeta Yadav and Suiying Huang in collaboration with the research group of Dr. Uri Samuni at Queens College in Flushing NY.

3.4.9 Cell Culture

The human normal lung cells MRC5 (ATCC® CCL-171™), endometrial cancer cells AN3CA (ATCC® HTB-111™), breast cancer cells MDA-MB-231 (ATCC® HTB-26™) and

cervical cancer cells HeLa (ATCC® CCL-2™) were purchased from ATCC. All cell based experiments were conducted under the supervision of Drs. John Koren and Gabriela Chiosis at the Memorial Sloan Kettering Cancer Center in New York, NY. The MDA-MB-231, HeLa and MRC5 cells were cultured in Dulbecco's Modified Eagle medium (DMEM) while AN3CA cells were in Minimum Essential Medium (MEM) supplemented with 10% (v/v) Fetal Bovine Serum (FBS) and 1% (v/v) penicillin/streptomycin (P/S) under 5% CO_2 at 37 ºC. For passaging cells were detached with 0.25% trypsin and re-suspended with complete culture medium.

3.4.10 Serum Stability Assay

siRNA hybrid samples (A1:S1, A12:S1:S1, A12:S12 and A123:S1:S2:S3) were hybridized as previously described in annealing buffer (0.75 µM, 10 mM Tris, 50 mM NaCl, 1 mM EDTA, pH 7.5–8.0, 1 mL). An aliquot (10 µL, 5 µM) was added to a 10% FBS solution (40 µL in phosphate buffer). The mixtures were incubated at 37 ºC and periodically (0 – 48 h) sample aliquots (10 µL) were removed and suspended in 1.5X TBE loading buffer (15 µL) and frozen at -80 ºC prior to analyses. Samples were thawed to room temperature (22 ºC) and analyzed on a 16% native, non-denaturing PAGE for 2.5 h. The gel was then visualized with a Stains-All (Sigma-Aldrich™) solution.

3.4.11 siRNA Transfections in AN3CA Cells

Briefly, the AN3CA endometrial cancer cells (ATCC® HTB-111™), 1 x 10^5, were plated in 6-well culture plates containing MEM culture media with 10% FBS. Cells were cultured for 48 h in a humidified incubator set at 37 ºC with 5% CO_2. Prior to transfections, the siRNA hybrids (5 µL, 2.5-12.5 µM, in DMEM, 250 µL) were mixed with the transfection reagents (Lipofectamine 2000™, SilentFect™ or RNAiMAX™, 2.5 – 7 µL in DMEM, 250 µL) according to the

manufacture's recommendation. The mixtures were incubated (10 min, 22 ºC) then added to the AN3CA cell culture and incubated at 37 ºC with 5% CO_2 over a three-day period. Cell growth over time (65-72 h) was monitored in an Incucyte™ (Essen BioScience).

3.4.12 Western Blots

The cell media was aspirated from the transfected culture and washed with PBS buffer for 2-3 min, twice. The cells were lysed using cell lysis buffer (1% Tween-20, 50 mM Tris, 130 mM NaCl, 5 mM EDTA) containing protease inhibitors and phosphatase inhibitors (Protease inhibitor, PSMF, Phos2, Phos3). Protein concentrations of lysates were determined using the BSA protein assay reagent (ThermoFisher Scientific Inc.). Proteins samples (15-20 mg, 20 µL) were dissolved in 5X loading buffer, boiled for 5-7 min, and resolved in 10% sodium dodecyl sulfate polyacrylamide gel electrophoresis (SDS-PAGE). The proteins were electrotransferred onto a polyvinylidene difluoride membrane (Bio-Rad Laboratories), which was blocked in Tris-buffered saline, pH 8.0, Tween-20, 5% (w/v) skimmed milk (TBST solution) for 1 h at room temperature (22 ºC). Membranes were then probed with the indicated primary antibodies (anti-PARP p85 fragment pAb, Promega Inc.; anti-GRP75 mAb, ThermoFisher Scientific Inc and anti-GRP94 pAb; anti-GRP78 pAb, Cell Signaling Inc.) in TBST solution at 4 ºC overnight. Next day, membranes were washed with TBST solution (3X, 10 min each) and incubated with horseradish peroxidase conjugated secondary antibodies (1:3000 v/v) at room temperature for 1 h followed by washing with TBST solution (3X, 10 min each). Immunoblotted protein bands were visualized by enhanced chemiluminescence reagent (ThermoFisher Scientific Inc.) and quantified using NIH imager (ImageJ).

3.4.13 Cell Cytotoxicity

Following transfection with GRPs specific siRNAs, a cytotoxicity assay was performed with all cells using the Cytotoxicity Detection Kit (ThermoFisher Scientific Inc.). With this kit, the rate of cell lysis was monitored by determination of the LDH amount released into the culture medium and quantified at 492 nm by the detection of the red formazan chromophore.

3.5 RESULTS AND DISCUSSION

3.5.1 siRNA Self-Assembly

The siRNA sequences described in this study (**Table 3.2**) are based on the target nucleotides for down-regulating GRP-75, 78 and 94 expression in human cancer cells.[49,61] The linear, V- and Y-shaped RNA templates were synthesized by semi-automated solid phase RNA synthesis following our previously reported procedure.[60] The RNA templates were purified by Reverse-Phase Ion-Pairing High Performance Liquid Chromatography (RP IP HPLC) in ≥96% purities and their identities were confirmed by electrospray ionization mass spectrometry (ESI MS) (**Table 3.2**).

NO.	Name	Sequence[a]	% Yield[b]	% Purity[c]	Mass[d]
1.	A1	5'-AUC AGA AUC UUC CAA CAC U-3'	91%	>99%	5949.6(5949.8)
2.	A2	5'-UCU AGU AUC AAU GCG CUC C-3'	90%	>99%	5958.6(5958.8)
3.	A3	5'-GUA ACA ACU GCA UGG GUA ACC UUC-3'	89%	>99%	7636.6(7636.8)
4.	S1	5'-AGU GUU GGA AGA UUC UGA U-3'	92%	>99%	6103.7(6103.7)
5.	S2	5'-GGA GCG CAU UGA UAC UAG A-3'	91%	>99%	6124.7(6124.2)
6.	S3	5'-GAA GGU UAC CCA UGC AGU UGU UAC-3'	90%	>99%	7653.6(7653.8)
7.	NS_A	5'-AGU UCA ACG AGU AUC AGC A-3'	92%	>99%	6068.7(6068.5)
8.	NS_S	5'-UGC UGA UAC UCG UUG AAC U-3'	91%	>99%	5998.8(5998.6)
9.	A11	2'3'-UCA CAA CCU UCU AAG ACU A-5' rU 3'5'-AUC AGA AUC UUC CAA CAC U-3'	82%	>98%	12266.4(12267.6)
10.	A12	2'3'-CCU CGC GUA ACU AUG AUC U-5' rU 3'5'-AUC AGA AUC UUC CAA CAC U-3'	80%	>99%	12275.4(12277.0)
11.	S11	2'3'-UAG UCU UAG AAG GUU GUG A-5' rU 3'5'-AGU GUU GGA AGA UUC UGA U-3'	83%	>99%	12574.5(12575.5)
12.	S12	2'3'-AGA UCA UAG UUA CGC GAG G-5' rU 3'5'-AGU GUU GGA AGA UUC UGA U-3'	79%	>99%	12595.6(12596.2)
13.	A2S1	2'3'-UAG UCU UAG AAG GUU GUG A-5' rU 3'5'-UCU AGU AUC AAU GCG CUC C-3'	81%	>99%	12429.7(12430.6)
14.	A1S1	2'3'-UAG UCU UAG AAG GUU GUG A-5' rU 3'5'-AUC AGA AUC UUC CAA CAC U-3'	80%	>99%	12421.2(12421.6)
15.	A111	2'3'-UCA CAA CCU UCU AAG ACU A-5' 5'-AUC AGA AUC UUC CAA CAC U-3'5'-U 3'5'-AUC AGA AUC UUC CAA CAC U-3'	71%	>96%	18278.0(18278.4)
16.	A123	2'3'-CCU CGC GUA ACU AUG AUC U-5' 5'-GUA ACA ACU GCA UGG GUA ACC UUC -3'5'-U 3'5'-AUC AGA AUC UUC CAA CAC U-3'	68%	>96%	19975.2(19975.8)
17.	S111	2'3'-UAG UCU UAG AAG GUU GUG A-5' 5'-AGU GUU GGA AGA UUC UGA U-3'5'-U 3'5'-AGU GUU GGA AGA UUC UGA U-3'	70%	>98%	18739.2(18740.6)
18.	S123	2'3'-AGA UCA UAG UUA CGC GAG G-5' 5'- GAA GGU UAC CCA UGC AGU UGU UAC -3'5'-U 3'5'-AGU GUU GGA AGA UUC UGA U-3'	64%	>99%	20531.2(20634.0)
19.	$GRP94_A$	5'-GGU AAU CAG AUG CUU CUU C-3'	93%	>99%	5999.6(5999.8)
20.	$GRP94_S$	5'-GAA GAA GCA UCU GAU UAC C-3'	92%	>99%	6068.7(6068.9)
21.	$GRP75_A$	5'-UUG UAU UCU CCG AGU CAG U-3'	93%	>98%	5976.6(5976.8)
22.	$GRP75_S$	5'-ACU GAC UCG GAG AAU ACA A-3'	91%	>99%	6091.8(6092.0)
23.	GRP7894	2'3'-CUU CUU CGU AGA CUA AUG G-5' rU 3'5'-AUC AGA AUC UUC CAA CAC U-3'	79%	>98%	12929.7(12929.9)
24.	GRP7875	2'3'-UGA CUG AGC CUC UUA UGU U'3' rU 3'5'-AUC AGA AUC UUC CAA CAC U-3'	76%	>98%	12906.7(12906.9)
25.	GRP9475	2'3'-UGA CUG AGC CUC UUA UGU U'3' rU 3'5'-GGU AAU CAG AUG CUU CUU C-3'	75%	>97%	12956.6(12956.8)
26.	GRP789475	2'3'-CUU CUU CGU AGA CUA AUG G-5' 5'-UUG UAU UCU CCG AGU CAG U-3'5'-U 3'5'-AUC AGA AUC UUC CAA CAC U-3'	62%	>97%	18395.9(18396.1)

Table 3.2 [a] Linear sequence number 1,2,3,7,19 and 21 represents antisense (A) siRNA sequence to its complimentary sense (S) sequences 4,5,6,8,20 and 22 respectively. V-shaped siRNA sequences 9-14 contains two siRNA sequences targeting GRP78 mRNA. Y-shaped siRNA sequences 15-18 contains three siRNA sequence targeting three different sites of GRP78 mRNA. Sequences 19-22 are linear siRNA sequences targeting GRP94 and GRP75. Sequences 23-25 are V-shape siRNA targeting two GRP mRNAs and sequence 26 is a Y-shape siRNA targeting three GRP mRNAs (GRP78, GRP94, GRP75). [b] Determined by UV-Vis Spectroscopy. [c] Obtained by RP-IP-HPLC using 0.1 mM TEAA in 0-20% MeCN, pH: 7.2 over 26 min. [d] Calculated mass (observed mass) by ESI-MS in negative mode (Novatia LLC, Newton, PA).

Based on the previous study on the requirements for stable 3CS hybrid formation (Chapter 2), the RNA templates were hybridized with their complementary strands in the stabilizing Tris buffer conditions. Each purified complementary strand was added to their corresponding RNA templates in stoichiometric ratios that favored hybrid formation and self-assembly of the putative siRNA nanostructures (**Figure 3.3**) in annealing buffer (10 mM Tris, 50 mM NaCl, 1 mM EDTA, pH 7.5–8.0, 13-15 μL). Hybridization and self-assembly were promoted by heating the RNA templates and their complementary sequences at 90 ºC (5-10 min) followed by slow cooling to room temperature (22 ºC) for 1 h, and overnight storage at 4 ºC. siRNA hybridization was confirmed by a native, non-denaturing 16% polyacrylamide gel electrophoresis (PAGE). In this assay, (**Figure 3.4**) the lower molecular weight templates (linear, V- and Y-shape RNA) migrated fastest on the gel and were found to be equivalent to the anticipated migration of the 23-50bp RNA ladder. The V-and Y-shaped RNA templates hybridized to their complementary RNA single strands (**Figure 3.4**, lanes 10,11 and lanes 8,9 respectively) migrated slower on the gels, with electrophoretic mobilities which were found to be comparable to the migration of the 30-50bp RNA ladder (V-shape siRNA hybrids, lanes 10,11) and the 150-300bp RNA ladder (Y-shape siRNA hybrids, lanes 8,9). The self-assembled V- (**Figure 3.4**, lanes 4-7) and Y-shape (**Figure 3.4**, lanes 2, 3) siRNA hybrids migrated the slowest on the gels. The self-assembled V-shape siRNA hybrids (lanes 4,5) migrated with similar electrophoretic mobility on gel when compared to the V-shape siRNA

hybrids formed with their complementary linear RNA sequences (lanes 10,11). The siRNA hybrid combinations formed with multiple Y- and V-RNA templates (lanes 2,3 and 6,7, respectively) were found to be ≥300bp RNA ladder suggesting the formation of higher-ordered siRNA nanostructures.

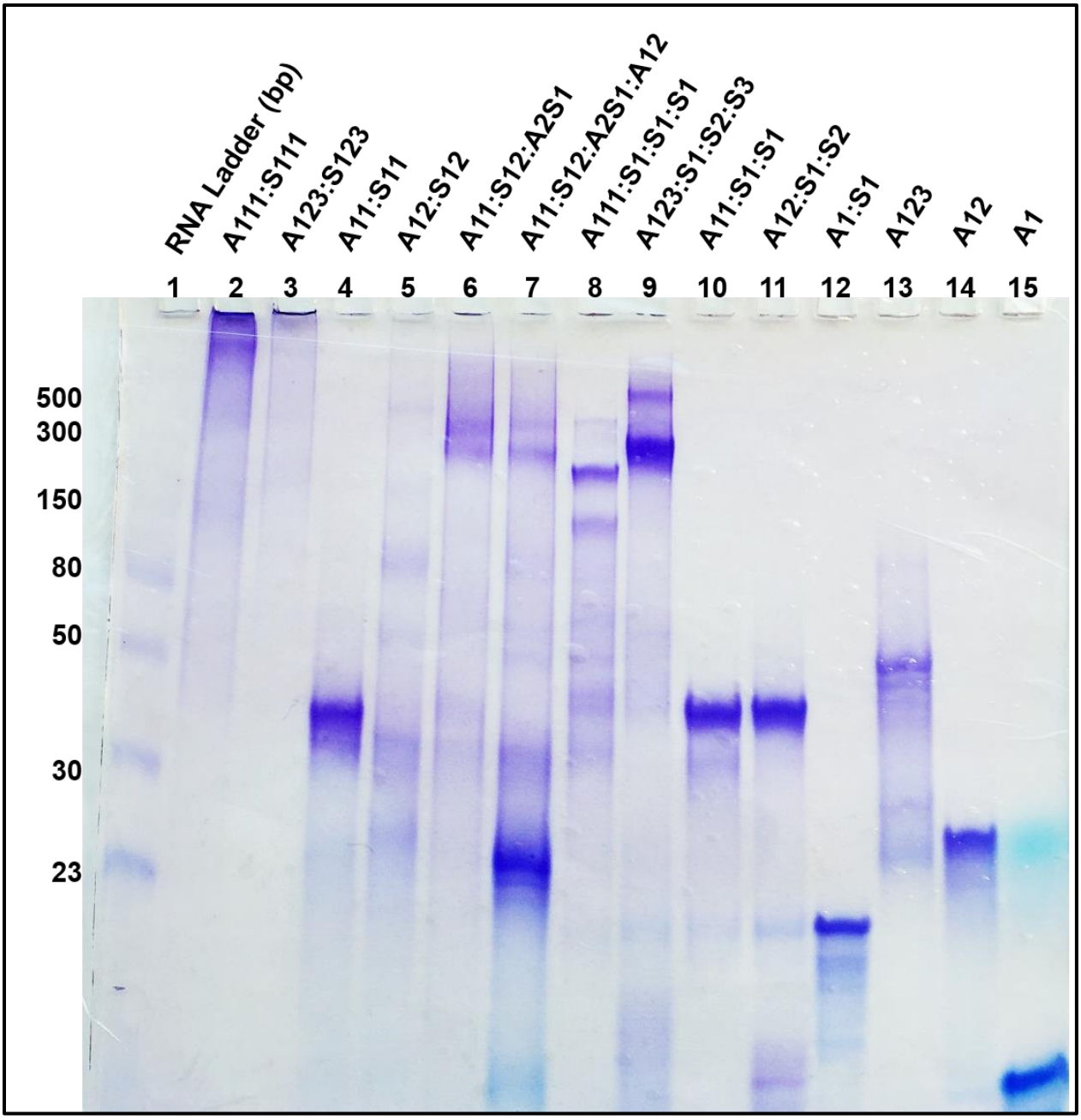

Figure 3.4 siRNA self-assembly. Native, non-denaturing 16% PAGE of self-assembled Y- (lanes 2-3), V-shape (lanes 4-7) siRNA hybrids, Y-shape RNA templates hybridized to linear complementary RNA sequences (lanes 8, 9), V-shape RNA templates hybridized to linear complementary RNA sequences (lanes 10, 11), linear siRNA (lane 12) along with Y-shape (lane 13), V-shape (lane 14) and linear (lane 15) RNA templates. The RNA ladder (23-500bp) was used to track the relative sizes of the siRNA hybrids on the gel (lanes 1).

3.5.2 Structural Analysis of siRNA Hybrids by Transmission Electron Microscopy

In order to determine the sizes and shapes of the siRNA hybrids detected on native PAGE, a transmission electron microscopy (TEM) study was conducted. Interestingly, the TEM images of the complementary hybrid V- and Y-shaped siRNAs revealed nanostructures of well-defined geometries and size distributions (**Figure 3.5**). For example, the siRNA hybrid A11:S11 was found to self-assemble into circular and rectangular nanostructures having size distributions of 60-100 nm (**Figure 3.5A**). Comparatively, the TEM image of the siRNA hybrids A12:S12 self-assembled to form squares (60-80 nm) with a few elongated (80-110 nm) rectangular shape nanostructures (**Figure 3.5B**). The nanoparticle formulation formed from hybridizing three complementary V-shape RNA templates, namely, A11:A2S1:S12, self-assembled into triangle-shaped siRNA nanostructures having mostly smaller size distributions of 10-50 nm (**Figure 3.5C**). Pushing the boundaries of siRNA self-assembly, the V-shape templates composed of A11:A2S1:S12:A12 generated pentagons of sizes 90-100 nm, squares and rectangles of sizes ranging from 60-80 nm and 100-120 nm, respectively, (**Figure 3.5D**). The siRNA hybrid formed from the Y-shape RNA templates, A123:S123, formed hexagonal shaped nanostructures ranging in sizes from 80-120 nm (**Figure 3.5F**). Comparatively, the siRNA hybrid A111:S111 was uniquely shown to self-assemble into porous spheres, with diameters ranging from ~20 - ~110 nm and with pore sizes as small as 3- 30 nm (**Figure 3.5E**). This novel type of RNA nanomaterial may be especially useful in small molecule encapsulation and release applications, such as those belonging to the stable RNA nanoparticles that have been used in drug delivery for cancer therapy.[62]

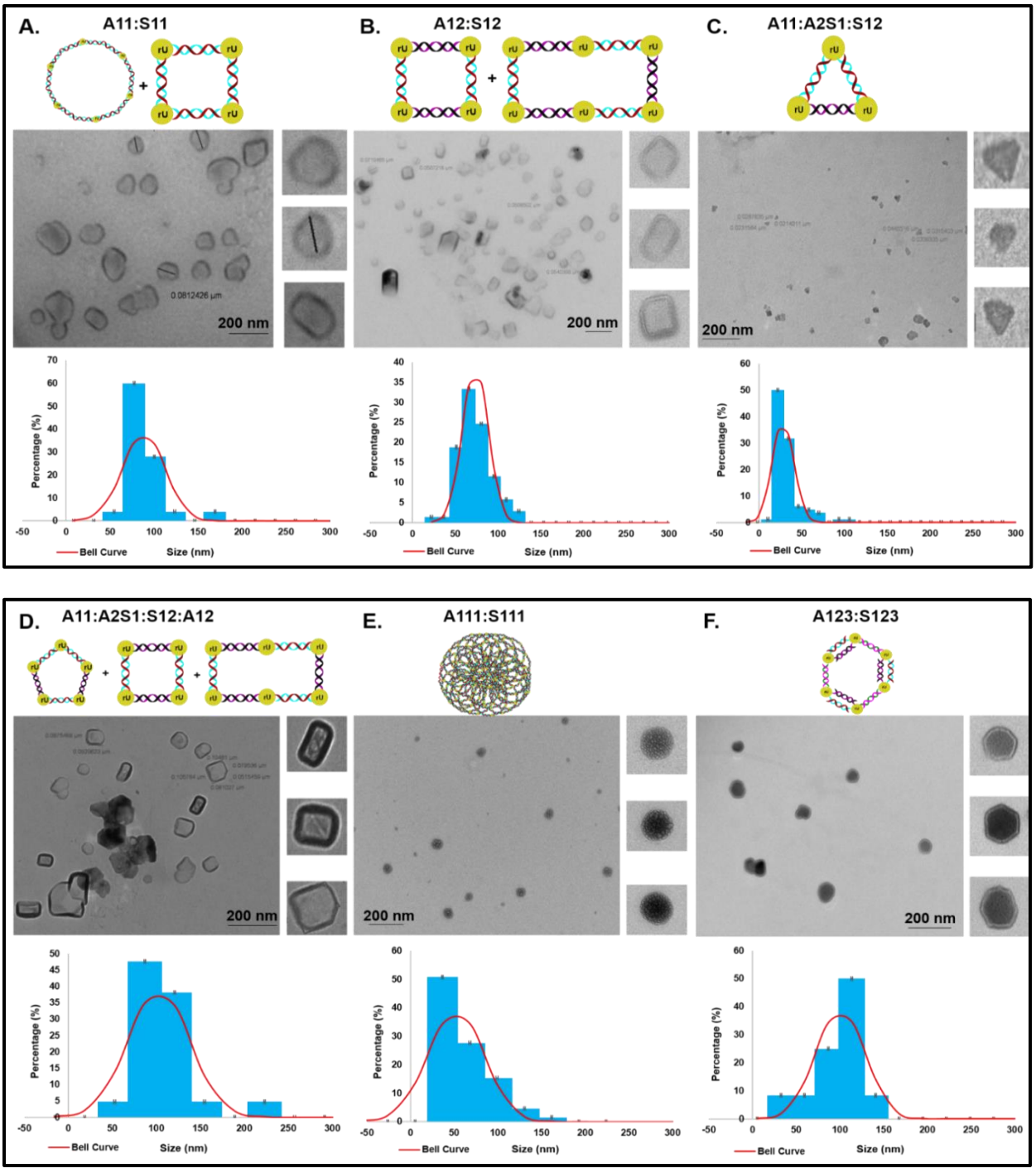

Figure 3.5 Sizes and shapes of siRNA nanostructures. TEM images and particle size distribution plots of (**A**) V-shape siRNA hybrids A11:S11, (**B**) V-shape siRNA hybrids A12:S12, (**C**) V-shape siRNA hybrids A11:A2S1:S12, (**D**) V-shape siRNA hybrids A11:A2S1:S12:A12, (**E**) Y-shaped siRNA hybrids A111:S111, and (**F**) Y-shaped siRNA hybrids A123:S123.

3.5.3 Thermal Denaturation (T_m) analysis of siRNA Hybrids by UV-Spectroscopy

siRNA hybrid stabilities were measured by thermal denaturation (T_m). The siRNA hybrids based on the V-shape RNA templates were found to be very stable, with high T_m values obtained for the A11:S11 (T_m = 84 ºC) and A12:S12 (T_m = 78 ºC), **Figure 3.6**. The V-shaped RNA templates hybridized with their complementary linear strands showed good thermal stabilities (A11:S1:S1, T_m = 76 ºC and A12:S1:S2, T_m = 77 ºC). Similarly, the siRNA hybrids, A111:S111 and A123:S123, based on the Y-shape RNA templates were also found to be stable, T_m = 69 ºC and T_m = 63 ºC, respectively. The Y-shaped RNA template hybridized to its complementary linear RNA strands formed siRNA hybrids which maintained good thermal stabilities (A111:S1:S1:S1, T_m = 62 ºC and A123:S1:S2:S3, T_m = 68 ºC), **Figure 3.6**.

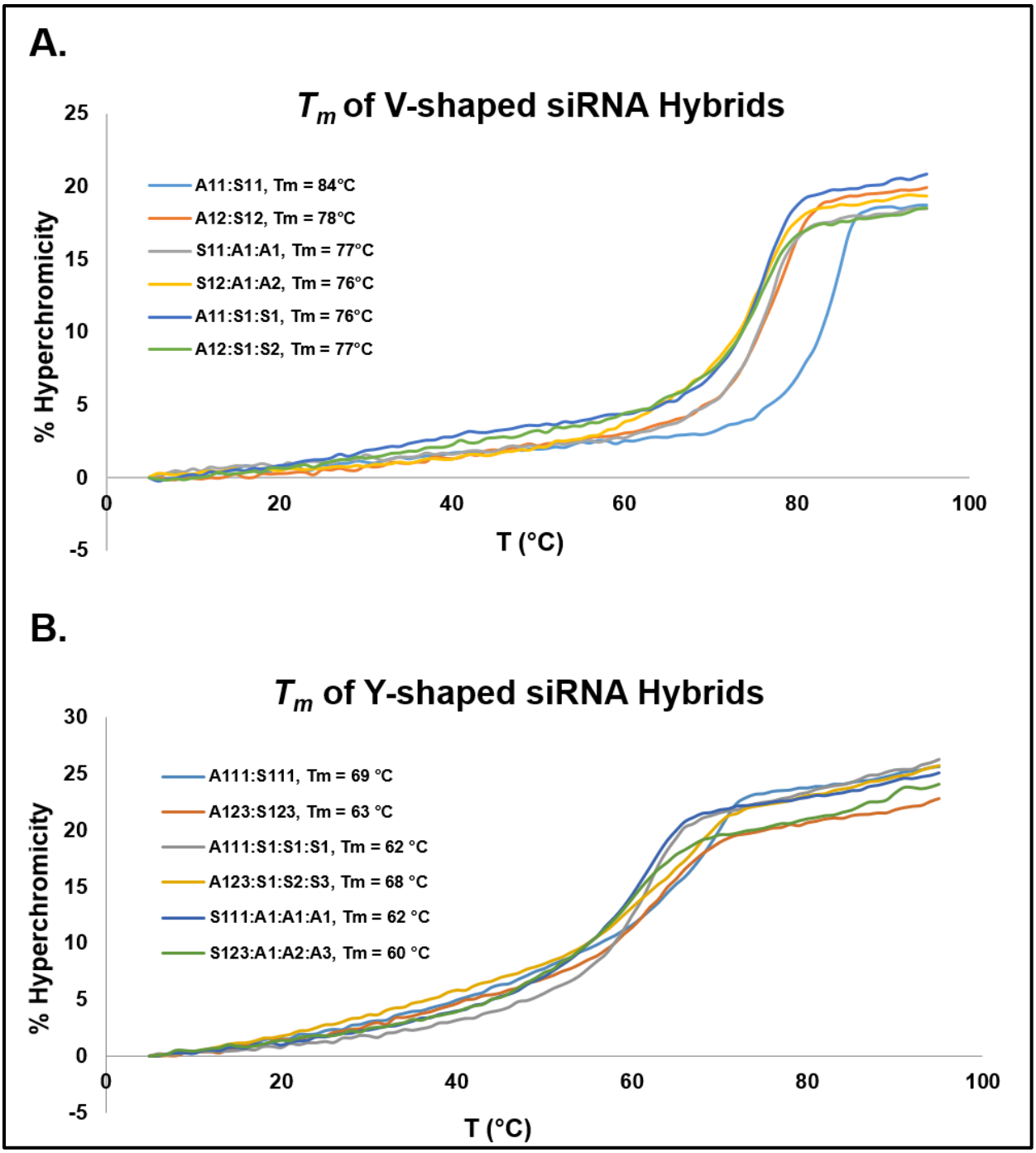

Figure 3.6. Thermal denaturation of V- and Y-shaped siRNAs. All sample hybrids were prepared by annealing equimolar quantities (0.75 µM) of antisense V-shaped (**A**) or Y-shaped (**B**) RNA to their complementary single or V- or Y-shaped RNA template strands. Samples were hybridized in anealing buffer (10 mM Tris, 50 mM NaCl, 1 mM EDTA, pH 7.5–8.0, 13-15 µL) by pre-heating at 95 ºC followed by slow cooling to room temperature over 1 h and overnight storage at 4 ºC prior to T_m analyses. Before running T_m, all samples were diluted in annealing buffer (1 mL) and the T_m analyses were observed at 260 nm between temperatures of 5-95 ºC.

3.5.4 Secondary Structural Analysis of siRNA Hybrids by Circular Dichroism Spectroscopy

Circular dichroism (CD) spectroscopy was used to explore whether the siRNA nanostructures maintained the prerequisite A-type helix geometry for RNAi applications.[63] The linear siRNAs displayed typical CD profiles for A-form helices, with a minimum peak at 240 nm and a broad maximum in between 250-290 nm.[64] In the case of the self-assembled V- and Y-shape siRNA hybrids (**Figure 3.7**), the A-type broad maximum and minimum bands were observed between 250-290 nm and 240 nm, respectively, albeit with a decrease in the amplitudes of the molar ellipticities at these characteristic wavelengths. Despite this change, the self-assembled V- and Y-shape siRNA hybrids maintained CD signatures that were consistent with the A-form RNA helix. Taken altogether, the siRNA hybrids were found to maintain thermally stable, A-type helices within their higher-ordered nanostructure formulations making them promising candidates for their applications in RNAi nanotechnology.

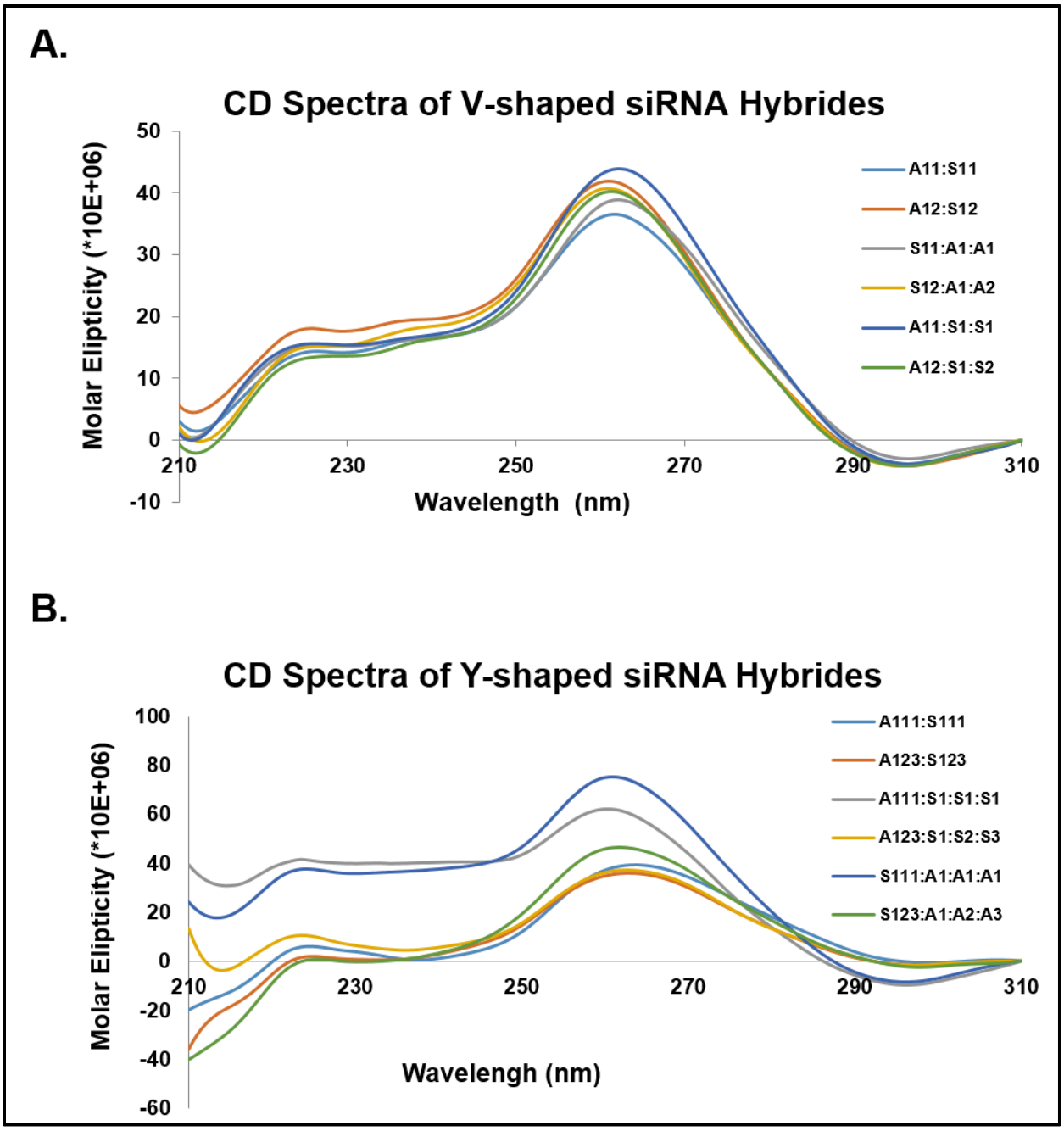

Figure 3.7 Circular dichroism spectroscopy of V- and Y-shaped siRNAs. All hybrid siRNA samples were prepared by annealing equimolar quantities (0.75 nM) of antisense V-shaped (**A**) or Y-shaped (**B**) RNA templates with their complementary linear or V- or Y-shaped RNA sequences. Samples were hybridized in annealing buffer (10 mM Tris, 50 mM NaCl, 1 mM EDTA, pH 7.5–8.0, 13-15 µL) by pre-heating at 95 ºC (3-5 min) followed by slow cooling to room temperature over 1 h and overnight storage at 4 ºC prior to CD analyses. All samples were diluted in annealing buffer (1 mL) and the CD analysis was observed from 205-310 nm.

3.5.5 Transfection Optimization of siRNA Hybrids

Prior to our RNAi screen, siRNA transfections were optimized within the GRP78 overexpressing AN3CA endometrial cancer cell line (ATCC® HTB-111™).[43,44,65-69] The linear, A1:S1, and the Y-shape, A123:S1:S2:S3 GRP78-targeting siRNAs were selected as test samples along with a non-specific (NS) RNA control. The benchmark transfection reagents, Lipofectamine 2000™, siLentFect™ and Lipofectamine RNAiMAX™ were tested for their transfection efficiencies according to the manufacture's protocol. Briefly, the transfection reagents (2.5-7 µL) were mixed with the siRNAs (15 and 30 nM) for 20 min at room temperature (22 ºC) and then added to the AN3CA cell culture which was incubated at 37 ºC for 72 h. Cell images were collected periodically during the incubation period and revealed the greatest extent of cell growth inhibition for the RNAiMAX-mediated siRNA transfections (**Figure 3.8A**). The enhanced efficiency of the RNAiMAX transfections was also supported by the most pronounced GRP78 knockdown effect (>90%) as detected by western blot (**Figure 3.10**), which also led to the most significant cell death response (35-55%) according to a cytotoxic lactate dehydrogenase (LDH) release assay (**Figure 3.8D**).[70] The Y-shape siRNA hybrids, A123:S1:S2:S3, were found to be more active than the linear siRNA control, A1:S1, exhibiting a greater GRP78 knockdown effect (>97 % *vs*. 90 %) which translated to a stronger inhibition of the AN3CA cells' growth (>99% *vs*. ~30 %) which ultimately led to a more pronounced cell death effect (58% *vs.* 32 %) at 30 nM and over a three day incubation period (**Figures 3.8-3.10**). The cells images of the transfected AN3CA cells obtained from the Incucyte™ clearly showed that the Y-shape siRNA (A123:S1:S2:S3) treated cells inhibited cell growth and the accumulation of cell debris during the incubation time was also observed in comparison to the linear nonspecific siRNA control (**Figure 3.9**). The anti-cancer effects of the siRNAs correlated with silencing of GRP78 activity according to western blot (**Figure 3.10**).

These results have effectively served to validate the potent anti-cancer effects of the multifunctional Y-shape siRNA, paving the way for a vigorous screening assay for evaluating the SARs of the GRP78-targeting siRNAs within the AN3CA EC cells.

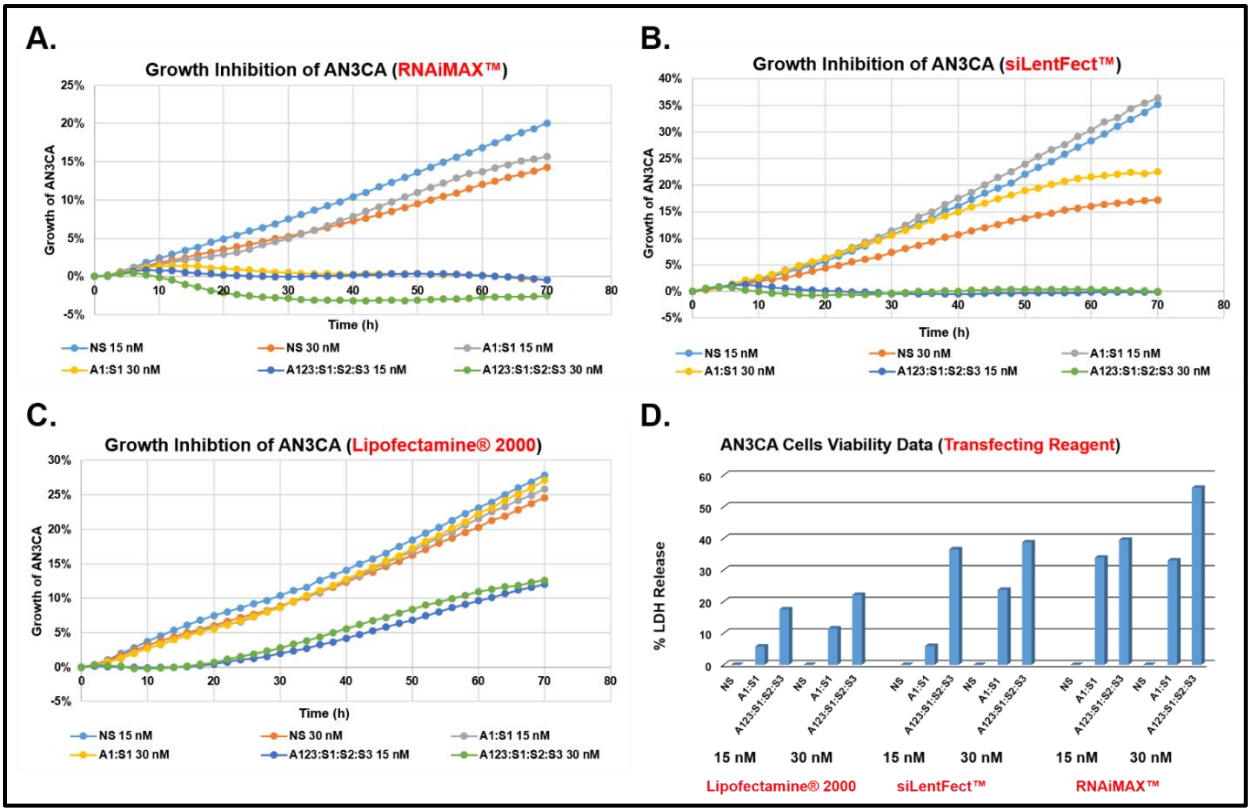

Figure 3.8 Optimization of siRNA transfections in AN3CA cells. The transfection efficiencies of the siRNAs, (NS, A1:S1 and A123:S1:S2:S3, 15 nM and 30 nM) using (**A**) Lipofectamine® 2000, (**B**) siLentFect™ and (**C**) RNAiMAX™ transfecting reagents were followed in the Incucyte™ (0 – 70 h) to obtain the AN3CA cell growth curves. (**D**) LDH release assay following siRNA transfections. Cell viability of AN3CA cells was measured by the % LDH released in the media and normalized according to the NS RNA treatment.

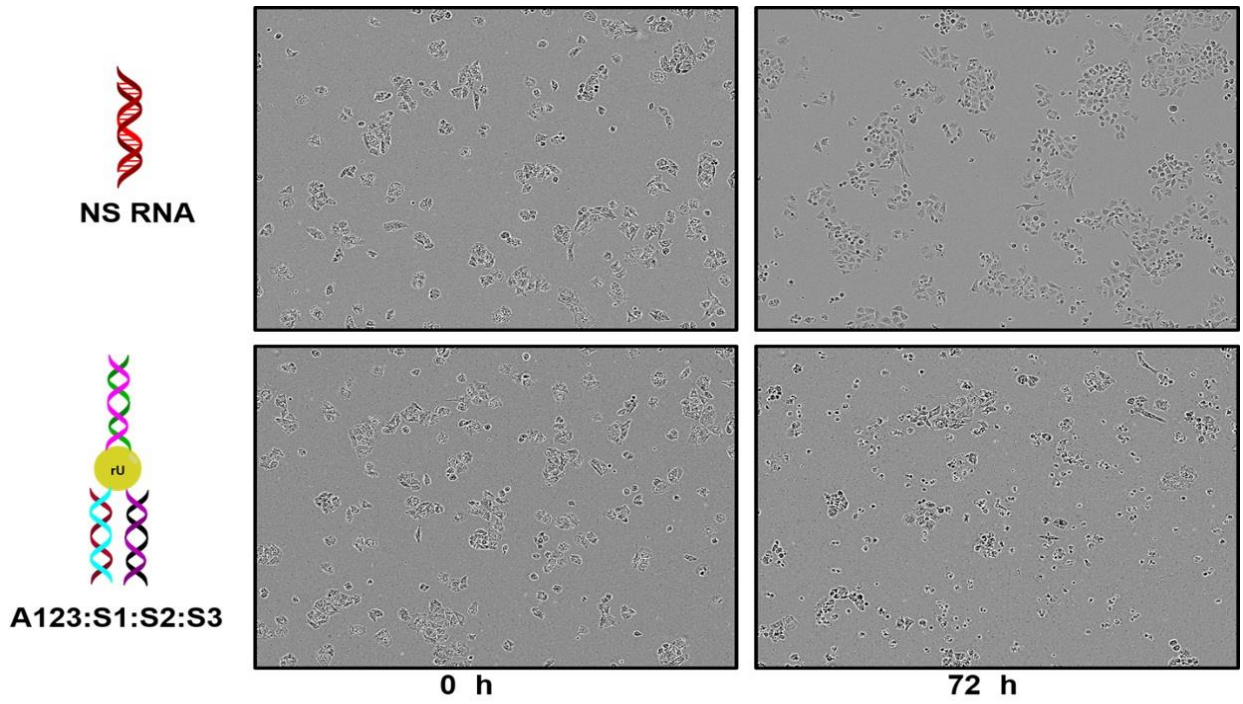

Figure 3.9 Cell growth images of the treated AN3CA EC cells. Images captured from the Incucyte™ represent treated cells (0 and 72 h) with the scrambled NS RNA control (30 nM) and the Y-shape siRNA composed of A123:S1:S2:S3 (30 nM) transfected with RNAiMAX™ (7 µL). AN3CA cells exhibited proliferative growth in the case of the NS RNA treatment, whereas, the Y-shape siRNA elicited growth inhibition and apparent cell death from the noticeable debris following 72 h incubation.

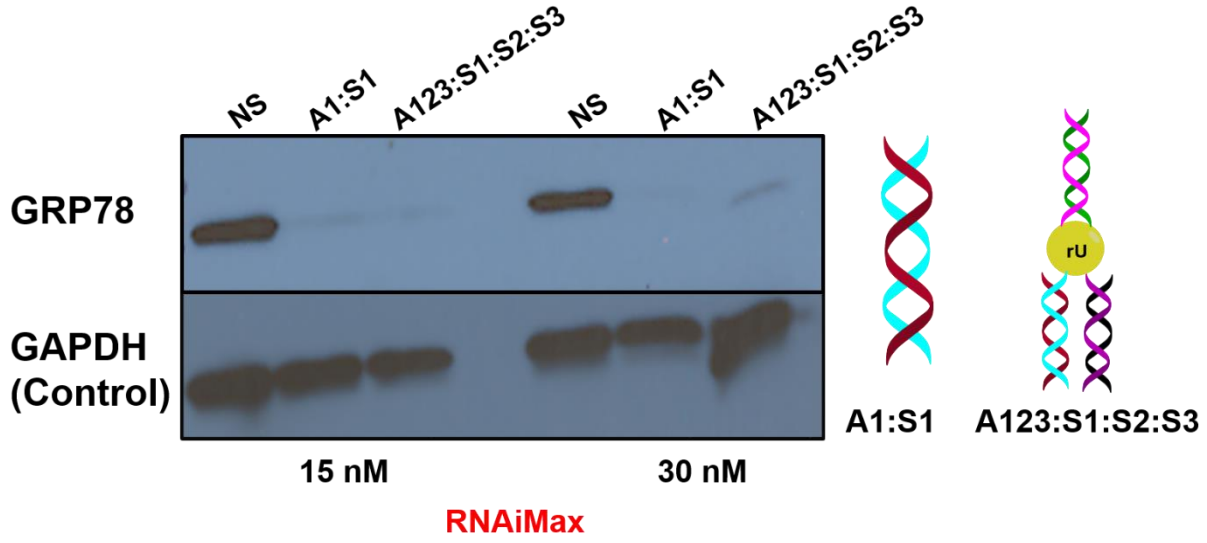

Figure 3.10 Western blot of the total GRP78 levels following siRNA transfections. siRNAs (A1:S1 and A123:S1:S2:S3, 15 and 30 nM) were transfected with RNAiMAX™ within the AN3CA cells. Following incubation (72 h), cells were lysed, protein concentrations were determined within the lysates, separated by SDS PAGE, transferred to a PVDF membrane which was blocked, immunoblotted with anti-GRP78 pAb and detected by chemiluminescence with HRP-conjugated secondary Ab. The loading control, GAPDH, was used to normalize the detected bands for quantitative densitometry using NIH imager (ImageJ).

3.5.6 24-siRNA Screen in the AN3CA EC Cells

Our hybridization and self-assembly approach has enabled the preparation of a small library of twenty-four (24) siRNA samples for evaluating their SARs in EC. RNAiMAX™ transfections of 24 siRNA samples at single doses (15 nM) within the AN3CA cells were evaluated over a three-day incubation period. Cell growth data obtained from the Incucyte™ (24-72 h) revealed the most significant growth inhibition (70-95 %) for the multifunctional siRNA nanostructures, while the control linear siRNAs and the NS RNA samples exhibited modest effects (5–50 %) on the growth of the AN3CA cells (**Figure 3.11A**). The western blots confirmed the anticipated GRP78 knockdown effects, with the siRNAs based on the V- (eg. A12:S1:S2) and Y-shape (eg. A123:S123) templates triggering the most potent responses (>95%) (**Figure 3.11B**). Interestingly, the Y-shape siRNAs targeting three different GRP78 mRNA sites (A123:S1:S2:S3 and A123:S123) produced the most marked effects on GRP78 knockdown (>95%) when compared to the linear siRNA controls targeting single (A1:S1, 15%), double (A1:S1 + A2:S2, 80%) and triple (A1:S1 + A2:S2 + A3:S3, 85%) oncogenic GRP78 mRNA sites. Moreover, these synergistic responses were also observed when monitoring the levels of the cleaved 85-kDa protein poly (ADP-ribose) polymerase (Cl-PARP), a molecular marker of apoptosis in cells (**Figure 3.11B**).[71] For example, the potent Y-shape siRNA (A123:S1:S2:S3) demonstrated significant GRP78 knockdown and growth inhibition (>90%, 15 nM), with notable increases in Cl-PARP levels (~50%). Comparatively, the linear control siRNAs (A1:S1 + A2:S2 + A3:S3) resulted in less (~30%) Cl-PARP expression (**Figure 3.11C**). Taken altogether, the multifunctional siRNAs stimulate synergistic anticancer responses in EC. These effects supersede those seen by the control siRNAs, even when added in combination, making the siRNA nanostructures more promising candidates for RNAi screening and cancer gene therapy applications.

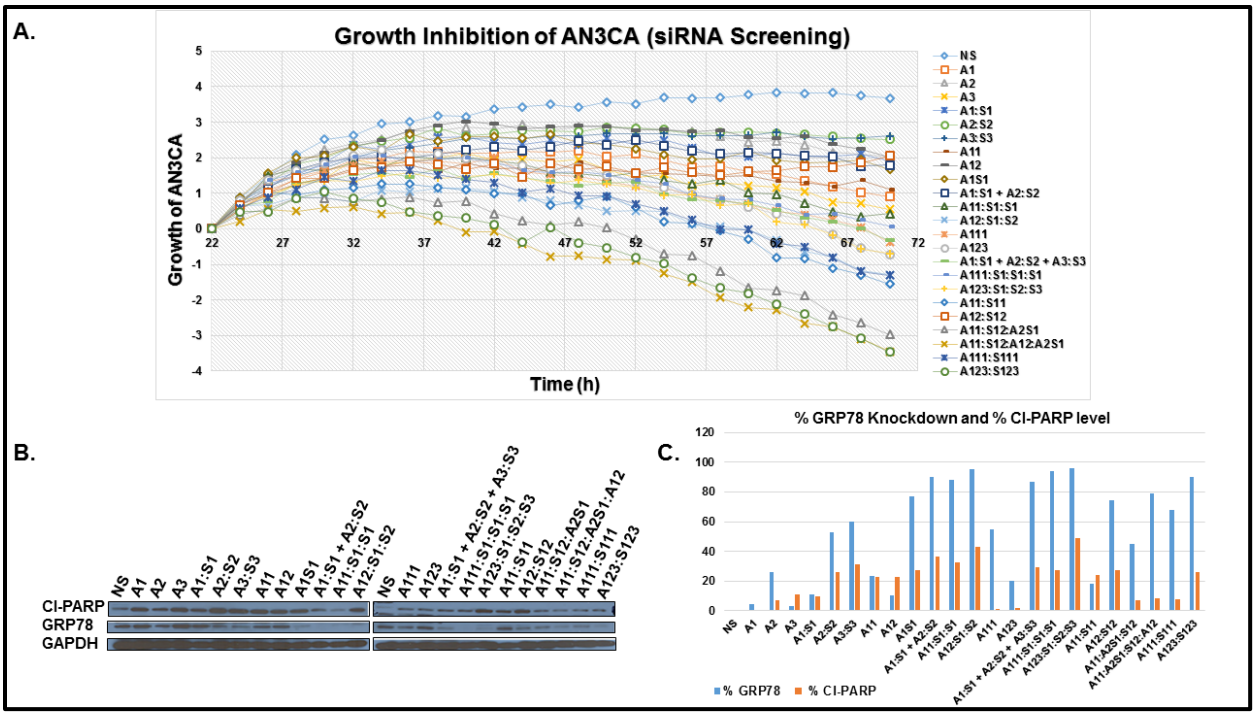

Figure 3.11 24-siRNA screen. (**A**) AN3CA cell growth curves following 24 siRNA transfections. siRNAs (15 nM) were transfected with RNAiMAX™ (7 µL) in endometrial AN3CA cancer cells and incubated (37 ºC, 72 h). Cell growth curves were obtained periodically (24 – 72 h) within the Incucyte™ and normalized according to the NS RNA (**B**) Western blots of the GRP78 knockdown and Cl-PARP levels following siRNA treatment. (**C**) The GRP78 (% knockdown) and Cl-PARP (% increase) levels were normalized according to GAPDH and quantified with respect to the NS RNA.

3.5.7 Transfection of the siRNA Leads

From the single dose 24 sample siRNA screen, four (4) V- (A12:S1:S2 and A12:S12) and Y-shape (A123:S1:S2:S3 and A123:S123) siRNA nanostructures were selected to validate the potency of their RNAi activity relative to their corresponding linear NS RNA and the siRNA (A1:S1, A2:S2, A3:S3, A1S1, A1:S1 + A2:S2, A1:S1 + A2:S2 + A3:S3) controls (**Figure 3.12**). The siRNA hybrids which exhibited the most pronounced anticancer effects, based on GRP78 knockdown, Cl-PARP levels and cell growth inhibition in our siRNA screen were selected as leads. As anticipated, the self-assembled siRNAs inhibited the AN3CA cells' growth to about a 40% greater extent relative to the controls (**Figure 3.12A**). A LDH release assay confirmed the cytotoxicities of the siRNA formulations, even at low dosages (5 nM), with the Y-shape A123:S1:S2:S3 siRNA exhibiting the most lethal (~10%) effects (**Figure 3.12B**). Moreover, western blot validated their potent GRP78 knockdown efficiencies, with ≥80% knockdown observed for the V- and Y-shape siRNA hybrids, while the linear controls exhibited at most ~75% GRP78 knockdown when added in combination (**Figure 3.12C** and **D**). Western blot also confirmed that the Cl-PARP levels indicative of apoptosis were observed at significantly increased levels in the cases of the V-shape (A12:S1:S2, ~75% and A12:S12, ~65%) and the Y-shape (A123:S1:S2:S3, ~77% and A123:S123, ~69%) siRNAs relative to their linear controls (~10-~65%). Interestingly, a direct correlation was observed in between GRP78 knockdown and increased levels of Cl-PARP indicating that GRP78 knockdown may be directly contributing to apoptosis in the AN3CA cells. Taken altogether, this study unveils the potent and long-lasting anticancer activities of the V- and Y-shape GRP78-targeting siRNA hybrids within the AN3CA EC cells at exceptionally low dosages (5 nM) and for an extended duration of action (72 h). Furthermore, these new siRNA motifs may be developed into multi-functional probes for

screening the influence of multiple oncogene targets on cancer cell biology and for enhancing the gene therapy effects within malignant tumors.

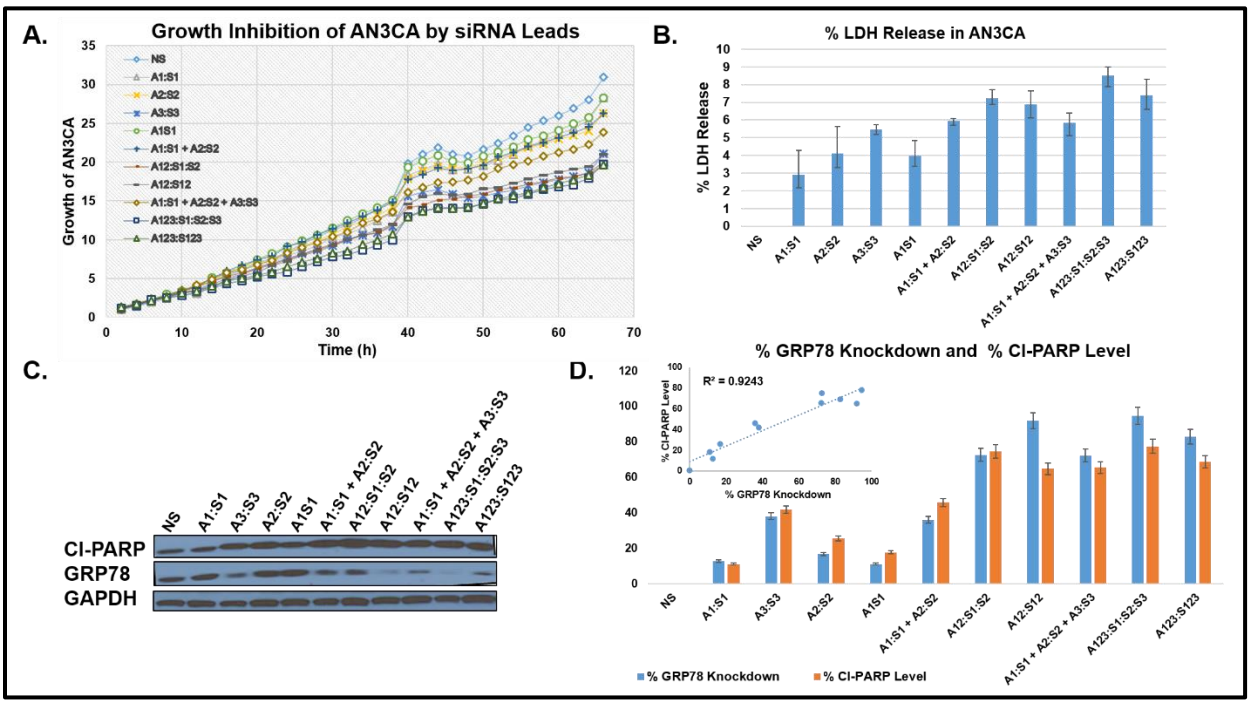

Figure 3.12 Biological evaluation of the siRNA leads. (**A**) The AN3CA cell growth curves (0 – 66 h) obtained from the Incucyte™ following RNAiMAX™ (7 µL) transfections of the siRNAs (5 nM). (**B**) LDH release assay following siRNA transfections. The % LDH released was measured for the siRNAs and normalized according to the NS RNA. (**C**) Western blot of the total GRP78 and Cl-PARP levels following siRNA transfections. The loading control, GAPDH, was used to normalize the detected bands for quantitative densitometry using NIH imager (ImageJ). (**D**) The % GRP78 knockdown and the % Cl-PARP levels were normalized according to the NS RNA control and quantitated following densitometry of the western blot. The linear (r^2 = 0.9243) correlation diagram in between the % GRP78 knockdown and the % Cl-PARP levels is provided as an inset. All experiments were replicated in triplicates with average values presented with their standard deviations about the mean. Statistical analyses produced error bars with acceptable variance ±SEM; N = 3, $p < 0.05$.

3.5.8 RNAi Screening of the GRP-Targeting siRNAs

The GRP overexpressing human cervical HeLa (ATCC® CCL-2™),[49] endometrial AN3CA[44,68,69] and breast MDA-MB-231 (ATCC® HTB-26™)[28] cancer cells in addition to a non-tumorigenic lung fibroblast MRC5 (ATCC®-CCL-171™)[72] cell line displaying normal GRP function were used as representative models to explore the influence of the glucose regulated chaperones, GRP-75, 78 and 94 on cell viability (**Figures 3.13-3.16**). The linear, V- and Y-shape siRNA hybrids respectively targeting single, double and all three GRPs were used as molecular probes for exploring cancer cell biology in our RNAi screening strategy (**Table 3.2**). The linear GRP-75, 78 and 94 siRNAs, used in combination demonstrated notable (20-90%) knockdown of GRP expression which translated to modest effects on cell growth inhibition (10-30%) and cell death (30-40%) in all cell lines tested. The V-shape siRNA hybrids targeting double chaperones (GRP7578, GRP7594 and GRP7894) showed sequence specific knockdown in all cell lines (20-95%) with varied effects on the expression levels of the non-targeted chaperone. For example, within the AN3CA cells, GRP-78 and 94 knockdown had little influence on the expression levels of GRP75, whereas GRP-75 and 94 knockdown led to a significant (40%) reduction in the GRP78 expression levels. Similar trends were delineated across different cell lines. For example, knockdown of GRP-75 and 94 led to a decrease in the expression levels of GRP78 within the AN3CA cells but not within the HeLa cells, suggesting that the cell lines have varied levels of GRP addiction. This assumption was validated by their varied effects on cell growth inhibition (30-50%) and death (20-40%). Representatively, GRP-75 and 94 knockdown translated to about a 2-fold increase in cell death within the HeLa relative to the AN3CA cell lines, underscoring a critical role of these chaperones on HeLa cell survival. The most potent anticancer effects were observed with the tri-functional Y-shape siRNA targeting GRP-75, 78 and 94. In this case, potent

(50-95%) knockdown was observed in all cancer cell lines which translated to significant levels of tumor cell cycle arrest (50-80%) and cancer cell death (50-60%). In comparison, the multiple GRP78-targeting Y-shape siRNA (A123:S1:S2:S3) triggered only about 10% AC3CA cell death whereas the GRP-75, 78 and 94 targeting Y-shape siRNA produced a 5-fold increase (50%) in cytotoxicity at low doses of 5 nM. The results observed for the Y-shape siRNA targeting GRP-75, 78 and 94 supersede the anticancer effects observed from all other siRNA hybrids tested in our study and underscores the synergistic influence of compromising chaperome activity in cancer. Moreover, GRP knockdown with the GRP-75, 78 and 94 targeting Y-shape siRNA had a more pronounced effect on tumor cell growth inhibition (50-80%) and death (50-60%) when compared to the control, non-tumorigenic MRC5 cell line which displayed modest growth inhibition (10-30%) and death (10-20%). These results correlate an addiction of human cancer cells to the overexpressed glucose regulated chaperome which may contribute towards cancer treatment selectivity.[73] Therefore, the self-assembled siRNA hybrids targeting multiple GRPs proved useful in screening these important oncogene targets for elucidating their role on cancer cell biology while improving siRNA therapeutic efficacy and specificity in cancer.

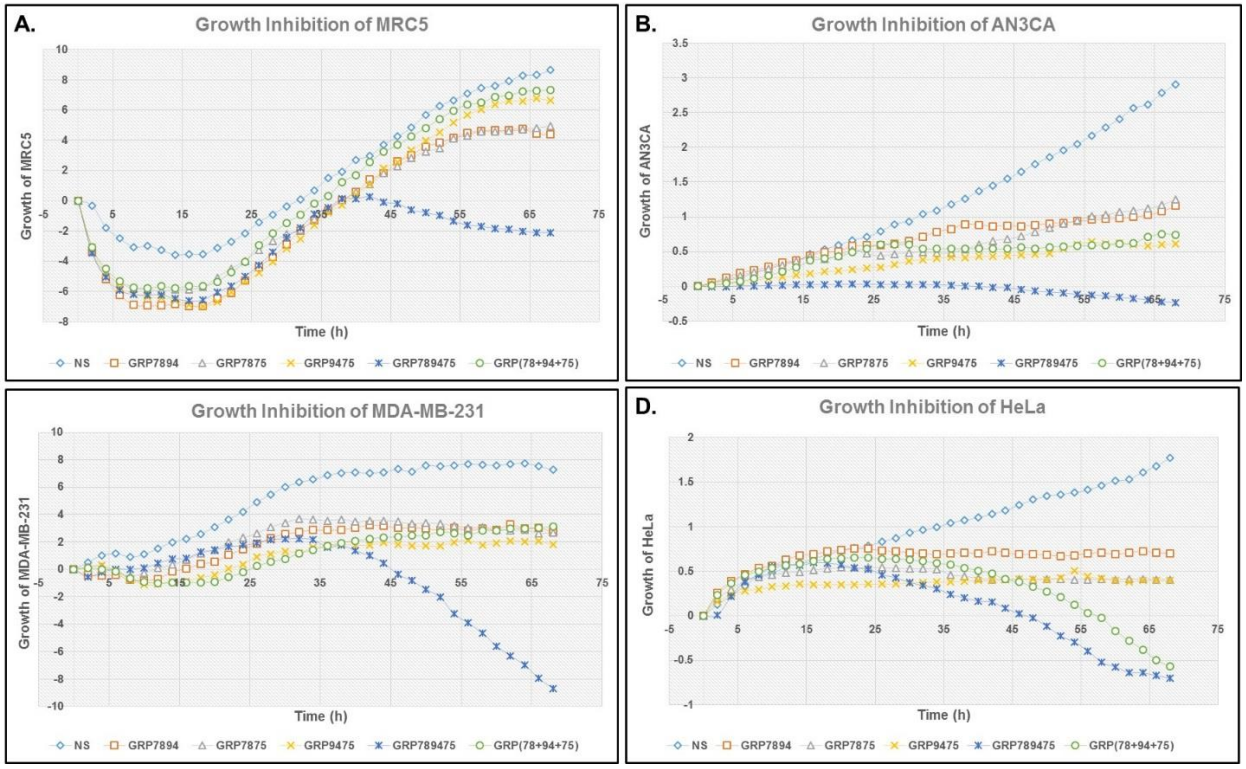

Figure 3.13 Cell Growth Curves. siRNA (5 nM) transfections with RNAiMAX™ (7 µL) in (**A**) MRC5, (**B**) AN3CA, (**C**) MDA-MB-231, and (**D**) HeLa cells were incubated at 37 °C for 72 h. Cell growth data was obtained periodically (every 2 h) within the Incucyte™ for 68-72 h, plotted and normalized according to the NS RNA. Data representative of three independently conducted experiments.

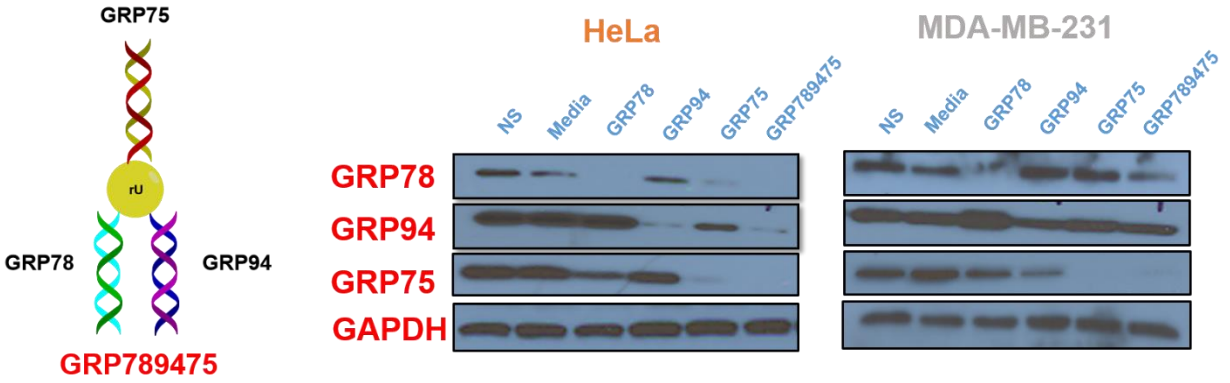

Figure 3.14 Western blots of the GRP78, 94 and 75 knockdown following siRNA treatment. Western blots showing 5 nM of siRNAs transfection in HeLa (Cervical cancer cells) and MDA-MB-231 (Breast cancer cells) following 72 h incubation at 37 ºC. The GRP78, GRP94 and GRP75 (% knockdown) levels were normalized according to GAPDH and quantified with respect to the NS RNA. Data represents comparative efficiency of linear siRNAs (GRP78, GRP94, GRP75) and Y-shape siRNA (GRP789475).

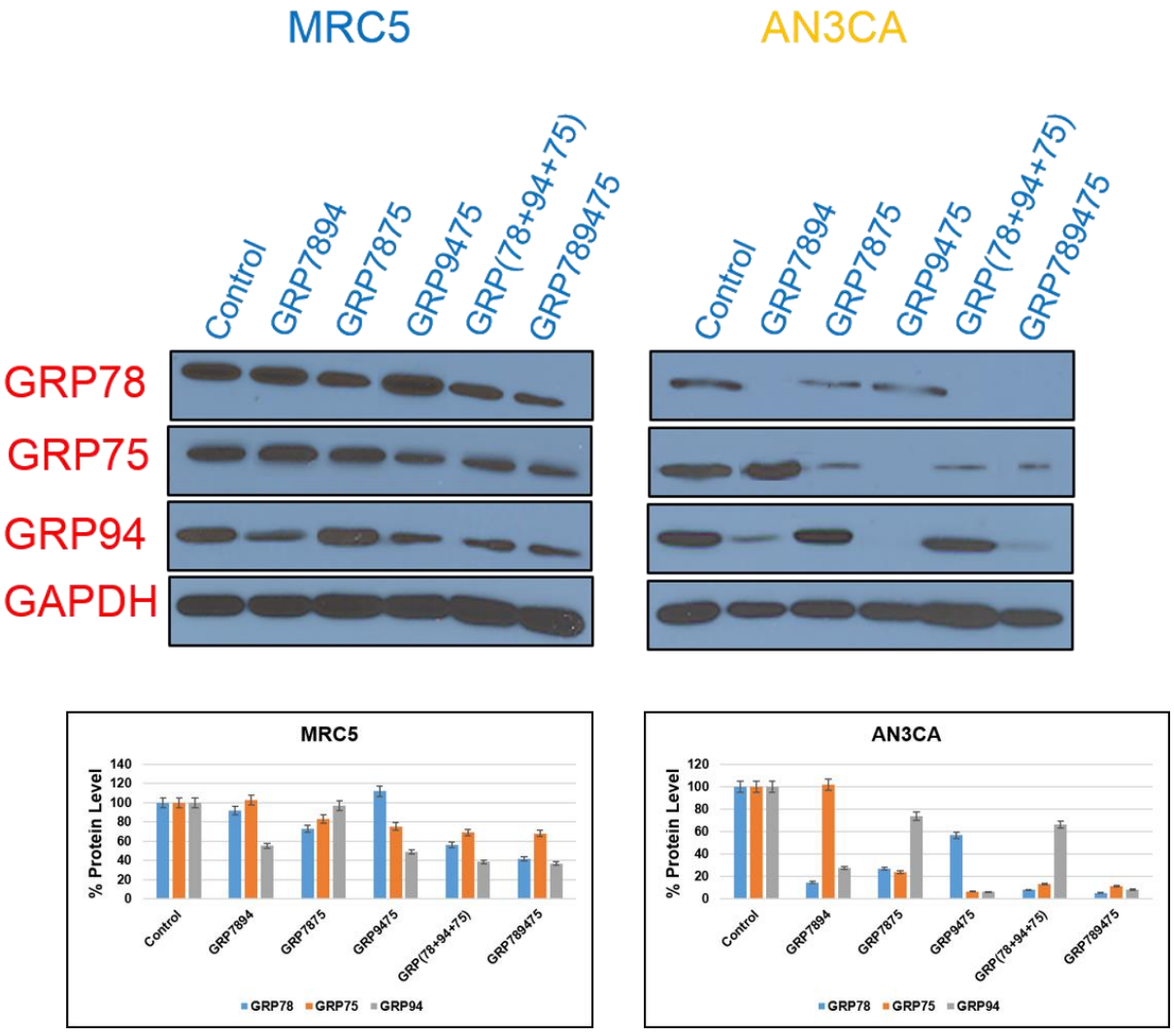
MRC5
AN3CA
Control
GRP7894
GRP7875
GRP9475
GRP(78+94+75)
GRP789475
GRP78
GRP75
GRP94
GAPDH
MRC5
% Protein Level
140
120
100
80
60
40
20
0
Control
GRP7894
GRP7875
GRP9475
GRP(78+94+75)
GRP789475
GRP78
GRP75
GRP94
AN3CA
% Protein Level
120
100
80
60
40
20
0
Control
GRP7894
GRP7875
GRP9475
GRP(78+94+75)
GRP789475
GRP78
GRP75
GRP94

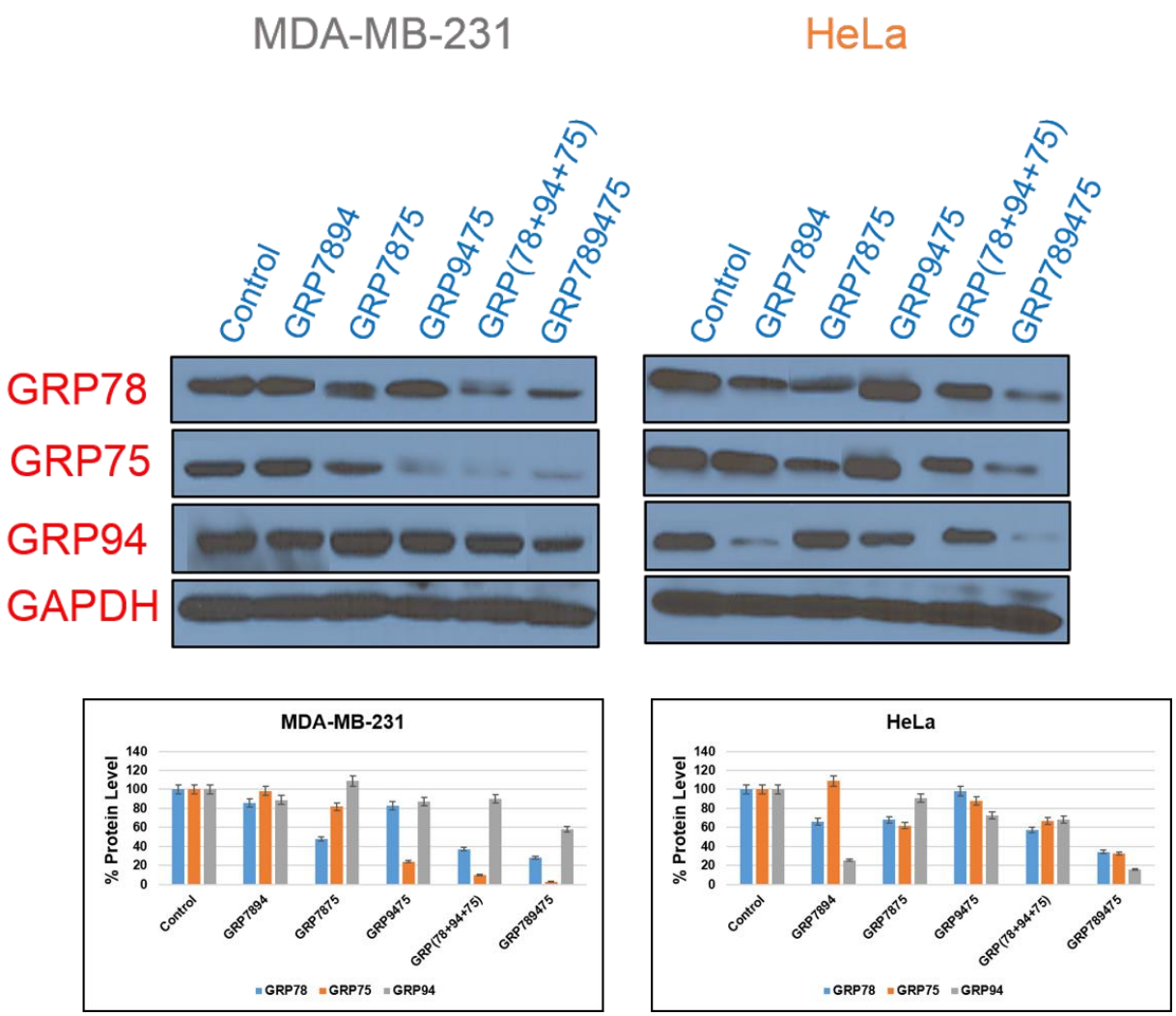

Figure 3.15 RNAi screening. Western blots measuring GRP78, GRP94 and GRP75 (% protein) levels following siRNA (5 nM) transfections in normal lung, MRC5, endometrial, AN3CA, breast, MDA-MB-231 and cervical, HeLa cancer cells. The GRP78, GRP94 and GRP75 levels were normalized according to GAPDH and quantified with respect to the NS RNA. Data represents knockdown efficiency of V-shape siRNAs (GRP7894, GRP7875, GRP9475), Y-shape siRNA (GRP789475) and the linear siRNAs (GRP78+GRP94+GRP75) added in combination. All experiments were replicated in triplicates with average values presented with their standard deviations about the mean. Statistical analyses produced error bars with acceptable variance ±SEM; N = 3, $p < 0.05$.

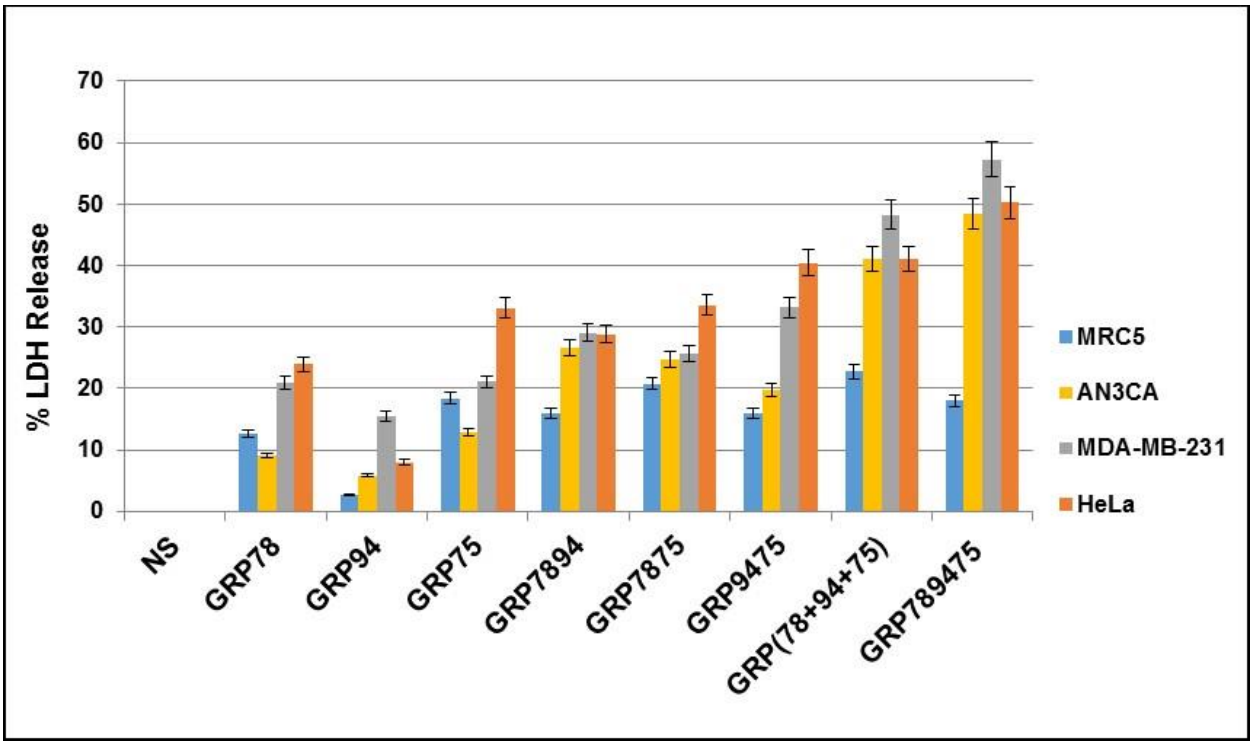

Figure 3.16 LDH Release Assay. The % LDH released was measured following transfections of all treated cell lines (MRC5, AN3CA, MDA-MB-231 and HeLa). The LDH levels were quantitated and normalized according to the NS RNA. All experiments were replicated in triplicates with average values presented with their standard deviations about the mean. Statistical analyses produced error bars with acceptable variance ±SEM; N = 3, $p < 0.05$.

3.5.9 Serum Stability of the siRNA Hybrids

The serum stability of selected siRNAs was next evaluated in fetal bovine serum (FBS). The linear (A1:S1), V- (A12:S12) and Y-shaped (A123:S1:S2:S3) siRNAs were hybridized in annealing buffer, treated with 10% FBS and incubated at 37 °C for 48 h. Periodically, aliquots were collected, concentrated and suspended in gel loading buffer, for 16% native PAGE analyses (**Figure 3.17**). As expected, the linear siRNA completely degraded, even after shorter incubation times of four hours. These results confirm the limited duration of action and therapeutic index of the native siRNAs that are readily degraded by nucleases present in serum.[36] In comparison, the siRNA nanostructures were shown to quickly (4 h) disassemble into shorter hybrid sequences and also into their native templates upon FBS treatment. In these cases, only partial degradation was observed even after 48 h treatment. In a separate FBS stability assay, (**Figure 3.18** and **3.19**) the linear (A1), V-shape (A12) and Y-shape (A123) RNA templates were completely degraded after 24 h treatment. However, the higher-order siRNA hybrids formed from the V- and Y-shape RNA templates (A12:S12, A12:S1:S2 and A123:S123, A123:S1:S2:S3, respectively) were found to undergo partial degradation after a 48 h incubation period. These results confirm that the higher-order siRNA nanostructures formed from the V-and Y-shape RNA templates impart partial stability to the nucleases present in serum which likely contributes to their prolonged duration of action relative to the linear siRNA hybrids. These results are consistent with the observed serum stability of other RNA nanostructures, suggesting that higher order structure formation may contribute to enhanced serum stability.[75] Moreover, site specific or gapmer modifications to the siRNA sequences have also been shown to improve resistance towards nuclease degradation, and may be incorporated to further enhance serum or plasma stability while retaining potent silencing activity.[76]

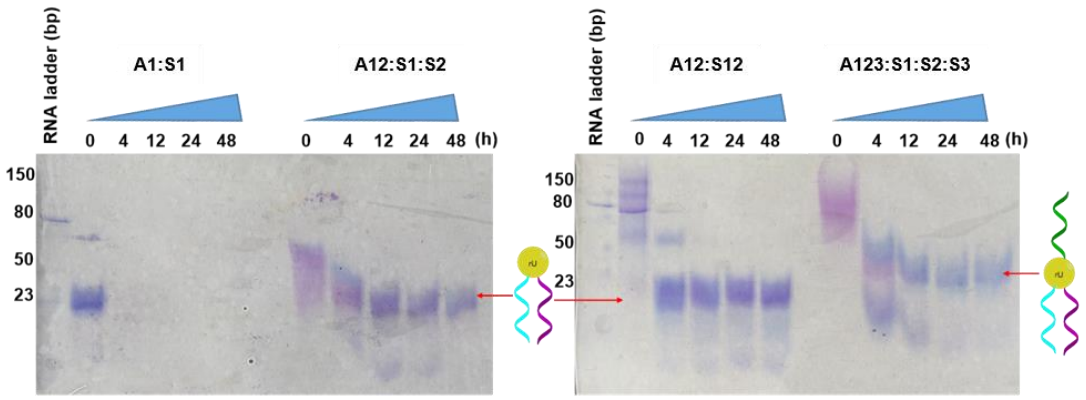

Figure 3.17 siRNA FBS stability assay (1). The native PAGE (16%) analyses of the serum stability of the linear siRNA (A1:S1) compared with the V- (A12:S1:S2 and A12:S12) and Y-shaped (A123:S1:S2:S3) siRNA nanostructures over 48 h in 10% FBS.

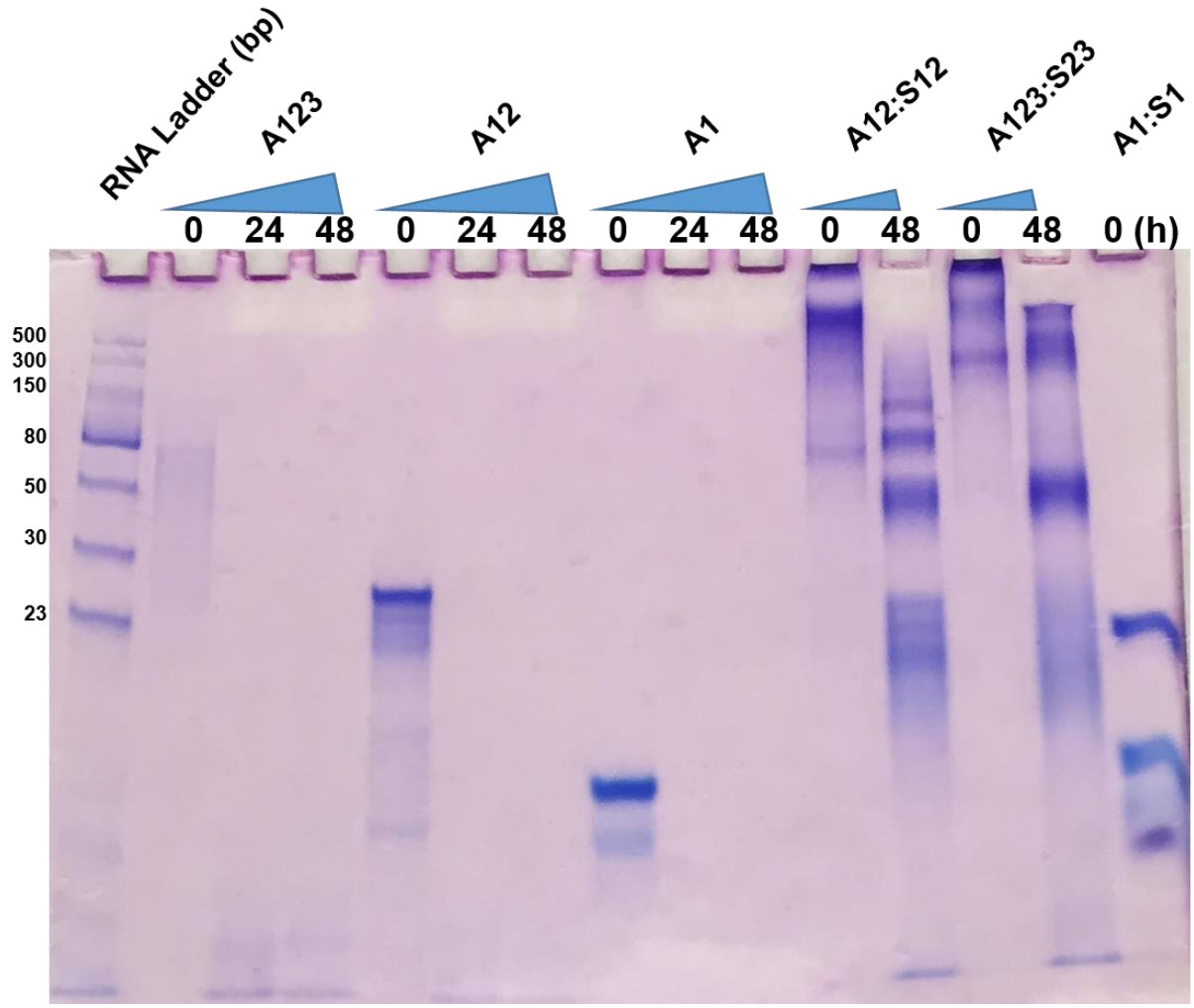

Figure 3.18. siRNA FBS stability assay (2). The native PAGE (16%) analyses of the serum stability of the Y-shape, V-shape and linear siRNA templates compared with the self-assembled V- (A12:S12) and Y-shaped (A123:S123) siRNA nanostructures over 48 h in 10% FBS. The RNA ladder (23-500bp) was used to track the relative sizes of the hydrolyzed siRNA components on the gels.

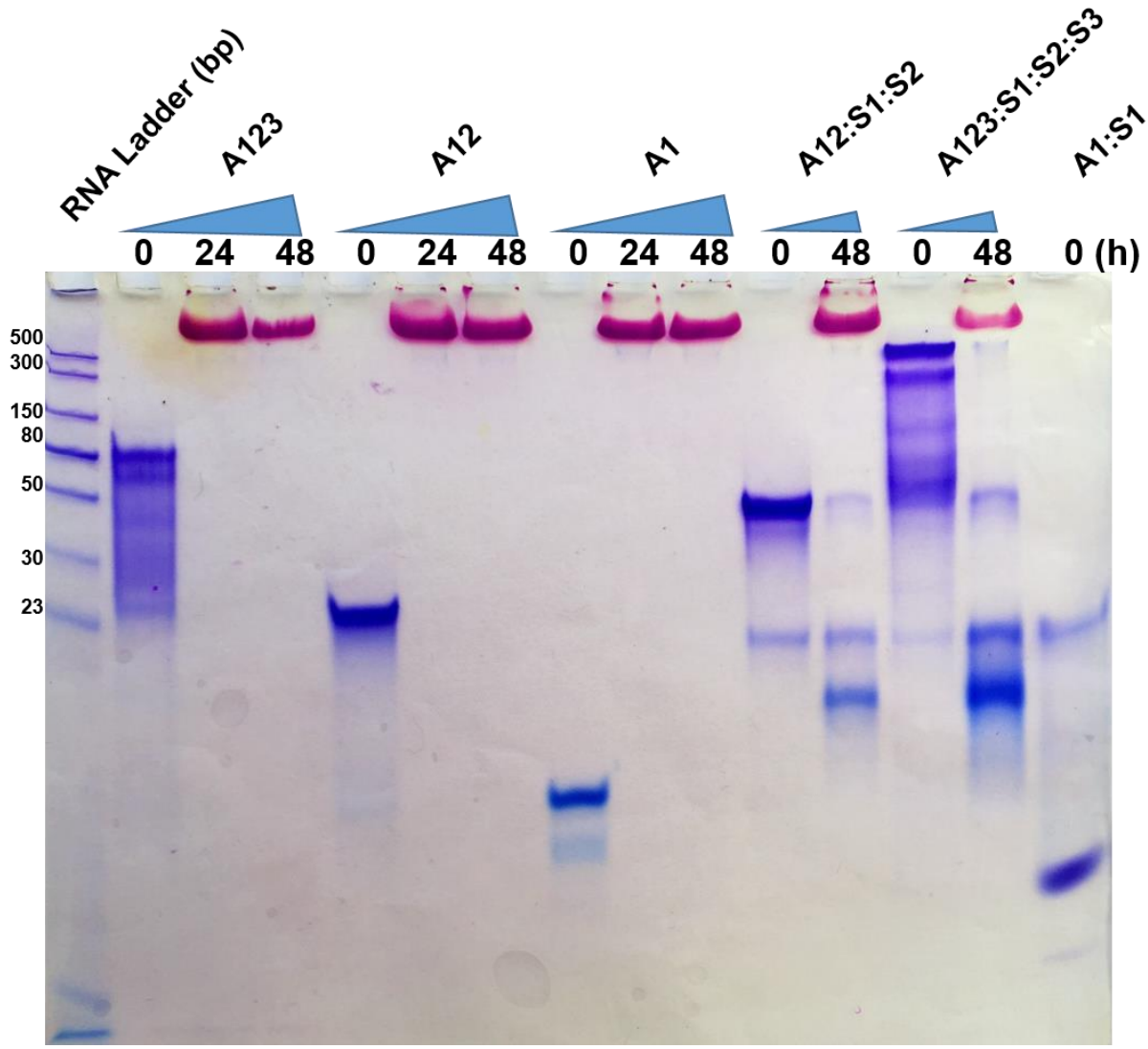

Figure 3.19. siRNA FBS stability assay (3). The native PAGE (16%) analyses of the serum stability of the Y-shape, V-shape and linear siRNA templates compared with the self-assembled V- (A12:S1:S2) and Y-shaped (A123:S1:S2:S3) siRNA nanostructures over 48 h in 10% FBS. The RNA ladder (23-500bp) was used to track the relative sizes of the hydrolyzed siRNA components on the gels.

3.6 CONCLUSIONS

We have effectively demonstrated the rational design and applications of RNA templates in the self-assembly of discrete, higher order siRNA nanostructures for RNAi screening and cancer gene therapy applications. The novel siRNA nanostructures created in this study have expanded the repertoire of multifunctional siRNAs. They were shown to adopt unique shapes and well defined structures according to TEM imaging. Moreover, thermal denaturation and CD spectroscopy were respectively used to confirm the prerequisite siRNA hybrid stabilities and A-form helices for invoking RNAi activity. In endometrial cancer, the higher-order siRNA hybrids were found to trigger synergistic anticancer effects, which surpassed those observed with the linear siRNAs. The V- and Y-shape siRNA hybrids induced potent (>95%) GRP78 knockdown, which inhibited tumor cell growth (35-55%) and stimulated programmed cell death according to the release of LDH and the increase in the 85-kDa Cl-PARP fragment, a molecular marker of apoptosis. In an RNAi screen across a panel of GRP overexpressing cancer cell lines and a non-tumorigenic control displaying regulated levels of GRP, the multi-functional V- and Y-shape siRNAs targeting GRP-75, 78 and 94 displayed synergistic anticancer effects which superseded their linear controls or the V- and Y-shape siRNAs targeting GRP78 alone. The RNAi screen also revealed the influence of GRP activity on cell viability. The GRP overexpressing cancer cells were sensitized to GRP-75, 78 and 94 knockdown resulting in greater tumor cell cycle arrest and cytotoxicity relative to the non-tumorigenic control. These studies revealed a greater dependence of human cancer cells to the overexpressed glucose regulated chaperome which was found to contribute to cancer treatment selectivity. A FBS serum stability assay provided preliminary mechanistic insights into the anticancer activity of the siRNA hybrids. In these experiments, the linear siRNAs and the non-hybridized RNA templates were found to degrade in the presence of

serum nucleases. Whereas, the siRNA nanostructures were found to undergo only partial degradation after a 48 h incubation period in 10% FBS. Therefore, the higher-order V- and Y-shape siRNA hybrids were found to confer greater resistance towards degradation in serum that may likely contribute to the long-lasting oncogene knockdown and anticancer effects observed in our study. Additional mechanistic studies are currently underway to elucidate the complete mechanism of action of the novel siRNA hybrids. In conclusion, these novel siRNA motifs encompass a new class of bio-probes for studying RNAi activity in cancer and also for screening important (single or multiple) oncogene targets for successful applications in cancer gene therapy.

3.7 REFERENCES

1. Shiu, R.P.; Pouyssegur, J.; Pastan, I. *Proc. Natl. Acad. Sci. USA* **1977**, *74*, 3840-3844.
2. Mizzen, L.A.; Chang, C.; Garrels, J.I.; Welch, W.J. *J. Biol. Chem.* **1989**, *264*, 20664-10675.
3. Luo, B.; Lee, A.S. *Oncogene* **2013**, *32*, 805-818.
4. Little, E.; Ramakrishnan, M.; Roy, B.; Gazit, G.; Lee, A.S. *Crit. Rev. Eukaryot Gene Expr*. **1994**, *4*, 1-18.
5. Chang, S.C.; Erwin, A.E.; Lee, A.S. *Mol. Cell Biol.* **1989**, *9*, 2153-2162.
6. Wang, M.; Wey, S.; Zhang, Y.; Ye, R.; Lee, A.S. *Antioxid Redox Signal* **2009**, *11*, 2307-2316.
7. Marzec, M.; Eletto, D.; Argon, Y. *Biochimi. Biophys. Acta* **2012**, *1823*, 774-787.
8. Wadhawa, R.; Yaguchi, T.; Hasan, M.K.; Mitsui, Y.; Reddel, R.R.; Kaul, S.C. *Exp. Cell Res.* **2002**, *274*, 246-253.
9. Ma, Y.; Hendershot, L.M. *Nat. Rev. Cancer* **2004**, *4*, 966-977.
10. Kaufman, R.J. *Genes Dev*. **1999**, *13*, 1211-1233.
11. Ron, D.; Walter, P. *Nat. Rev. Mol. Cell Biol.* **2007**, *8*, 519-529.
12. Hetz, C. *Nat. Rev. Mol. Cell Biol.* **2012**, *13*, 89-102.
13. Luo, S.; Baumeister, P.; Yang, S.; Abcouwer, S.F.; Lee, A.S. *J. Biol. Chem.* **2003**, *278*, 37375-37385.
14. Lee, K.; Tirasophon, W.; Shen, X.; Michalak, M.; Prywes, R.; Okada, T.; Yoshida, H.; Mori, K.; Kaufman, R. *J. Genes Dev.* **2002**, *16*, 452-466.
15. Lee, A.S. *Nat. Rev. Cancer* **2014**, *14*, 263-276.
16. Zhang, L. H.; Zhang, X. *J. Cell Biochem.* **2010**, *110*, 1299-1305.
17. Shin, B.K.; Wang, H.; Yim, A.M.; Le Naour, F.; Brichory, F.; Jang, J.H.; Zhao, R.; Puravs, E.; Tra, J.; Michael, C.W.; Misek, D.E.; Hanash, S.M. J Biol Chem. **2003**, *278*, 7607-7616.
18. Verras, M.; Papadreou, I.; Lim, A.L.; Denko, N.C. *Mol.Cell Biol.* **2008**, *28*, 7212-7224.
19. Misra, U.K.; Gonzalez-Gronow, M.; Gawdi, G.; Pizzo, S.V. *J. Immunol.* **2005**, *174*, 2092-2097.
20. Burikhanov, R.; Zhao, Y.; Goswami, A.; Qiu, S.; Schwarze, S.R.; Rangnekar, V.M. *Cell* **2009**, *138*, 377-388.
21. Misra, U.K.; Gonzalez-Gronow, M.; Gawdi, G.; Hart, J.P.; Johnson, C.E.; Pizzo, S.V. *J. Biol. Chem*. **2002**, *277*, 42082-42087.
22. Misra, U.K.; Pizzo, S.V. *PLoS One* **2012**, *7*, e51735
23. Zhang, Y.; Tseng, C.C.; Tsai, Y.L.; Fu, X.; Schiff, R.; Lee, A.S. *PLoS One* **2013**, *8*, e80071.
24. Kelber, J.A.; Panopoulos, A.D.; Shani, G.; Booker, E.C.; Belmonte, J.C.; Vale, W.W.; Gray, P.C. *Oncogene* **2009**, *28*, 2324-2336.
25. Wanderling, S.; Simen, B.B.; Ostrovsky, O.; Ahmed, N.T.; Vogen, S.M.; Gidalevitz, T.; Argon, Y. *Mol. Biol. Cell* **2007**, *18*, 3764-3775.
26. Hua, Y.; White-Gibertson, S.; Kelner, J.; Rachidi, S.; Usmani, S.Z.; Chiosis, G.; Depinho, R.; Li, Z.; Liu, B. *Clin. Cancer Res*. **2013**, *19*, 6242-6251.
27. Morales, C.; Rachidi, S.; Hong, F.; Sun, S.; Ouyang, X.; Wallace, C.; Zhang, Y.; Garret-Mayer, E.; Wu, J.; Liu, B.; Li, Z. *Cancer Res.* **2014**, *74*, 446-459.

28. Dejeans, N.; Glorieux, C.; Guenin, S.; Beck, R.; Sid, B.; Rousseau, R.; Bisig, B.; Delvenne, P.; Buc Calderon, P.; Verrax, J. *Free Radic. Biol. Med.* **2012**, *52*, 993-1002.
29. Wadhwa, R.; Takano, S.; Robert, M.; Yoshida, A.; Nomura, H.; Reddel, R.R.; Mitsui, Y.; Kaul, S.C. *J. Biol. Chem.* **1998**, *273*, 29586-29591.
30. Mizukoshi, E.; Suzuki, M.; Loupatove, A.; Uruno, T.; Hayashi, H.; Misono, T.; Kaul, S.C.; Wadhwa, R.; Imamura, T. *Biochem. J.* **1999**, *343*, 461-466.
31. Zhou, H.; Zhang, Y.; Fu, Y.; Chan, L.; Lee, A.S. *J. Biol. Chem.* **2011**, *286*, 25687-25696.
32. Martin-Perez, R.; Niwa, M.; Lopez-Rivas, A. *Apoptosis* **2012**, *17*, 349-363.
33. Tsai, Y.L.; Zhang, Y.; Tseng, C.C.; Stanciauskas, R.; Pinaud, F.; Lee, A.S. *J. Biol. Chem.* **2015**, *290*, 8049-8064.
34. Pujari, R.; Jose, J.; Bhavani, V.; Kumar, N.; Shastry, P.; Pal, J. K. *Int. J. Biochem. Cell Biol.* **2016**, *77*, 57-67.
35. Jin, H.; Ji, M.; Chen, L.; Liu, Q.; Che, S.; Xu, M.; Lin, Z. *J. Exp. Clin. Cancer Res.* **2016**, *35*, 42-51.
36. Yang, L.; Guo, W.; Zhang, Q.; Li, H.; Liu, X.; Yang, Y.; Zuo, J.; Liu, W. *J. Mol. Biol.* **2011**, *414*, 654-666.
37. Yoo, J.Y.; Ryu, J.; Gao, R.; Yaguchi, T.; Kaul, S.C.; Wadhawa, R.; Yun, C.O. *J. Gene Med.* **2010**, *12*, 586-595.
38. Wadhwa, R.; Ando, H.; Kawasaki, H.; Taira, K.; Kaul, S.C. *EMBO Rep.* **2003**, *4*, 595-601.
39. Wadhawa, R.; Sugihara, T.; Yoshida, A.; Nomura, H.; Reddel, R.R.; Simpson, R.; Maruta, H.; Kaul, S.C. *Cancer Res.* **2000**, *60*, 6818-6821.
40. Wittrup, A.; Zhang, S.; Svensson, K.J.; Kucharzewska, P.; Johansson, C.M.; Morgelin, M.; Belting, M. *Proc. Natl. Acad. Sci.* **2010**, *107*, 13342-13347.
41. Ermakova, S.P.; Kang, B.S.; Choi, B.Y.; Choi, H.S.; Schuster, T.F.; Ma, W.Y.; Bode, A.M.; Dong, Z. *Cancer Res.* **2006**, *66*, 9260-9269.
42. Yeung, B.H.; Kwan, B.W.; He, Q.Y.; Lee, A.S.; Liu, J.; Wong, A.S. *Oncogene* **2008**, *27*, 6782-6789.
43. Bifulco, G.; Miele, C.; Di Jeso, B.; Beguinot, F.; Nappi, C.; Di Carlo, C.; Capuozzo, S.; Terrazzano, G.; Insabato, L.; Ulianich, L. *Gynecol. Oncol.* **2012**, *125*, 220-225.
44. Cali, G.; Insabato, L.; Conza, D.; Bifulco, G.; Parrillo, L.; Mirra, P.; Fiory, F.; Miele, C.; Raciti, G.A.; Di Jeso, B.; Terrazzano, G.; Beguinot, F.; Ulianich, L. *J. Cell. Physiol.* **2014**, *229*, 1417-1426.
45. Roller, C.; Maddalo, D. *Front Pharmacol.* **2013**, *4*, 10.
46. Chang, Y.J.; Huang, Y.P.; Li, Z.L.; Chen, C.H. *PLoS One.* **2012**, *7*, e35123.
47. Yi, X.; Luk, J.M.; Lee, N.P.; Peng, J.; Leng, X.; Guan, X.Y.; Lau, G.K.; Beretta, L.; Fan, S.T. *Mol. Cell Proteomics.* **2008**, *7*, 315-25.
48. Firczuk, M.; Gabrysiak, M.; Barankiewicz, J.; Domagala, A.; Nowis, D.; Kujawa, M.; Jankowska-Steifer, E.; Wachowska, M.; Glodkowska-Mrowka, E.; Korsak, B.; Winiarska, M.; Golab, *J. Cell Death Dis.* **2013**, *4*, e741.
49. Suzuki, T.; Lu, J.; Zahed, M.; Kita, K.; Suzuki, N. *Arch. Biochem. Biophys.* **2007**, 468, 1-14.
50. Naldini, L. *Nature* **2015**, *526*, 351-360.
51. Ajith, T. A. *J. Exp. Ther. Oncol.* **2015**, *11*, 33-39.
52. Masiero, M.; Nardo, G.; Indraccolo, S.; Favaro, E. *Mol. Aspects Med.* **2007**, *28*, 143-166.

53. Lam, J.K.; Chow, M.Y.; Zhang, Y.; Leung, S.W. *Mol. Ther. Nucleic Acids.* **2015**, *4*, e252.
54. Gaglione, M.; Messere, A. *Mini Rev. Med. Chem.* **2010**, *10*, 578-595.
55. Guo, P. *Nat. Nanotechnol.* **2010**, 5, 833-842.
56. Shukla, G.C.; Haque, F.; Tor, Y.; Wilhelmsson, L.M.; Toulmé, J.J.; Isambert, H.; Guo, P.; Rossi, J.J.; Tenenbaum, S.A.; Shapiro, B.A. *ACS Nano.* **2011**, *5*, 3405-3418.
57. Afonin, K.A.; Viard, M.; Kagiampakis, I.; Case, C.L.; Dobrovolskaia, M.A.; Hofmann, J.; Vrzak, A.; Kireeva, M.; Kasprzak, W.K.; KewalRamani, V.N.; Shapiro, B.A. *ACS Nano*. **2015**, *9*, 251-259.
58. Afonin, K.A.; Viard, M.; Koyfman, A.Y.; Martins, A.N.; Kasprzak, W.K.; Panigaj, M.; Desai, R.; Santhanam, A.; Grabow, W.W.; Jaeger, L.; Heldman, E.; Reiser, J.; Chiu, W.; Freed, E.O.; Shapiro, B.A. *Nano Lett*. **2014**, *14*, 5662-5671.
59. Nakashima, Y.; Abe, H.; Abe, N.; Aikawa, K.; Ito, Y. *Chem. Commun*. **2011**, 47, 8367-8369.
60. Maina, A.; Blackman, B.A.; Parronchi, C.J.; Morozko, E.; Bender, M.E.; Blake, A.D.; Sabatino, D. *Bioorg. Med. Chem. Lett.* **2013**, *23*, 5270-5274.
61. Saar Ray, M.; Moskovich, O.; Iosefson, O.; Fishelson, Z. *J. Biol. Chem.* **2014**, *289*, 15014-15022.
62. Shu, Y.; Pi, F.; Sharma, A.; Rajabi, M.; Haque, F.; Shu, D.; Leggas, M.; Evers, B.M.; Guo, P. *Adv. Drug Deliv. Rev.* **2014**, *66*, 74-89.
63. Chiu, Y.L.; Rana, T. M. *RNA.* **2003**, *9*, 1034-1048.
64. Gray, D.M.; Hung, S.H.; Johnson, K.H. *Methods Enzymol.* **1995**, *246*, 19-34.
65. Gray, M.J.; Mhawech-Fauceglia, P.; Yoo, E.; Yang, W.; Wu, E.; Lee, A.S.; Lin, Y.G. *Int. J. Cancer*. **2013**, *133*, 21-30.
66. Ulianich, L; Insabato, L. *Front. Med.* **2014**, *1*, 55-60.
67. Matsuo, K; Gray, M.J; Yang, D.Y; Srivastava, S.A; Tripathi, P.B; Sonoda, L.A; Yoo, E. I; Duebeau, L; Lee, A.S; Lin, A.S. *Gynecol. Oncol.* **2013**, *128*, 552-559.
68. Luvsandagya, B.; Nakamura, K.; Kitahara, Y.; Aoki, H.; Murata, T.; Ikeda, S.; Minegishi, T. *Gynecol. Oncol.* **2012**, *126*, 132-139.
69. Wang, H.; Liu, Z.; Gou, Y.; Qin, Y.; Xu, Y.; Liu, J.; Wu, J.Z. *Int. J. Nanomedicine* **2015**, *10*, 5505-5512.
70. Chan, F. K.; Moriwaki, K.; De Rosa, M. *J. Methods Mol. Biol.* **2013**, *979*, 65-70.
71. Boulares, A.H.; Yakovlev, A.G.; Ivanova, V.; Stoica, B.A.; Wang, G.; Iyer, S.; Smulson, M. *J. Biol. Chem.* **1999**, *274*, 22932-22940.
72. Rubporn, A.; Srisomsap, C.; Subhasitanont, P.; Chokchaichamnankit, D.; Chiablaem, K.; Svasti, J.; Sangvanich, P. *Cancer Genomics Proteomics.* **2009**, *6*, 229-237.
73. Taldone, T.; Ochiana, S.O.; Patel, P.D.; Chiosis, G. *Trends Pharmacol. Sci.* **2014**, *35*, 592-603.
74. Hickerson, R.P.; Vlassov, A.V.; Wang, Q.; Leake, D.; Ilves, H.; Gonzalez-Gonzalez, E.; Contag, C.H.; Johnston, B.H.; Kaspar, R.L. *Oligonucleotides* **2008**, *18*, 345-354.
75. Martinez, J.; Patkaniowska, A.; Urlaub, H.; Lührmann, R.; Tuschl, T. *Cell* **2002**, *110*, 563-574.
76. Grabow, W.W.; Zakrevsky, P.; Afonin, K.A.; Chworos, A.; Shapiro, B.A.; Jaeger, L. *Nano Lett*. **2011**, *11*, 878-887.

77. Afonin, K.A.; Kireeva, M.; Grabow, W.W.; Kashlev, M.; Jaeger, L.; Shapiro, B.A. *Nano Lett.* **2012**, *12*, 5192-5195.

CHAPTER 4: CONCLUSIONS AND CONTRIBUTIONS TO KNOWLEDGE

4.1 CONCLUSIONS AND CONTRIBUTIONS TO KNOWLEDGE MADE IN THIS THESIS

4.1.1 Prerequisites for the Self-Assembly of Stable RNA Three Component Systems (3CS)

RNA nanotechnology has emerged as a powerful tool in the study of structure and function of biologically relevant RNA. In order to gain in-depth knowledge on the RNA hybridization and self-assembly requirements, Chapter-2 describes the influence of RNA sequence composition, length and buffer on RNA self-assembly into stable 3CS. This study involved the solid-phase synthesis of template RNA strands (**RNA_{T15}**, **RNA_{T20}** and **RNA_{T30}**) and its complementary RNA sequences (**RNA_{C15}**, **RNA_{C23}**) (**Table 2.1**). The synthesized RNAs were obtained in high crude yields (**≥84%**) and purities (**≥98%**) according to UV-Vis spectroscopy and IP-RP-HPLC. The identity of the RNA sequences were confirmed by molecular weight analysis using ESI-MS. The hybridization properties were investigated by native PAGE in different buffer conditions (**Figure 2.8**). The 30nt RNA template **RNA_{T30}** displayed the most stable RNA hybrid 3CS in Tris buffer, with the complementary RNA sequences (**RNA_{C15}**, **RNA_{C23}**). Thermal denaturation indicated the thermal stabilities of the RNA 3CS, in which the lengthier template provided the most stable hybrid structures (**RNA_{T30}>RNA_{T20}>RNA_{T15}**) in each buffer condition (**Figure 2.9**). The double transitions (T_m: 45 ºC and 77 ºC), indicative of denaturation of two hybrid strands confirmed that the lengthy 30 nt RNA template, **RNA_{T30}**, provided the highest thermal stability in Tris buffer. The secondary structure analysis of the RNA hybrid 3CS were studied by CD spectroscopy. The pre-requisite A-type RNA helical trajectory was confirmed for all RNA hybrid 3CS (**Figure 2.10**), in Tris buffer which maintained the most pronounced CD signature, asserted by absorbance

minima and maxima. Taken altogether, the chemical and biophysical characterization studies revealed the most stable helical RNA hybrid 3CS with the 30nt RNA template and with the complementary 15 nt and 23 nt RNA sequences in Tris buffer conditions. These findings are not only important for understanding the requirements for RNA hybridization and self-assembly, but also for promoting higher-order RNA structures that have biological importance and therapeutic relevance for cancer gene therapy applications (Chapter 3).

4.1.2 siRNA Nanostructures for Cancer Gene Therapy

In the realm of RNA nanotechnology, siRNA based nanostructures provide particular promise in RNAi-mediated cancer gene therapy applications. As discussed in Chapter 1, RNA nanotechnology favors the self-assembly of multiple RNA motifs within a single molecular structure that may synergize the therapeutic responses. The self-assembly of RNA requires the careful design of template sequences that may self-assemble with complementary sequences into higher-order structures with improved biological function and enhanced chemical and thermal stabilities. The optimization studies described in Chapter 2 for the stable self-assembly of RNA 3CS provided a platform for the design of novel siRNA nanostructures that proved to be useful in screening important oncogene targets while potentiating the cancer gene therapy effects. In Chapter 3, a new class of siRNA nanostructures based on linear, V-shape and Y-shape RNA templates were self-assembled with their complementary RNA sequences to afford higher-order RNA structures of well-defined sizes and shapes **(Figures 3.3** and **3.5**). The synthesis of V-shape and Y-shape RNA templates were completed with the incorporation of the ribouridine branchpoint synthon. The siRNAs were synthesized in good crude yields (≥62%) and purified using IP-RP-HPLC to obtained sequence purities (≥97%) whose identities were confirmed by ESI-MS, (**Table 3.2**).

The RNA templates were hybridized with their complementary sequences in Tris annealing buffer using stoichiometric ratios that promoted the self-assembly of the putative siRNA nanostructures, (**Figure 3.3**). A native PAGE was used to confirm hybridization and self-assembly into higher-order structures, (**Figure 3.4**). The sizes and shapes of the siRNA hybrids were elucidated by TEM imaging. The images revealed unique structural geometries for the self-assembled V- and Y-shape siRNA hybrids into genetically encoded circles, triangles, squares, rectangles, pentagons, hexagons and porous sphere-type structures with varying pore sizes 15-160 nm (**Figure 3.5**). Moreover, thermal denaturation and CD studies revealed high thermal stability (**Figure 3.6**) and the A-type helical geometries (**Figure 3.7**), of the siRNAs nanostructures for RNAi activity.

The RNAiMax^{TM} mediated transfection efficiency was initially optimized (**Figure 3.8-3.10**) within the GRP78 overexpressing AN3CA endometrial cancer cells. Following optimization of the transfection procedure, a 24 sample siRNA screen (**Figure 3.11**) was conducted in order to identify the most potent siRNA leads. The lead siRNAs produced the most pronounced GRP78 knockdown and apoptosis of the AN3CA cancer cells. More specifically, the lead Y-shape siRNA targeting three different sites of oncogenic GRP78 mRNA showed the greatest GRP78 knockdown efficiency (>90%) which translated into notable cell growth inhibition (~40%) and cell death effects (~10%) at low (5 nM) siRNA doses (**Figure 3.12**).

Furthermore, this study also revealed the influence of multiple GRPs (GRP-75, 78 and 94) on MDA-MB-231 (breast cancer), HeLa (cervical cancer), AN3CA (endometrial cancer) and MRC5 (non-tumorigenic lung cells) cells' survival. The multi-chaperone (GRP-75, 78 and 94) targeting V- and Y-shape siRNA hybrids revealed synergistic effects of silencing the GRP chaperome in cancer. More specifically, cancer cells were found to be more profoundly affected

by the siRNAs relative to the control, non-cancerous cells (**Figure 3.14-3.16**). Therefore, the self-assembled siRNA hybrids targeting multiple GRPs may provide specific and more potent anticancer activities. These findings are not only important for enhancing the gene therapy effects of siRNAs but also for screening the influence of oncogene targets on the progression of cancer. Finally, the stability of linear, V- and Y-shape siRNA hybrids were assessed in 10% FBS. Interestingly, the linear hybrid siRNA was completely degraded within 4 h post treatment while, the V- and Y-shape siRNA hybrids were shown to disassemble into the native RNA template strands, without further degradation, even after 48 h treatment (**Figure 3.17**). These results are also important, as they provide mechanistic insights into the prolonged (72 h) activity of the siRNA hybrids. In these cases, the template V- and Y-shape RNAs may contribute to the potent RNAi effects observed in cancer cells. Future work will be dedicated to study the complete mechanism of action while evaluating the efficacy of the siRNA nanostructures in mice tumor xenograft models.

4.2 PUBLICATIONS, INVENTION DISCLOSURES AND CONFERENCE PRESENTATIONS

4.2.1 Accepted Manuscripts for Publication

- Patel, L.P.; Rana, N.K.; Patel, M.R.; Kozuch, S.D.; Sabatino, D. **Nucleic Acid Bioconjugates and Their Potential in Cancer Therapy.** *ChemMedChem*, **2015,** *11*, 252-269.

4.2.2 Manuscripts in Review

- Patel, M.R.; Kozuch, S.D.; Cultrara, C.N.; Yadav, R.; Huang, S.; Samuni, U.; Koren, J.; Chiosis, G.; Sabatino, D. **RNAi Screening of the Glucose Regulated Chaperones in Cancer with Self-Assembled siRNA Nanostructures.** *ACS Nano Lett.* **2016,** manuscript doi: nl-2016-02274r

4.2.3 Oral and Poster Presentations

- Patel, M. R.; Sabatino, D. **siRNA Nanotechnology: A platform of cancer gene therapy**, *TIDES Meeting*, Long Beach, CA. May 2016. (**Oral and Poster Presentation**)

- Patel, M. R.; Sabatino, D. **siRNA Nanotechnology: A platform of cancer gene therapy**, *New York Academy of Sciences Meeting*, New York, NY, May 2016. (**Oral and Poster Presentation**)

- Carrión, E.N.; Kozuch, S.D.; Patel, M.R.; Patel, H.; Patel, P.L.; Borland, E.; Sabatino, D.; Gorun, S.M. **Cancer-Targeting fluoroalkyl metal phthalocyanine bioconjugates for photodynamic therapy**, *New York Academy of Sciences Meeting*, New York, NY, May 2016. (**Poster Presentation**)

- Patel, M. R.; Sabatino, D. **Self-Assembled siRNA Nanostructures: Modern approach for targeting multiple site of GRP78 oncogene for gene cancer therapy**, *27th Annual Dr. George Perez Research Colloquium*, Seton Hall University, April 2016. (**Poster Presentation**)

- Patel, M. R.; Sabatino, D. **Self-Assembled siRNA Nanostructures: Modern approach for targeting multiple site of GRP78 oncogene for gene cancer therapy**, *Petersheim Academic Exposition*, Seton Hall University, April 2016. (**Poster Presentation**)

- Patel, M. R.; Sabatino, D. **The assembly of stable, high-order oligonucleotide structure and their application in cancer gene therapy**, *ACS 247th National Meeting*, San Francisco, CA Aug 2014. (**Poster Presentation**)

- Patel, M. R.; Sabatino, D. **Modifying the sizes and shapes of nucleic acids by chemical synthesis**, *Petersheim Academic Exposition*, Seton Hall University, April 2014. (**Poster Presentation**)

- Patel, M. R.; Sabatino, D. **Exploring the basis for stable oligonucleotide interactions and their relevance in regulating gene expression**, *ACS 245th National meeting*, New Orleans, LA, April 2013. (**Poster Presentation**)

- Patel, M. R.; Sabatino, D. **The assembly of stable, higher-order oligonucleotide structures and their applications in regulating gene expression**, *Petersheim Academic Exposition*, Seton Hall University, April 2013. (**Poster Presentation**)

- Patel, M. R.; Sabatino, D. **Characteristics of three component nucleic acids**, *57th Annual New Jersey Academy of Science Meeting*, Seton Hall University, April 2012. (**Poster Presentation**)

- Patel, M. R.; Sabatino, D**. Antisense strategy to developed stable high-order structure and their application in regulating gene expression**, *Petersheim Academic Exposition*, Seton Hall University, April 2012. (**Poster Presentation**)

4.2.4 Awards and Scholarships

- Awarded **Dr. Robert DeSimone Fellowship (2014-2016)**

APPENDIX

TABLE OF CONTENTS

A. Supplemental IP-RP-HPLC Chromatograms and MS values

Figure A1. RP IP LC/MS analysis of V-shape A11 RNA (**9**)

SAMPLE INFORMATION

Sample Name:	MPVA11-GRP78	Acquired By:	System
Sample Type:	Unknown	Sample Set Name:	siRNA PURITY CHECK
Vial:	42	Acq. Method Set:	RNA_MP03_28_12_2489MS
Injection #:	1	Processing Method:	oligoprocessing
Injection Volume:	100.00 ul	Channel Name:	260
Run Time:	23.0 Minutes	Proc. Chnl. Descr.:	W2489 ChA
Date Acquired:	5/14/2014 1:35:13 PM EDT		
Date Processed:	5/20/2014 6:29:07 PM EDT		

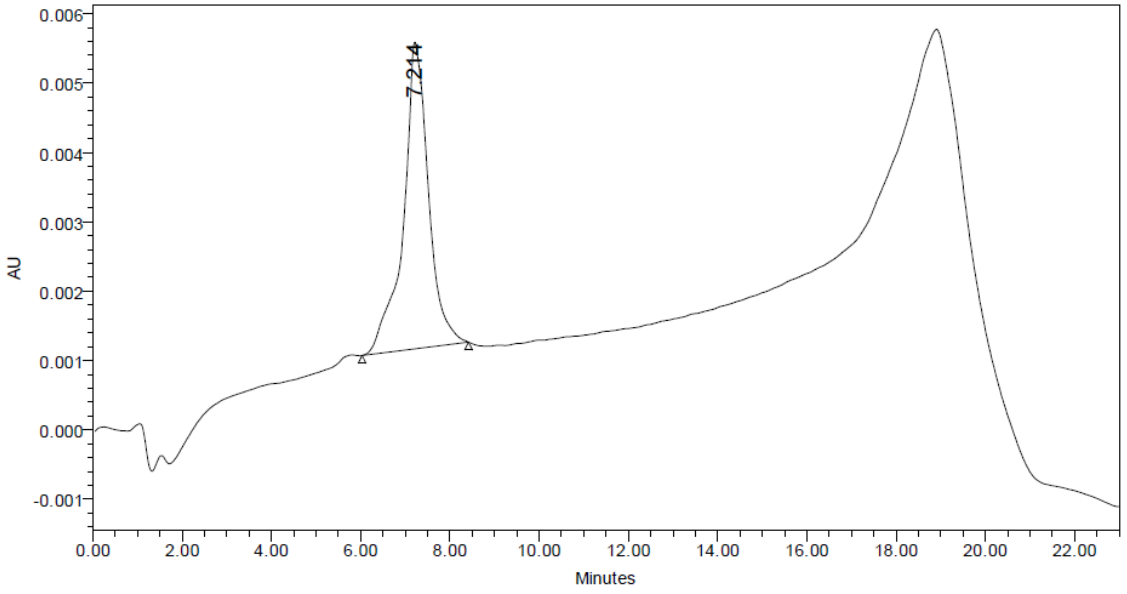

	RT	% Area	Area (µV*sec)
1	7.21	100.00	172533

9) A11:

2'3'-UCA CAA CCU UCU AAG ACU A-5' **MS. Calc. 12266.4 g/mol**

rU **Found 12266.6 g/mol**

3'5'-AUC AGA AUC UUC CAA CAC U-3'

Figure A2. RP IP LC/MS analysis of V-shape A12 RNA (**10**)

SAMPLE INFORMATION

Sample Name:	MPVA12-GRP78	Acquired By:	System
Sample Type:	Unknown	Sample Set Name:	siRNA PURITY CHECK
Vial:	43	Acq. Method Set:	RNA_MP03_28_12_2489MS
Injection #:	1	Processing Method:	oligoprocessing
Injection Volume:	100.00 ul	Channel Name:	260
Run Time:	23.0 Minutes	Proc. Chnl. Descr.:	W2489 ChA
Date Acquired:	5/14/2014 2:01:31 PM EDT		
Date Processed:	5/20/2014 6:29:07 PM EDT		

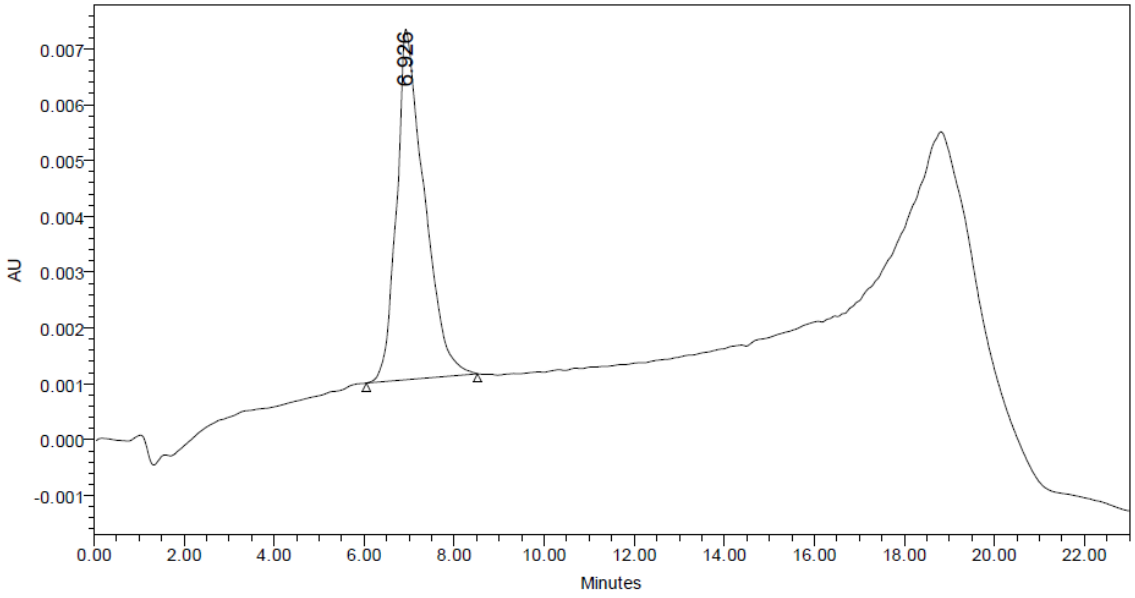

	RT	% Area	Area (µV*sec)
1	6.93	100.00	267375

10) A12:

2'3'-CCU CGC GUA ACU AUG AUC U-5' **MS. Calc. 12275.4 g/mol**

rU **Found 12277.0 g/mol**

3'5'-AUC AGA AUC UUC CAA CAC U-3'

Figure A3. RP IP LC/MS analysis of V-shape S11 RNA (**11**)

SAMPLE INFORMATION

Sample Name:	MPVS11-GRP78	Acquired By:	System
Sample Type:	Unknown	Sample Set Name:	siRNA PURITY CHECK
Vial:	44	Acq. Method Set:	RNA_MP03_28_12_2489MS
Injection #:	1	Processing Method:	oligoprocessing
Injection Volume:	100.00 ul	Channel Name:	260
Run Time:	23.0 Minutes	Proc. Chnl. Descr.:	W2489 ChA
Date Acquired:	5/14/2014 2:27:49 PM EDT		
Date Processed:	5/20/2014 6:29:07 PM EDT		

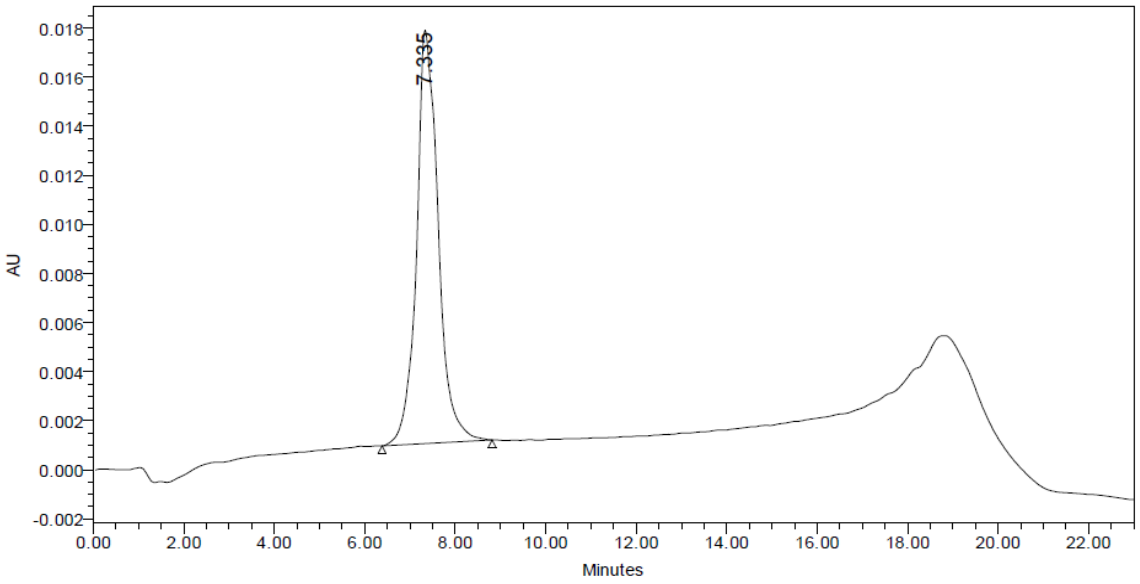

	RT	% Area	Area (µV*sec)
1	7.33	100.00	560309

11) S11:

2'3'-UAG UCU UAG AAG GUU GUG A-5' **MS. Calc. 12574.5 g/mol**

rU **Found 12575.5 g/mol**

3'5'-AGU GUU GGA AGA UUC UGA U-3'

Figure A4. RP IP LC/MS analysis of V-shape S12 RNA (**12**)

SAMPLE INFORMATION

Sample Name:	MPVS12-GRP78	Acquired By:	System
Sample Type:	Unknown	Sample Set Name:	siRNA PURITY CHECK
Vial:	45	Acq. Method Set:	RNA_MP03_28_12_2489MS
Injection #:	1	Processing Method:	oligoprocessing
Injection Volume:	100.00 ul	Channel Name:	260
Run Time:	23.0 Minutes	Proc. Chnl. Descr.:	W2489 ChA
Date Acquired:	5/14/2014 2:54:08 PM EDT		
Date Processed:	5/20/2014 6:29:07 PM EDT		

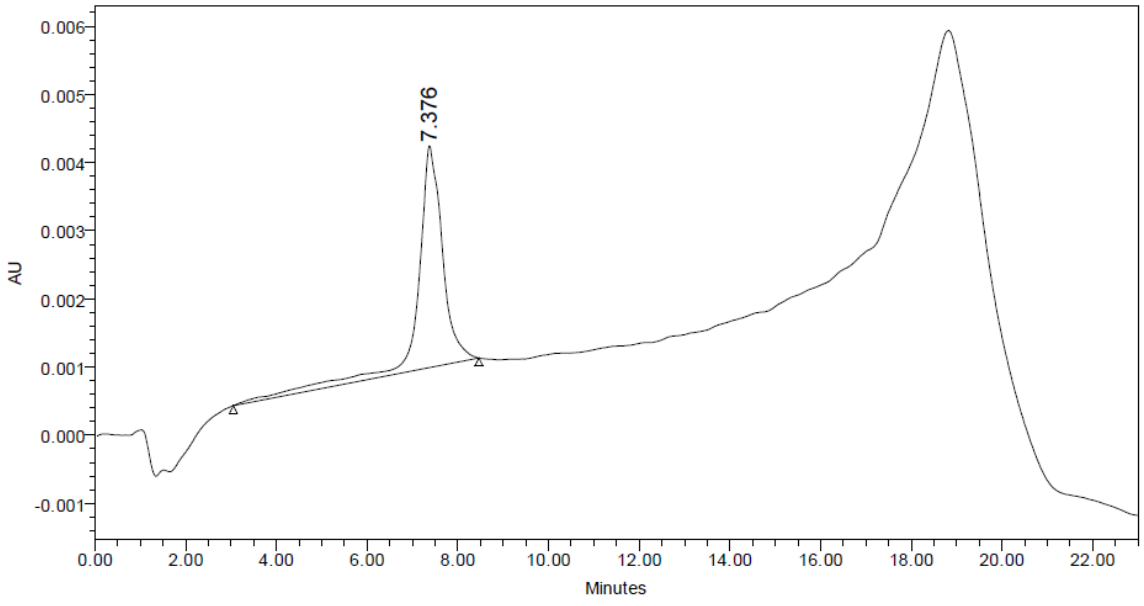

	RT	% Area	Area (µV*sec)
1	7.38	100.00	123755

12) S12:

2'3'-AGA UCA UAG UUA CGC GAG G-5' **MS. Calc. 12595.6 g/mol**

rU **Found 12596.2 g/mol**

3'5'-AGU GUU GGA AGA UUC UGA U-3'

Figure A5. RP IP LC/MS analysis of V-shape A2S1 RNA (**13**)

SAMPLE INFORMATION

Sample Name:	MPVAS21-GRP78	Acquired By:	System
Sample Type:	Unknown	Sample Set Name:	siRNA PURITY CHECK
Vial:	46	Acq. Method Set:	RNA_MP03_28_12_2489MS
Injection #:	1	Processing Method:	oligoprocessing
Injection Volume:	100.00 ul	Channel Name:	260
Run Time:	23.0 Minutes	Proc. Chnl. Descr.:	W2489 ChA
Date Acquired:	5/14/2014 3:20:25 PM EDT		
Date Processed:	5/20/2014 6:29:07 PM EDT		

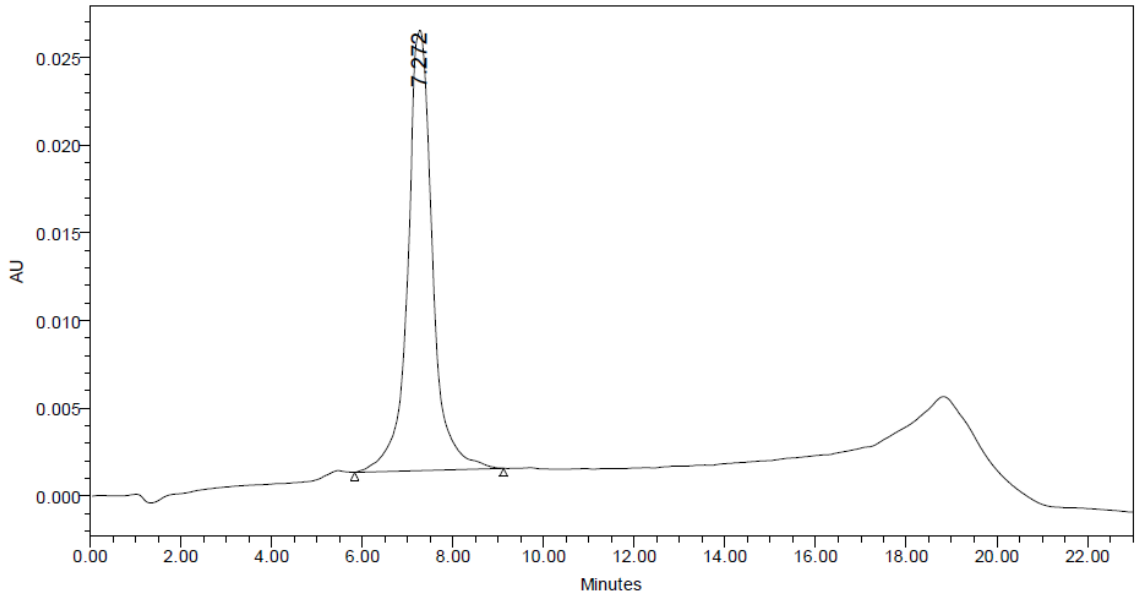

	RT	% Area	Area (µV*sec)
1	7.27	100.00	954295

13) A2S1

2'3'-UAG UCU UAG AAG GUU GUG A-5' **MS. Calc. 12429.7 g/mol**

rU **Found 12430.6 g/mol**

3'5'-UCU AGU AUC AAU GCG CUC C-3'

Figure A6. RP IP LC/MS analysis of V-shape A1S1 RNA (**14**)

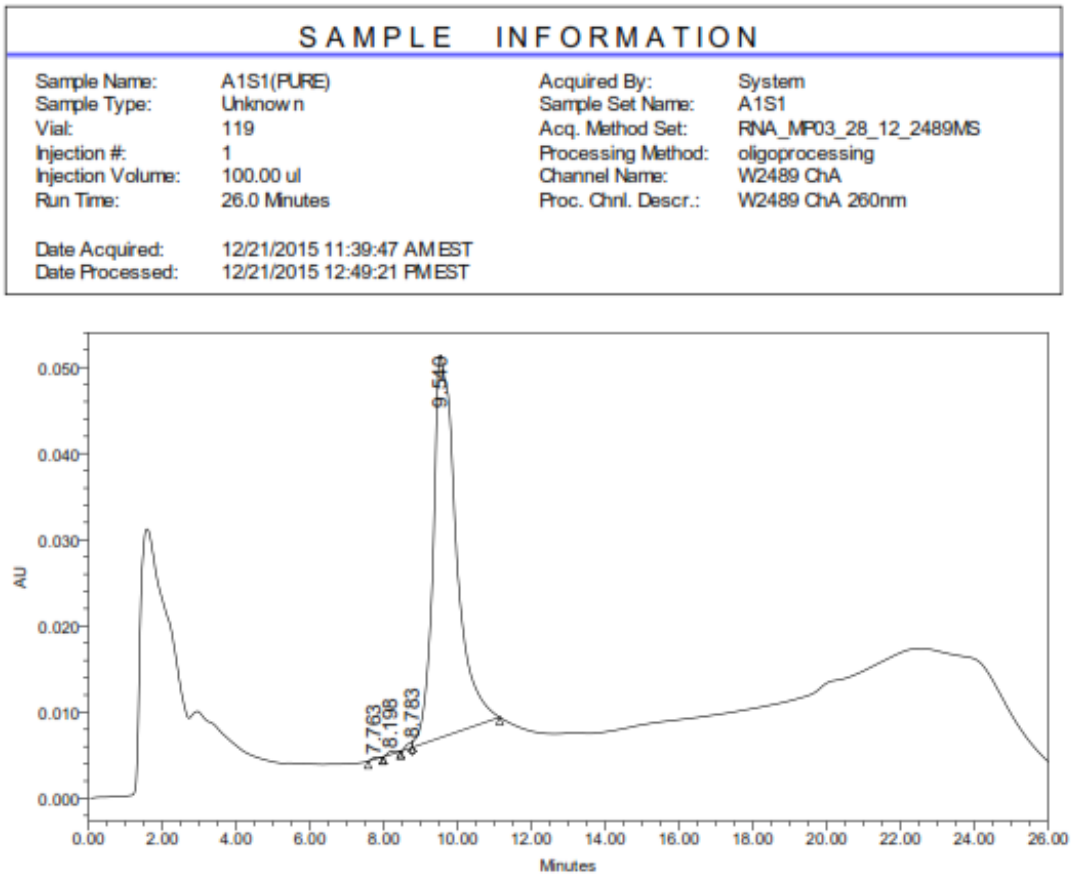

	RT	% Area	Area (μV*sec)
1	7.76	0.13	2470
2	8.20	0.25	4835
3	8.78	0.37	7239
4	9.54	99.26	1951612

14) A1S1

2'3'-UAG UCU UAG AAG GUU GUG A-5' **MS. Calc. 12421.2 g/mol**

rU **Found 12421.6 g/mol**

3'5'-AUC AGA AUC UUC CAA CAC U-3'

Figure A7. RP IP LC/MS analysis of Y-shape A111 RNA (**15**)

SAMPLE INFORMATION

Sample Name:	MPYA111-GRP78	Acquired By:	System
Sample Type:	Unknown	Sample Set Name:	PURITY CHECK
Vial:	31	Acq. Method Set:	RNA_MP03_28_12_2489MS
Injection #:	1	Processing Method:	oligoprocessing
Injection Volume:	100.00 ul	Channel Name:	260
Run Time:	23.0 Minutes	Proc. Chnl. Descr.:	W2489 ChA
Date Acquired:	5/14/2014 10:37:32 AM EDT		
Date Processed:	5/20/2014 6:27:39 PM EDT		

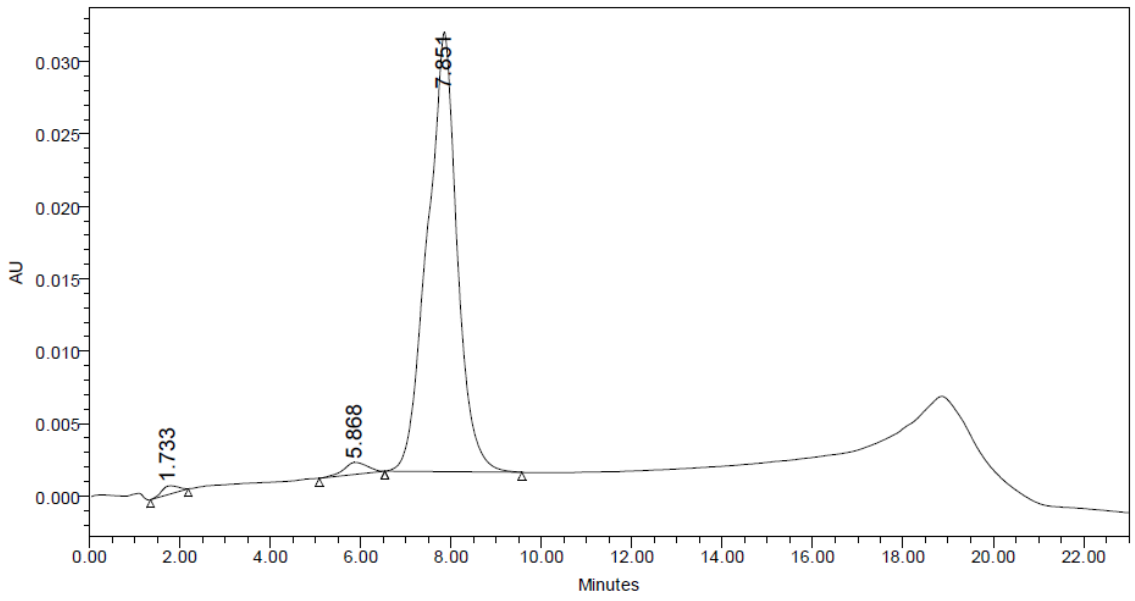

	RT	% Area	Area (µV*sec)
1	1.73	1.02	14580
2	5.87	2.08	29866
3	7.85	96.90	1388382

15) A111:

2'3'-UCA CAA CCU UCU AAG ACU A-5' **MS. Calc. 18278.0 g/mol**

5'-AUC AGA AUC UUC CAA CAC U-3'5'-U **Found 18278.4 g/mol**

3'5'-AUC AGA AUC UUC CAA CAC U-3'

Figure A8. RP IP LC/MS analysis of Y-shape A123 RNA (**16**)

SAMPLE INFORMATION

Sample Name:	MPYA123-GRP78	Acquired By:	System
Sample Type:	Unknown	Sample Set Name:	PURITY CHECK
Vial:	32	Acq. Method Set:	RNA_MP03_28_12_2489MS
Injection #:	1	Processing Method:	oligoprocessing
Injection Volume:	100.00 ul	Channel Name:	260
Run Time:	23.0 Minutes	Proc. Chnl. Descr.:	W2489 ChA
Date Acquired:	5/14/2014 11:03:50 AM EDT		
Date Processed:	5/20/2014 6:22:44 PM EDT		

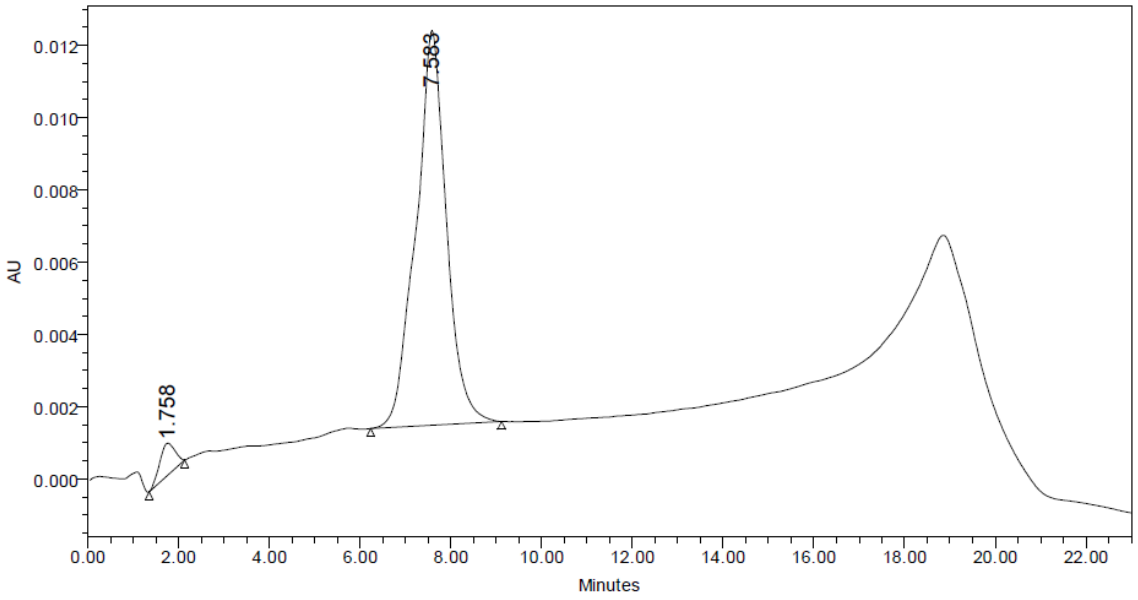

	RT	% Area	Area (µV*sec)
1	1.76	3.94	20934
2	7.58	96.06	509742

16) A123:

2'3'-CCU CGC GUA ACU AUG AUC U-5' **MS. Calc. 19975.2 g/mol**

5'-GUA ACA ACU GCA UGG GUA ACC UUC-3'5'-U **Found 19975.8 g/mol**

3'5'-AUC AGA AUC UUC CAA CAC U-3'

Figure A9. RP IP LC/MS analysis of Y-shape S111 RNA (**17**)

SAMPLE INFORMATION

Sample Name:	MPYS111-GRP78	Acquired By:	System
Sample Type:	Unknown	Sample Set Name:	PURITY CHECK
Vial:	33	Acq. Method Set:	RNA_MP03_28_12_2489MS
Injection #:	2	Processing Method:	oligoprocessing
Injection Volume:	100.00 ul	Channel Name:	260
Run Time:	23.0 Minutes	Proc. Chnl. Descr.:	W2489 ChA
Date Acquired:	5/14/2014 11:56:26 AM EDT		
Date Processed:	5/20/2014 6:29:07 PM EDT		

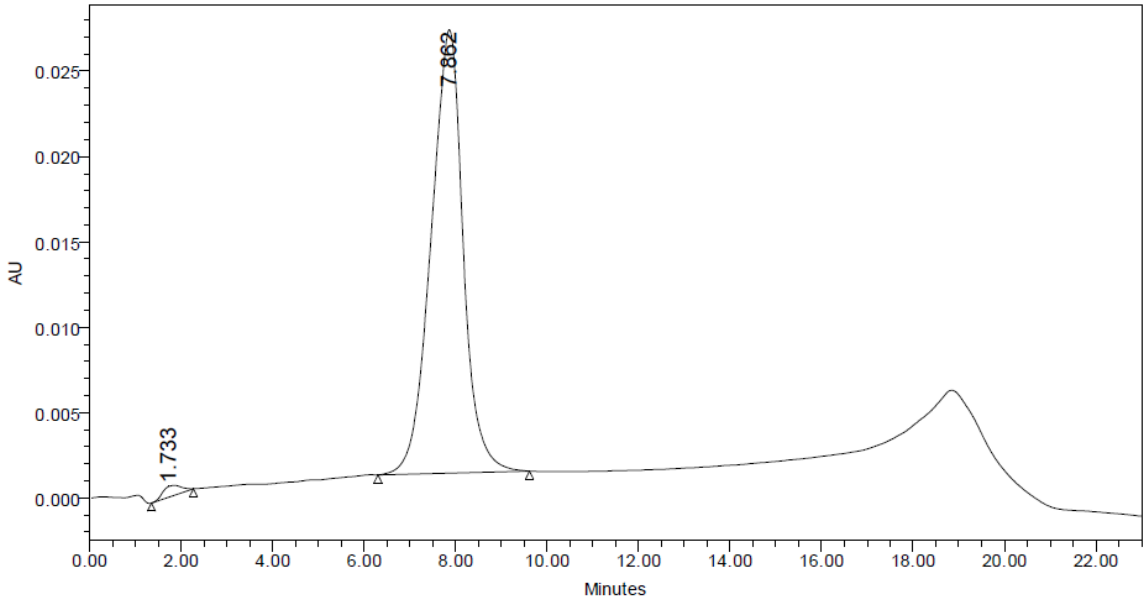

	RT	% Area	Area (µV*sec)
1	1.73	1.33	17142
2	7.86	98.67	1268433

17) S111:

2'3'-UAG UCU UAG AAG GUU GUG A-5' MS. Calc. 18739.2 g/mol

5'-AGU GUU GGA AGA UUC UGA U-3'5'-U Found 18740.6 g/mol

3'5'-AGU GUU GGA AGA UUC UGA U-3'

Figure A10. RP IP LC/MS analysis of Y-shape S123 RNA (**18**)

SAMPLE INFORMATION

Sample Name:	MPYS123-GRP78	Acquired By:	System
Sample Type:	Unknown	Sample Set Name:	siRNA PURITY CHECK
Vial:	34	Acq. Method Set:	RNA_MP03_28_12_2489MS
Injection #:	1	Processing Method:	oligoprocessing
Injection Volume:	100.00 ul	Channel Name:	260
Run Time:	23.0 Minutes	Proc. Chnl. Descr.:	W2489 ChA
Date Acquired:	5/14/2014 12:42:21 PM EDT		
Date Processed:	5/20/2014 6:29:07 PM EDT		

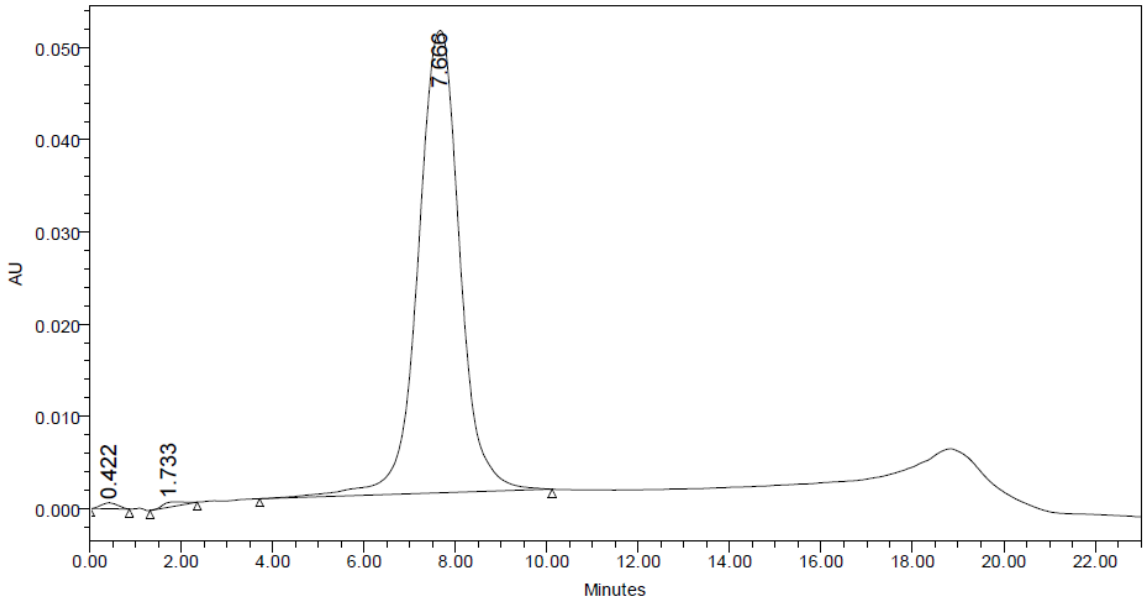

	RT	% Area	Area (μV*sec)
1	0.42	0.50	16165
2	1.73	0.49	15729
3	7.67	99.01	3180262

18) S123:

2'3'-AGA UCA UAG UUA CGC GAG G-5' **MS. Calc. 20531.2 g/mol**

5'-GAA GGU UAC CCA UGC AGU UGU UAC-3'5'-U **Found 20534.0 g/mol**

3'5'- AGU GUU GGA AGA UUC UGA U-3'